POLITECNICO DI TORINO

Department of Mechanical and Aerospace Engineering

Master degree course in Aerospace Engineering

Master Degree Thesis

Dynamic and thermal model for hydraulic shock absorbers

Advisor:
Domenic D'Ambrosio

Co-Advisor:
Roberto Marsilio

Candidate
Riccardo Andrighetto

Academic Year 2017-2018

Summary

The purpose of the thesis is to develop a compressible and thermal model for automotive dampers. The selected approach is a lumped parameter modelling which shortens preliminary design sizing process if compared to a time-consuming detailed CFD.
Twin tube configuration is taken as reference: four main regions are identified such as rebound, compression and reserve chamber which are filled with the damper medium while the fourth is constituted by the gas chamber.

Starting from the simplest formulation, the incompressible one, each model is analysed including progressively compressibility and thermal effects.
In the lumped system analysis also damper main solid parts are modelled. Temperature influence on viscosity is accounted for in both local and wall-friction losses.

Numerical verification is provided to guarantee mass and energy conservation. For MATLAB implementation classical ODE resolution and mass-matrix formulation is investigated in terms of CPU time.

To my family,

Riccardo Andrighetto

Contents

List of Tables V

List of Figures VI

List of Symbols VIII

Introduction 1

1 Lumped parameter model 5
- 1.1 Reference configuration description . . . 5
- 1.2 Piston rod law motion . . . 6
- 1.3 Governing equations . . . 8
- 1.4 Compressibility and coefficient of thermal expansion . . . 8
- 1.5 Characteristic time and pressure variation in each chamber . . . 9
- 1.6 Damping force computation . . . 9
- 1.7 Friction and local losses modelling . . . 10

2 Incompressible twin tube damper model 13
- 2.1 Adiabatic process for gas chamber . . . 14
- 2.2 Pressure field in a simplified incompressible model . . . 14
- 2.3 Hysteresis effects on the F-V diagrams in the incompressible model . . . 15
  - 2.3.1 Initial gas volume effect on hysteresis . . . 18
  - 2.3.2 Initial gas volume and working point . . . 19

3 Compressible model for an isothermal twin tube damper 21
- 3.1 Formulation of the compressible model . . . 21
- 3.2 Mass conservation equation for the three chambers . . . 22
  - 3.2.1 Compressibility influence on characteristic diagrams . . . 22
  - 3.2.2 Mass flow through orifices . . . 24
- 3.3 Compliance of the cylinder wall . . . 26
  - 3.3.1 Another expression for cylinder compliance . . . 26
  - 3.3.2 Analysis of the compliance effect . . . 28
- 3.4 Piston-wall leakage modelling . . . 29
- 3.5 A geometrical model with a simplified blow-off valve . . . 30
  - 3.5.1 The impact of blow-off valve on damper characteristics . . . 32

3.5.2 Summary of the phenomenology appreciated 42

4 A simplified non-caviting twin tube for experimental testing 45
4.1 Orifices geometry analysis 45
4.1.1 Piston orifices 46
4.1.2 Base valve orifices 47
4.2 Possible configurations for experimental testing 49
4.2.1 Configuration with fixed orifice 50
4.2.2 Twin tube with 60% reduced piston orifice area in the rebound phase 51
4.2.3 Twin tube with 50% reduced piston area orifice in the rebound phase 52
4.3 Constant k model and Reynolds dependent model comparison 53

5 Dynamic behaviour of the damper at high frequency 55
5.1 Damping work 57
5.2 Spring Power 57

6 A compressible and thermal model for a dual tube damper 59
6.1 Thermal working fluid 59
6.2 Equation of state for gas 60
6.3 Mass conservation equations for the thermal model 60
6.4 Energy equations 61
6.4.1 Gas energy equation 62
6.4.2 Energy equation for orifices 62
6.5 Heat transfer modelling on solid parts 63
6.6 Justification of the lumped system analysis 64
6.6.1 Biot number computation for the solid parts 65
6.7 Temperature influence on viscosity 66
6.8 Definition of fluxes through boundaries 67

7 Implementation of the model in Matlab 71
7.1 Classical ODE resolution 71
7.2 Mass matrix implementation method 72
7.3 CPU time measurements for the two methods 72
7.3.1 CPU time: Heat fluxes disabled 72
7.3.2 CPU time: Heat fluxes enabled 73
7.4 Numerical verification of mass and energy conservation 76
7.4.1 Thermal model with no heat fluxes 76
7.4.2 Thermal model with heat fluxes enabled 78
7.5 A mass non-conserving model 80
7.5.1 Coefficient of thermal expansion effect on density 82

8 Conclusions 85

Appendix 87

Bibliography 101

List of Tables

2.1 Geometry configuration for incompressible model 16
2.2 Initial gas volume input on the incompressible model 18
3.1 Value of compressibility used to highlight compressibility effect 23
3.2 Cylinder compressibility factor 28
3.3 Geometrical configuration for parameter study 33
3.4 Value of β used to show compressibility effect 34
3.5 Blow-off equivalent effect on damper properties 36
3.6 Input parameters to show the pre-load force effect 39
3.7 Value of cylinder-wall gap simulated in the compressible model 40
4.1 Geometry configuration for incompressible model 45
4.2 Orifice configuration for the fixed orifice model 50
4.3 Orifice configuration for the third orifice model with 50% area reduction in rebound 51
4.4 Orifice configuration for the third orifice model with 50% area reduction in rebound 52
6.1 Calculation of Biot number for solid parts 65
7.1 CPU time required for the thermal model with heat flux disabled 72
7.2 CPU time required with heat flux enabled 73
7.3 Mass and energy conservation for the thermal model - numerical verification 80
7.4 Mass value comparison for frequency f=3 Hz and time T=5 s 81

List of Figures

1 Conflict diagram for Ride-Handling (dis)qualities 1
2 Monotube and Twin-tube shock absorber schemes 2
3 Valve assembly scheme 3
4 Example of a real-life piston valve assembly 3
5 Real-life components of a shock absorber 4
1.1 Reference model of the twin tube damper 6
1.2 Slider crank mechanism 7
1.3 Piston rod displacement and velocity for excitation frequency f = 1 Hz . . 7
1.4 Forces acting on the piston for damping force computation 10
1.5 $\lambda - Re$ correlation used for friction losses 11
1.6 Empirical function for C_d in case of sharp-edge orifices 12
2.1 Characteristic diagrams 16
2.2 Gas Pressure vs Time assuming incompressible medium 17
2.3 Pressure trends vs Time assuming incompressible medium 17
2.4 Effect of initial gas volume on F-V diagram hysteresis 18
2.5 Gas pressure for same input geometry and different excitation frequency . 19
2.6 Reserve chamber pressure at different excitation frequency 20
3.1 Hysteresis effect due to compressibility at frequency 1 Hz 23
3.2 Compressibility effect at high frequency (f = 4 Hz) 24
3.3 Comparison of mass flow through orifices for different β 25
3.4 Deformation cylinder effect on F-V diagram 28
3.5 Wall-cylinder leakage scheme 30
3.6 Interface implemented in app-designer 31
3.7 F-X diagram for excitation frequency 1 Hz, $k = 800\ \mathrm{N\,m^{-1}}$ 32
3.8 F-V diagram for f= 1 Hz, $k = 800\ \mathrm{N\,m^{-1}}$ and $\mathrm{F_{pre\text{-}charge}}$= 20 N 33
3.9 Hysteresis effect due to compressibility magnified by blow-off valve 35
3.10 Force-displacement diagram for different k 37
3.11 Force-velocity diagram for $k = 80$, 800 and 10^4 N/m 38
3.12 Force-velocity diagram for $F_{precharge} = 40$ N 39
3.13 Force-velocity diagram for different cylinder-wall gap 41
3.14 Characteristic diagram for a typical twin tube with blow-off valve 43
4.1 Rebound chamber pressure for two diameters of the piston orifices 47
4.2 Rebound chamber pressure for two diameters of the piston orifices 48
4.3 Compression chamber pressure with a condition of cavitation 49
4.4 F-V diagram for fixed orifice model 51

4.5 F-V diagram with 60% closure of orifice in piston valve in rebound phase 52
4.6 F-V diagram with closure of orifice in piston valve in rebound 53
4.7 Constant k model and k(Re) model for fixed orifice configuration 53
4.8 Constant k model and k(Re) model with 60% reduction in rebound 54
4.9 Constant k model and k(Re) model with 50% reduction in rebound 54
5.1 Frequency behaviour for incompressible model 56
5.2 Frequency behaviour for compressible model 56
5.3 Damping work for various frequencies 57
5.4 Classical and fixed maximum velocity stroke comparison 58
5.5 F-V diagram without stroke changing for various excitation frequencies . 58
5.6 F-V diagram at fixed maximum velocity for various excitation frequencies 58
6.1 Convection-Conduction in the lumped system 64
6.2 Pressure and temperature trends with enthalpy convection 68
6.3 Pressure and temperature trends with mean value enthalpy 69
7.1 CPU time comparison for the thermal model with heat flux disabled . . . 74
7.2 CPU time comparison for the thermal model with heat flux enabled . . . 75
7.3 Temperature trends for solid parts (heat fluxes disabled) 76
7.4 Fluid part pressures and temperatures for heat fluxes disabled model . . . 77
7.5 Temperature trends for solid parts (heat fluxed enabled) 78
7.6 Fluid part pressures and temperatures for heat fluxes enabled model . . . 79
7.7 Example of pressure trend for a non conserving model 81
7.8 Example of pressure trend for a conserving model 81
7.9 Pressure trend for a typical coefficient of thermal expansion 82
7.10 Pressure trend for coefficient of thermal expansion $\varphi = 0$ 83

List of Symbols

α	Coefficient of thermal convection	$[\mathrm{W\,m^{-2}\,K^{-1}}]$
β	Isothermal compressibility coefficient	$[\mathrm{Pa^{-1}}]$
β_c	Compressibility factor of the cylinder	$[\mathrm{Pa^{-1}}]$
$\dot{m}$	Mass flux through orifice	$[\mathrm{kg\,s^{-1}}]$
ϵ	Elastic strain	
ϵ_s	Absolute roughness	[m]
γ	Specific heat ratio	
λ	Thermal conductivity	$[\mathrm{W\,m^{-1}\,K^{-1}}]$
λ_f	Friction factor	
μ	Dynamic viscosity	[Pa s]
ν	Kinematic viscosity	$[\mathrm{m^2\,s^{-1}}]$
ν	Poisson's coefficient	
Φ	Heat exchanged with the environment	[W]
ρ	Density	$[\mathrm{kg\,m^{-3}}]$
$\sum A_{fcomp-res}$	Total base valve orifice area	$[\mathrm{m}^2]$
$\sum A_{freb-comp}$	Total base valve orifice area	$[\mathrm{m}^2]$
τ	Shear stress	[Pa]
φ	Coefficient of thermal expansion	$[\mathrm{K^{-1}}]$
a	Acceleration of piston rod	$[\mathrm{m\,s^{-2}}]$
a	Speed of sound	$[\mathrm{m\,s^{-1}}]$
A_p	Piston area	$[\mathrm{m}^2]$

A_r	Rod area	$[\mathrm{m}^2]$
A_{cyl}	Internal cross section of the cylinder	$[\mathrm{m}^2]$
$A_{orifice}$	Orifice area	$[\mathrm{m}^2]$
A_{ref}	Reference area	$[\mathrm{m}^2]$
A_{valve}	Valve area	$[\mathrm{m}^2]$
Amp	Length of the crank	[m]
b	Cylinder wall clearance	[m]
C_d	Discharge coefficient	
c_p	Specific heat at constant pressure	$[\mathrm{J\,kg^{-1}K^{-1}}]$
c_v	Specific heat at constant volume	$[\mathrm{J\,K^{-1}\,kg^{-1}}]$
C_{corr}	Corrective term (flow not completely known near valve)	
C_{d_∞}	Coefficient of discharge for Re $\rightarrow \infty$	
D_e	External diameter of the cylinder	[m]
D_h	Hydraulic diameter	[m]
D_p	Piston diameter	[m]
E	Young's modulus	[Pa]
e_k	Specific kinetic energy (per unit mass)	$[\mathrm{J\,kg^{-1}}]$
e_p	Specific potential energy (per unit mass)	$[\mathrm{J\,kg^{-1}}]$
f	Frequency	[Hz]
F_D , F_{app}	Damping force	[N]
F_{fric}	Friction between piston ring-tube and rod-seal	[N]
$F_{pre-charge}$	Pre-charge force of the blow of valve	[N]
h	Specific enthalpy (per unit mass)	$[\mathrm{J\,kg^{-1}}]$
K	Bulk modulus	[Pa]
k_{loss}	Coefficient of flow resistance	
L	Cylinder length	[m]
L	Length of the connecting rod	[m]

l	Cylinder thickness	[m]
L_c	Inner cylinder length	[m]
L_{ref}	Reference length	[m]
Lc_{inner}	Characteristic length of inner cylinder	[m]
Lc_{outer}	Characteristic length of outer cylinder	[m]
m_i	Mass of the solid part	[kg]
M_{mg}	Gas molar mass	$[\mathrm{g\,mol^{-1}}]$
p	Pressure	[Pa]
p_0	Reference pressure	[Pa]
P_{sp}	Spring Power	[W]
q	Heat flux	[W]
Q_m	Mass flow rate	$[\mathrm{kg\,s^{-1}}]$
Q_{BC}	Volumetric flux from compression to reserve chamber	$[\mathrm{m^3\,s^{-1}}]$
Q_{EC}	Volumetric flux from rebound to compression chamber	$[\mathrm{m^3\,s^{-1}}]$
Q_{leak}	Volumetric flow due to piston-wall clearance	$[\mathrm{m^3\,s^{-1}}]$
Q_{leak}	Volumetric flux due to cylinder-wall leakage	$[\mathrm{m^3\,s^{-1}}]$
R_e	Outer cylinder radius	[m]
R_i	Inner cylinder radius	[m]
R_{12}	Friction losses in the orifice	$[\mathrm{J\,kg^{-1}}]$
Re	Reynolds number	
T_0	Reference temperature	[K]
T_g	Gas temperature	[K]
U	Circumference of the cross section area of the cylinder	[m]
$u(y)$	Streamwise velocity component in parallel channel	$[\mathrm{m\,s^{-1}}]$
v	Velocity of oil through orifice	$[\mathrm{m\,s^{-1}}]$
v_p	Piston speed	$[\mathrm{m\,s^{-1}}]$
$v_{comp-res}$	Flow velocity between compression and reserve chamber	$[\mathrm{m\,s^{-1}}]$

V_{comp}	Rebound chamber oil volume	$[\mathrm{m}^3]$
V_g	Gas chamber volume	$[\mathrm{m}^3]$
V_{oil}	Total volume occupied by gas in the damper	$[\mathrm{m}^3]$
$v_{reb-comp}$	Flow velocity between compression and rebound chamber	$[\mathrm{m\,s}^{-1}]$
V_{reb}	Rebound chamber oil volume	$[\mathrm{m}^3]$
V_{res}	Reserve chamber oil volume	$[\mathrm{m}^3]$
W_d	Damping work	[J]
$x_p(t)$	Piston position	[m]
y	Deflection of the blow-off valve	[m]
$\dot{W}_a$	Power provided from the external to the control volume	[W]
Bi	Biot number	
E	Specific total energy (per unit mass)	$[\mathrm{J\,kg}^{-1}]$
R	Universal constant for gases	$[\mathrm{J\,Kmol}^{-1}\,\mathrm{K}^{-1}]$
z	Height of the fluid with respect to reference height	[m]

Introduction

The suspension system of a vehicle has to provide the best compromise of a number of requirements which can be divided in two main subjects: Ride and Handling. Ride means driving comfort and it is concerned with the protection of isolated side components (e.g. chassis, driver and passengers) from the motion of the input side (e.g. road or wheel)[3]. Handling is strictly related to vehicle reaction to steering manoeuvre. Usually, a suspension system consists of a spring and a damper.
Energy temporary stored by the spring is dissipated and converted into heat by damper with a decaying amplitude of oscillations. The effect of the spring and damper, which together constitute the so called *damper module*, may be combined into a polar plot, the passenger-tyre discomfort loop.

The opposing ride-handling qualities give birth to the *conflict diagram* (Figure 1). The diagram needs to be plotted for various values of suspension ride-handling parameter f_{SRH} which takes into account stiffness k, damping coefficient C and mass m of the equivalent system [8].

$$f_{SRH} = \sqrt[3]{\frac{kC}{m^2}}$$

For normal vehicle it falls in the range 1-2 s^{-1}.

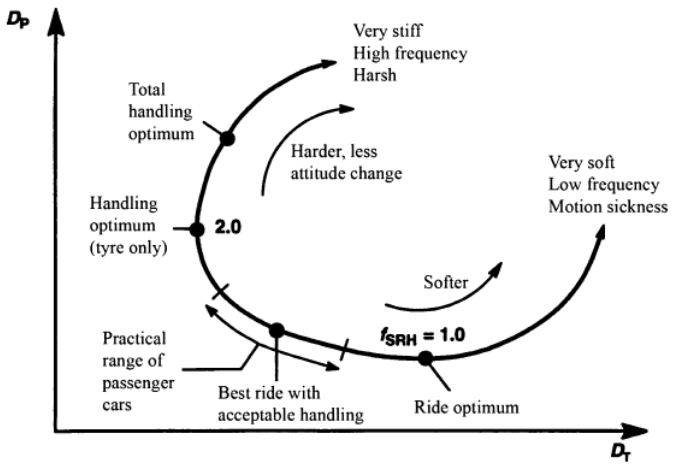

Figure 1: Example of conflict diagram (D_p = passenger discomfort on the y-axis, D_r = tyre discomfort on the x-axis)

Moving forward into the description, let's concentrate on the subject of study: *shock absorbers*. They can be divided in two categories:

- Monotube dampers;
- Dual tube dampers;

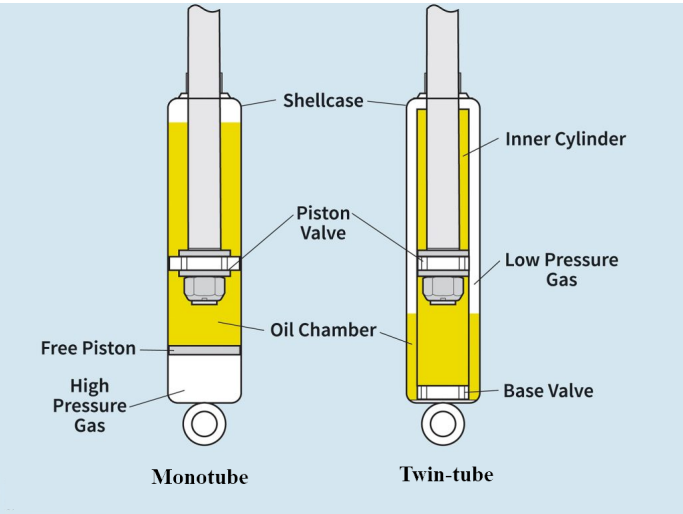

Figure 2: Monotube (left) and Twin-tube (right) shock absorber [source:http://dsportmag.com/]

The difference between these two types of shock absorbers consists on how volume variation due to piston rod movement is compensated. The reader can see their schematic configuration in Figure 2.

In both cases a compression chamber, a rebound and a gas chamber can be identified. The dual tube (also *twin tube*) damper is characterized by a reserve chamber filled with oil which is in direct contact with gas. Conversely, in the monotube configuration a floating piston (also *free piston*) separates the compression chamber from the gas chamber (typically nitrogen or air).
The role of the gas chamber is permitting volume variations in the compression and extension phases due to the movement of the piston rod. In fact, the compressibility of oil is not enough to compensate these volumetric changes, as performed by gas.

Rebound and compression chambers are separated by a piston valve assembly which is a combination of blow-off valves, leak restrictions and intake valves. Intake valve is a check valve that allows flow only in a predetermined direction, while restricted channels engender pressure drop by viscous dissipation. On the other hand, blow-off valves constitute a passive self tuning of the damper preventing the value of the damping force from getting too high (Figure 3). What can be said is that the primary damping mechanism is proportional to flow restrictions. Low speed damping forces are dominated by bleed orifices (permanent flow) while blow-off valves progressively open at high velocity.

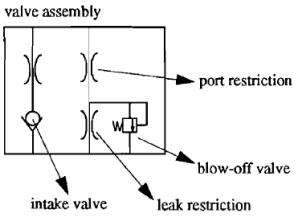

Figure 3: Scheme of a valve assembly [9]

Another flow path is the piston-wall leakage. Although undesirable, it is very difficult to remove. A real-life piston assembly is reported in Figure 4.

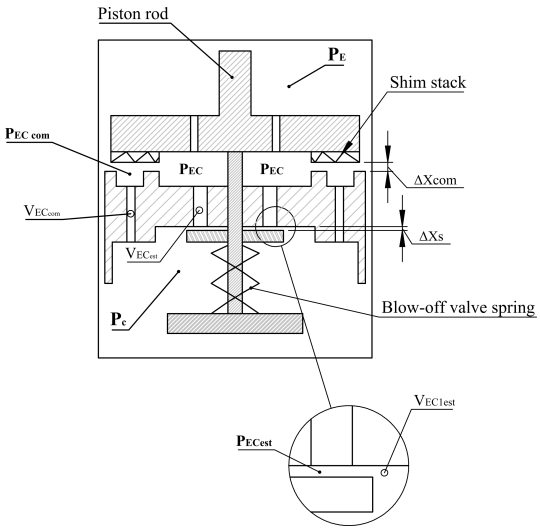

Figure 4: Example of a real-life piston valve assembly

A brief comparison between dual-tube and monotube shock absorber is useful to highlight how although similar physical principles respond differently to accomplish requirements.

Pure monotube shock absorber

- Oil separated from gas;
- High pressure gas to prevent cavitation;
- Larger oil capacity and improved heat dissipation;
- High-pressure gas can lead to stress on seals and causes larger friction;

Pure twin tube shock absorber

- The presence of base valve allow to keep a lower gas pressure. Hence stress is avoided and friction is low;

- Aeration is possible;
- The size of the piston is not large as the one in the monotube;
- Minor manufacturing costs;

In concrete terms, this combination of valves is realized using assemblies of shim stacks and extension/compression valve springs. Different flow paths are designed in rebound and compression phase to obtain an asymmetric F-V diagram, which will be introduced later.
Pre-charge forces, elastic constant of the shim stack and blow-off valve are the key factors governing damper's dynamics.

Figure 5: On the top, examples of real-life components of a shock absorber, on the bottom a piston valve [8]

Chapter 1

Lumped parameter model

This part is focused on the basic elements the lumped parameter model is derived from. It includes the definition of the geometrical configuration for a pure twin tube damper, the law of motion for the piston rod and the introduction to compressibility and to thermal expansion effects.

The distinctive mark of a lumped parameter analysis is that it relinquishes a point to point description preferring modelling the phenomena with lumped elements.
The application of this integral approach assigns a set of properties (temperature, pressure) at each working chamber.

1.1 Reference configuration description

The subject of study is a damper in a dual tube configuration. In the classical twin tube damper we can identify three regions filled with the liquid medium (oil):

- A rebound chamber, the upper region in contact with the piston rod;
- A compression chamber, located in the middle between the rebound and the reserve chamber. It communicates with the rebound chamber through the piston orifices and with the reserve chamber through the base valve (also *foot valve*);
- A reserve chamber in communication with the compression chamber through the base valve;

The system is completed by a gas chamber which is in direct contact with the oil in the reserve chamber. The role of the gas is to compensate volume variations caused by the variable length of the piston rod portion in the rebound chamber during the rebound and compression phases.
The main difference between twin tube and monotube dampers lies in the presence, for the latter, of a *floating piston* whose function is to separate the gas-oil interface introducing an inertial factor.

Coming back to the twin tube description, the whole system is contained inside what will be called the outer cylinder, with the internal regions (rebound and compression) divided from the external ones from the inner cylinder. In this work, piston and base

valves are constituted only by bleed orifices. At the oil-gas interface, what will be called *compatibility condition* reads:

$$p_g = p_{reserve} \tag{1.1}$$

$$\frac{\mathrm{d}p_g}{\mathrm{d}t} = \frac{\mathrm{d}p_{reserve}}{\mathrm{d}t} \tag{1.2}$$

It is equivalent to say that the reserve chamber pressure is bounded to that assumed by the gas.
A schematic representation of the model is reported in Figure 1.1.

In the upward movement of the piston, the oil flows from the rebound chamber into the compression chamber, but to compensate the change of the compression chamber volume an oil flow from the reserve chamber to the compression chamber takes place. The key mechanism lies in the different volume variation of compression and rebound chamber due to the presence of the piston in the latter one. The reverse scenario to that described develops when the piston moves downward : the oil flows from the compression to the rebound chamber; again, the volume occupied by the piston rod forces part of the oil to flow through the base valve.

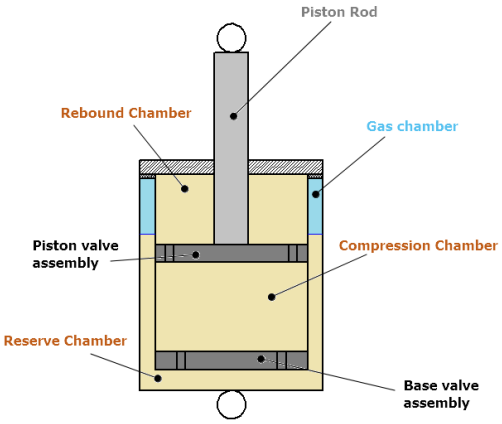

Figure 1.1: Reference model of the twin tube damper

1.2 Piston rod law motion

In order to analyse the damper behaviour, the motion of the piston rod is imposed and therefore, known. The piston rod movement is derived from the inspection of the slider-crank mechanism (Figure 1.2): From geometrical relations it is possible to write:

$$\begin{cases} x_p = L\cos\varphi + Amp\cos\theta \\ L = Amp\cos(\pi - \theta - \varphi) + x_p\cos\varphi \end{cases} \tag{1.3}$$

Expanding the second of (1.3), using trigonometry identity $\sin^2\theta + \cos^2\theta = 1$, we obtain

$$\sin\varphi = \frac{Amp}{L}\sin\theta \tag{1.4}$$

Expression (1.4), after trigonometrical manipulation, lead to:

$$1 - cos^2\theta = \frac{Amp^2}{L^2}\sin^2\theta \tag{1.5}$$

Thus,

$$x = \sqrt{L^2 - Amp^2\sin^2\theta} + Amp\cos\theta \tag{1.6}$$

From the relation between angle θ and frequency of the stroke

$$\theta = \pi + 2\pi ft$$

The final form for the displacement reads:

$$x_p = \sqrt{L^2 - Amp^2\sin^2(2\pi ft)} - Amp\cos(2\pi ft) \tag{1.7}$$

Deriving with respect to time, we find the velocity of the piston:

$$\dot{x} = v_p = -\frac{\pi f Amp^2\sin(4\pi ft)}{\sqrt{L^2 - Amp^2\sin^2(2\pi ft)}} + 2\pi f Amp\sin(2\pi ft) \tag{1.8}$$

In Figure 1.3 the origin has been shifted by subtracting the quantity $L - Amp$ from (1.7).

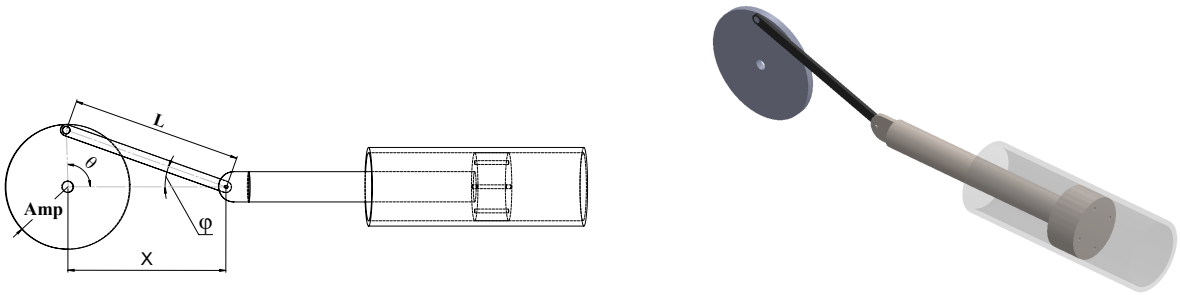

Figure 1.2: Slider crank mechanism

If not specified differently, the values of Amp and L assumed are respectively:

$$Amp = 15 \cdot 10^{-3}\,[\text{m}] \qquad L = 4.5 \cdot 10^{-2}\,[\text{m}]$$

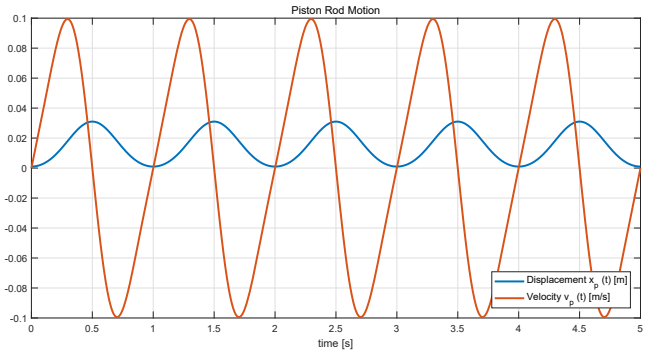

Figure 1.3: Piston rod displacement and velocity for excitation frequency f = 1 [Hz]

1.3 Governing equations

The physical model is based on the application of the following governing equations:

1. Mass balance equation:

$$\frac{D}{\mathrm{D}t}\int_{V(t)}\rho\,\mathrm{d}V = 0 \tag{1.9}$$

$$\frac{\partial}{\partial t}\int_{V}\rho\,\mathrm{d}V + \int_{S}\rho\mathbf{V}\cdot\mathbf{n}\mathrm{d}S = 0 \tag{1.10}$$

2. Energy balance equation:

$$\frac{\partial}{\partial t}\int_{V(t)}(\rho E)\mathrm{d}V+\int_{S(t)}(\rho E)\mathbf{v}\cdot\mathrm{d}\mathbf{S} = \Phi-\int_{V(t)}\boldsymbol{\nabla}\cdot(p\mathbf{v})\mathrm{d}V+\int_{V(t)}\boldsymbol{\nabla}\cdot(\tau\cdot\mathbf{v})\mathrm{d}V-\int_{V(t)}\boldsymbol{\nabla}\cdot q\mathrm{d}V-\dot{W}_a \tag{1.11}$$

Each equation is specialized for the model adopted. For isothermal models, the energy equation is not needed. The closure of the system of equation is obtained through the state-equation.

1.4 Compressibility and coefficient of thermal expansion for the damper medium

The density of a liquid is affected by the pressure level. The bulk modulus K of a substance provide a measure of the volume variation caused by a pressure field:

$$K = -V\frac{\mathrm{d}P}{\mathrm{d}V} \tag{1.12}$$

Compressibility β is the reciprocal of the bulk modulus:

$$\beta = \frac{1}{K} = \frac{1}{\rho}\frac{\partial\rho}{\partial p} \tag{1.13}$$

Density ρ of the medium increases with pressure. A typical value for pure clean oil [8] is

$$\beta \approx 0.05\%/MPa$$

In service condition the entrained air bubbles greatly increase compressibility. If not specified, the value of β adopted in the simulation is $\beta = 2.5\cdot10^{-9}\,\mathrm{Pa}^{-1}$. The coefficient of thermal expansion is defined as:

$$\varphi = -\frac{1}{\rho}\frac{\partial\rho}{\partial T} \tag{1.14}$$

An increment of temperature causes ρ to diminish. The order of magnitude of this coefficient is $\phi \approx 10^{-3}\,\mathrm{K}^{-1}$.

1.5 Characteristic time and pressure variation in each chamber

The development of a model requires the inspection of phenomena time scale taking place inside the damper. A relationship which bounds the speed of sound a and the isothermal compressibility factor β, yields to:

$$a^2 = \frac{\mathrm{d}p}{\mathrm{d}\rho} \tag{1.15}$$

Together with (1.13):

$$\beta = \frac{1}{\rho}\frac{\mathrm{d}\rho}{\mathrm{d}p} = \frac{1}{\rho a^2} \tag{1.16}$$

Consequently a typical value of the speed of sound is:

$$a = \frac{1}{\sqrt{\beta\rho}} \approx 1300 \quad \mathrm{m/s} \tag{1.17}$$

At this point, considering a reference length $L_{ref} = 10^{-1}$ m for the column of oil, a reference time-scale is found to be:

$$t = \frac{L_{ref}}{a} \approx 10^{-4} \quad \mathrm{s} \tag{1.18}$$

The results obtained states that a perturbation of pressure propagates in each chamber of oil almost instantaneously. In fact, this time corresponds to a frequency of approximately 10 KHz.

For the excitation frequency considered, the process can be regarded as quasi stationary and it is possible to attribute to each chamber a single pressure value at the generic instant t.

1.6 Damping force computation

The piston rod assembly is subjected to a force F_D generating from the differential pressure between rebound and compression chamber. Pressure acts on different areas because of the presence of piston rod. As a result, a static force (offset) exists at rest which is given by the term $p_{g_0}A_r$.

$$F_D = p_{rebound}(A_p - A_r) - p_{compression}A_p + p_{g_0}A_r - \mathrm{sgn}\left(\frac{\mathrm{d}x_p}{\mathrm{d}t}\right)F_{fric} \tag{1.19}$$

A_p and A_r indicate the piston area and the rod area respectively, while p_{g_0} refers to the initial gas pressure. In experimental testing the value of friction F_{fric} can be estimated and is not considered in the model. The frictional force for standard dampers falls in the range of 20 N and 60 N. An improvement in modelling friction phenomena in sliding condition is given in [13].

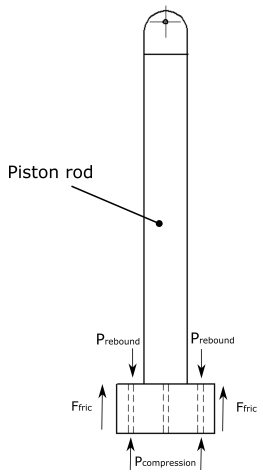

Figure 1.4: Forces acting on the piston for damping force computation

1.7 Friction and local losses modelling

In principle, two kinds of losses are distinguished observing the mechanism of energy dissipation:

- *Wall friction losses*: they have a close causal connection with the viscosity of the fluid and no-slip condition. Friction loss arises from shear stress at the wall, producing a momentum flux;

- *Local losses* (also *concentrated* losses) which appear in presence of geometrical (cross-section) changes. Dissipation is produced by separation of the flow;

Friction losses are modelled using friction correlation for laminar, transition and turbulent flow [7]. Friction factor λ is therefore expressed using a power law of Re. Precisely, the correlation used is is given as a rational fraction of rational fractions of power laws [7].

$$\lambda_f = -D_h \frac{\frac{\mathrm{d}p}{\mathrm{d}x}}{\frac{\rho U^2}{2}} \tag{1.20}$$

In fact, the non-dimensional parameter which governs the phenomenon is Reynolds number:

$$Re = \frac{\rho v D_h}{\mu} \tag{1.21}$$

The geometrical input required are the hydraulic diameter D_h and the length of the orifices. The correlation used is reported below:

$$\begin{aligned} F_a &= \frac{64}{Re} \\ F_b &= 4.1 \cdot 10^{-16} Re^4 \\ F_c &= 0.351 Re^{-0.255} \\ F_d &= 0.118 Re^{-0.165} \\ F_1 &= F_a + \frac{F_b - F_a}{\sqrt{1 + \left(\frac{Re}{2900}\right)^{-50}}} \\ F_2 &= F_c + \frac{F_d - F_c}{\sqrt{1 + \left(\frac{Re}{240000}\right)^{-1}}} \end{aligned} \tag{1.22}$$

$$\lambda_f = F_1 + \frac{F_2 - F_1}{\sqrt{1 + \left(\frac{Re}{3050}\right)^{-50}}} \tag{1.23}$$

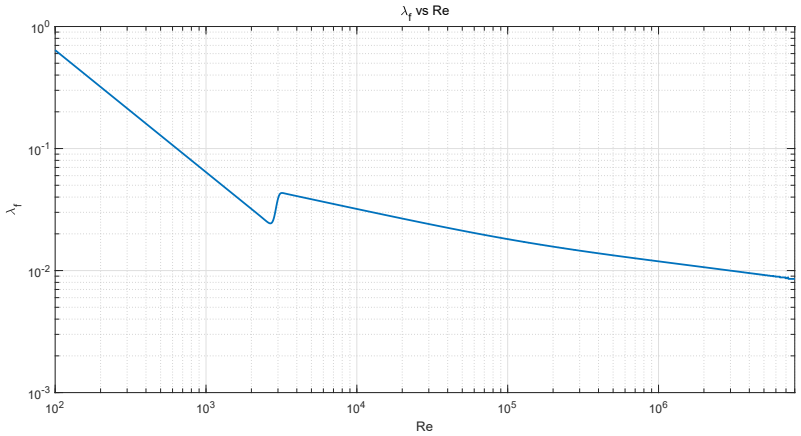

Figure 1.5: $\lambda - Re$ correlation used [7]

Even though roughness has negligible influence, the code contemplates also absolute roughness as input. In this case, an efficient resolution of Colebrook-White equation is provided [6]:

$$\frac{1}{\sqrt{\lambda_f}} = -2\log_{10}\left(\frac{\epsilon_s}{3.7} + \frac{2.51}{Re\sqrt{\lambda_f}}\right) \tag{1.24}$$

The flow rate Q through an orifice can be modelled introducing a discharge coefficient C_d applying Bernoulli's equation [16]. It is function of acceleration number $\frac{al}{\nu^2}$, Reynolds number $\frac{\rho\nu l}{\mu}$, Cauchy number $\beta\nu^2\rho$ and thickness to length ratio $\frac{s}{l}$.

$$C_d = f\left(\frac{al}{\nu^2}, \frac{\mu}{\rho\nu l}, \beta\nu^2\rho, \frac{s}{l}\right) \tag{1.25}$$

so that

$$Q = C_d A_{orifice} \sqrt{\frac{2\Delta p}{\rho}} \tag{1.26}$$

In first approximation C_d can be assumed as constant at high Reynolds number but its value may change significantly especially for small openings. According to [22] the following empirical model is used:

$$C_d = C_{d_\infty}(1 + ae^{-\frac{\delta_1}{C_{d_\infty}}\sqrt{Re}} + be^{-\frac{\delta_2}{C_{d_\infty}}\sqrt{Re}}) \tag{1.27}$$

In case of sharp-edge orifice (1.27) becomes:

$$C_d = 0.61(1 + 1.07e^{-0.126\sqrt{Re}} - 2.07e^{-0.246\sqrt{Re}}) \tag{1.28}$$

The discharge coefficient trend vs $\sqrt{Re}$ is reported in Figure 1.6. When the flow is turbulent and fully developed viscosity has negligible impact and $C_d \to C_{d_\infty}$. In some cases the introduction of the flow resistance k_{loss} is preferred. Its relation with discharge coefficient is:

$$k_{loss} = \frac{1}{{C_d}^2}$$

so the flow rate is:

$$Q = A_{orifice} \sqrt{\frac{2\Delta p}{\rho k_{loss}}} \tag{1.29}$$

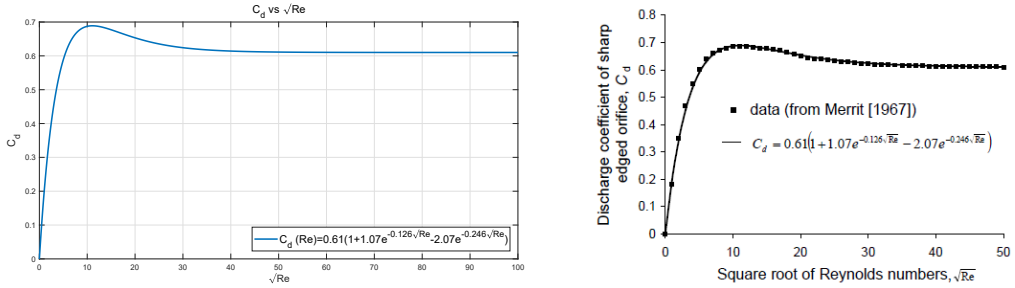

Figure 1.6: On the left the empirical function for sharp-edge orifices, on the right the comparison with experimental data [22]

Chapter 2

Incompressible twin tube damper model

In this section the assumptions an incompressible model is based on will be investigated. The limits of these hypothesis are explored and compared to the benefits of a more extended modelling including compressibility and thermal effects.

Assuming as reference Figure 1.1, the incompressibility statement results in a isothermal compressibility coefficient equal to zero:

$$\frac{1}{\rho}\frac{\partial \rho}{\partial p} = \beta = 0 \tag{2.1}$$

This consideration allows to face the problem writing an explicit relation between volumetric fluxes Q and piston movement v_p. In fact, when the piston rod progressively enters the rebound chamber, the volume variation for this chamber is:

$$\frac{\mathrm{d}V_{reb}}{\mathrm{d}t} = v_p(t)(A_p - A_r) \tag{2.2}$$

At the same time, the piston causes a variation of the volume in the compression chamber:

$$\frac{\mathrm{d}V_{comp}}{\mathrm{d}t} = -v_p(t)A_p \tag{2.3}$$

Considering the continuity equation for incompressible medium, the volumetric flow rate interesting the rebound chamber (having the normal to the control volume pointing outward) is:

$$v_p(A_p - A_r) + Q_{reb-comp} = 0 \tag{2.4}$$

At this point should be evident that due to the volume occupied by the rod, an amount of oil equal to v_pA_r (in volumetric terms) is forced to flow from the compression to the reserve chamber. The total flow rate $Q_{tot} = v_pA_r$ is easily obtained writing the mass conservation equation for the other two chambers containing oil:

$$-v_pA_p - Q_{reb-comp} + Q_{comp-res} = 0 \tag{2.5}$$

For the reserve chamber:

$$\frac{\mathrm{d}V_{res}}{\mathrm{d}t} - Q_{comp-res} = 0 \tag{2.6}$$

It follows that for an incompressible model, the volumetric fluxes are an explicit function of the piston velocity, as mentioned at the beginning of the section:

$$Q_{tot} = Q_{comp-res} = v_p(t)A_r \tag{2.7}$$

2.1 Adiabatic process for gas chamber

The process of compression - expansion of the gas in direct contact with the oil can be expressed assuming adiabatic process. The frequency of excitation and the high speed of the piston leave no time to the gas to exchange heat with the surroundings.
On this basis, the heat flux is neglected and the process is idealized as adiabatic:

$$p_{g_1}V_1^{\gamma} = p_{g_2}V_2^{\gamma} \tag{2.8}$$

As the pre-charge pressure p_{g_0} and the initial volume of the gas V_{g_0} are known, the volume variation in the gas chamber is readily obtained:

$$\frac{\mathrm{d}p_g}{\mathrm{d}t} + \gamma\frac{p_g}{V_g}\frac{\mathrm{d}V_g}{\mathrm{d}t} = 0 \tag{2.9}$$

2.2 Pressure field in a simplified incompressible model

Since $\frac{\mathrm{d}V_g}{\mathrm{d}t} = -\frac{\mathrm{d}V_{res}}{\mathrm{d}t}$ and it is a quantity known from (2.7), the time integration is carried out:

$$p_g = \left(p_{g_0}^{-\frac{1}{\gamma}} - \frac{A_r}{p_{g_0}^{\frac{1}{\gamma}}V_{g_0}}(x_p - x_{p_0})\right)^{-\gamma} \tag{2.10}$$

Pressure in the gas chamber is a function of the initial condition (initial pressure p_{g0}, volume V_{go} and piston position x_0) and the piston position $x_p(t)$. Rearranging (2.5) and (2.4) remembering that in the incompressible model the density ρ has a constant value, mass conservation is simply a volumetric conservation:

$$v_{comp-res} = \frac{v_p A_r}{\sum A_{fcomp-res}} \tag{2.11}$$

$$v_{reb-comp} = -v_p\frac{A_p - A_r}{\sum A_{freb-comp}} \tag{2.12}$$

Using 1.29 on page 12 to represent the pressure drop in the pipe, the pressure of each chamber is found:

$$p_{comp} = p_{res} + \frac{1}{2}\,\mathrm{sgn}(v_{comp-res})k_{loss_{comp-res}}v_{comp-res}^2 \tag{2.13}$$

$$p_{reb} = p_{comp} + \frac{1}{2}\,\mathrm{sgn}(v_{reb-comp})k_{loss_{reb-comp}}v_{reb-comp}^2 \tag{2.14}$$

Once the pressure field in each chamber has been computed, the damping force is found using 1.19 on page 9. The assumption of adiabatic process will be made also in chapter 3 treating a compressible formulation for the damper medium.
We highlight that isothermal models such as the ones mentioned above (incompressible and compressible) do not contemplate the temperature as variable involved in the balance equations. This is the fundamental reason of introducing the adiabatic hypothesis.

2.3 Hysteresis effects on the F-V diagrams in the incompressible model

The incompressible model, assuming as constant the value of density, is not able to capture the non linearities caused by the compressibility effects. It follows that valve openings and orifice flows are generated by pressure drops proportional to the piston movement.
Idealizing the physical model as series connection of a damper and spring elements, the system responds instantaneously. In other words there are no delays related to the compressibility of the medium.

Nevertheless, Figure 2.1 shows large hysteresis in the force-velocity (F-V) diagram. In fact, the presence of the gas gives the so called *spring effect*. In the incompressible formulation, this contribution is independent from velocity and a function of only the piston position.
As a result, the initial gas volume performs an important role in preventing the pressure in the rebound chamber to drop below the vapour pressure of the oil and leading to cavitation.

A simplified geometry which includes three chambers filled with the oil and with the gas chamber is taken as reference to explore pressure and damping force trends. Rebound, compression and reserve chamber interchange the oil through the orifices as already indicated in 1.1. The geometrical configuration of the twin tube damper is reported in Table 4.1.

Figure 2.1 shows the typical diagrams for a damper: the force - velocity and force - displacement diagrams. As mentioned above, in the F - V diagram it is evident the hysteresis effect caused by the gas compression. At the same velocity (i.e. $v_p = 0$), the force takes two different values.
The gas spring effect is responsible for the non-zero value of the damping force when the piston is fully extended (where x_p reaches the maximum value), as shown in Figure 2.2.

In that condition, the gas pressure reaches the peak value because the piston rod, entering the rebound chamber for its maximum length allowed, forces the reserve chamber to occupy a larger volume (its maximum for single cycle) and thus compressing the gas.

Table 2.1: Geometry configuration for incompressible model

Data Geometry	
$\boldsymbol{A_p}$ [m^2]	$1.590 \cdot 10^{-3}$
$\boldsymbol{A_r}$ [m^2]	$3.142 \cdot 10^{-4}$
N° piston orifices	3
Diameter piston orifice [m]	$2.50 \cdot 10^{-3}$
N° base valve orifices	1
Diameter base valve orifice [m]	$2.50 \cdot 10^{-3}$
Internal Cylinder Length $\boldsymbol{L_{c_{in}}}$ [m]	$1.425 \cdot 10^{-1}$
$\boldsymbol{\gamma}$ **(specific heat ratio)**	1.4
$\boldsymbol{p_{g_0}}$ [Pa]	$1.00 \cdot 10^5$
$\boldsymbol{V_{g_0}}$ [m^3]	$3.584 \cdot 10^{-5}$

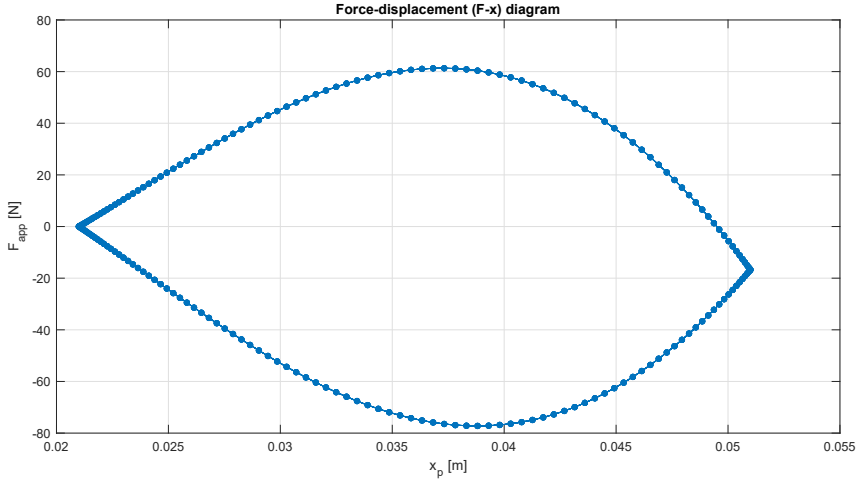

(a) *Force-displacement diagram*

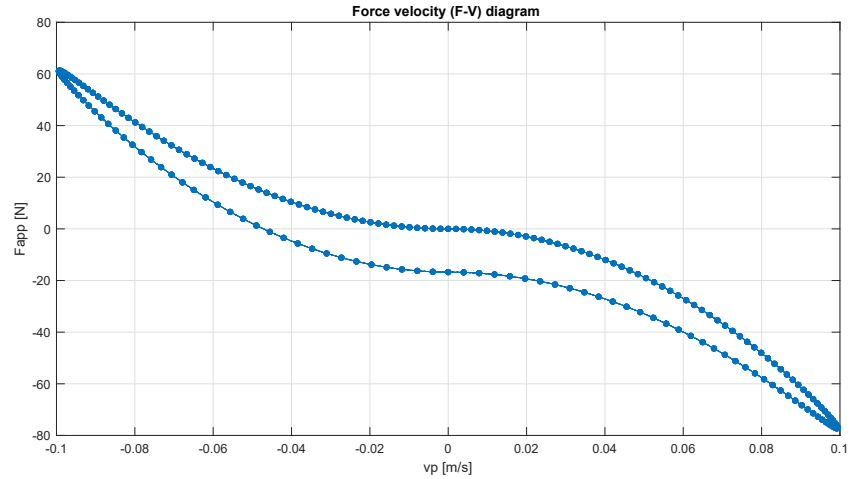

(b) *Force-velocity diagram*

Figure 2.1: Characteristic diagrams

In Figure 2.2, the pressure trends for each chamber are compared. As we can see, at time = 0.5 s corresponding to half cycle ($f = 1$ Hz), the pressure value is the same in the whole system. Thus, (1.19) reduces to

$$F_{app} = -A_r(p_{res} - p_{g0}) \quad \text{with} \quad p_g = p_{res} = p_{comp} = p_{reb}$$

When the rod is inserted for its maximum value $p_g \neq p_{g0}$, a non - zero force is acting on the cylinder.

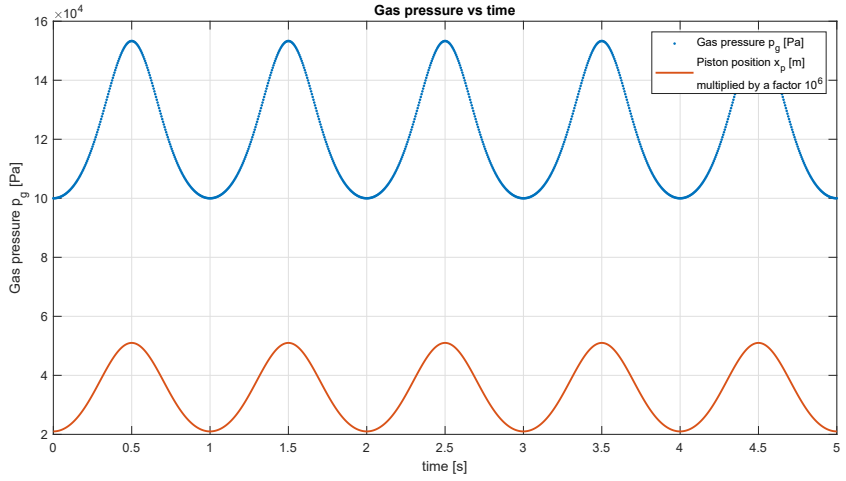

Figure 2.2: Gas Pressure vs Time assuming incompressible medium

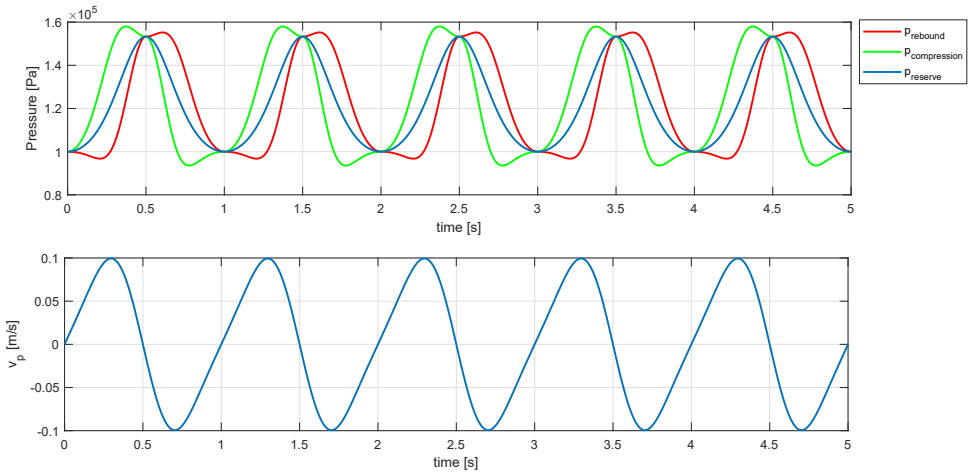

Figure 2.3: Pressure trends vs Time assuming incompressible medium

2.3.1 Initial gas volume effect on hysteresis

With reference to the same geometrical configuration reported in Table 4.1, we underline the effect of the initial volume on hysteresis which is apparent in F-V diagram.

The behaviour of the gas in the twin tube chamber can be idealized to that of a spring. Diminishing the volume occupied by the gas is equivalent to increase the elastic constant k of the spring. Reminding (2.8), since the volume variation depends only on the geometrical configuration:

$$p_{g0}V_{g0}^{\gamma} = \Big(p_g + \mathrm{d}p_g\Big)\Big(V_g - \mathrm{d}V_g\Big)^{\gamma} \tag{2.15}$$

The less the gas initial volume the more the gas pressure is increased for the same value of volume variation $\mathrm{d}V_g$. Figure 2.4 shows the different hysteresis cycles for the initial gas volumes listed in Table 2.2.

Table 2.2: Initial gas volume input on the incompressible model

$\boldsymbol{V_{g0}}$ [m^3]
$2.628 \cdot 10^{-5}$
$3.584 \cdot 10^{-5}$
$7.168 \cdot 10^{-5}$
$9.557 \cdot 10^{-5}$

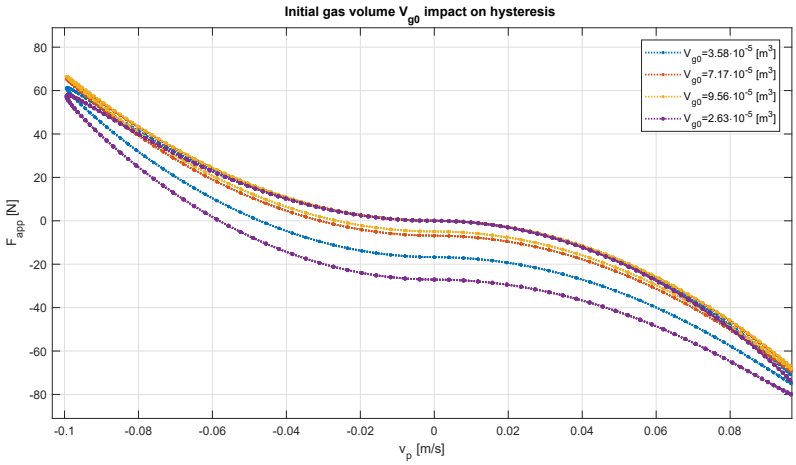

Figure 2.4: Effect of initial gas volume on F-V diagram hysteresis

2.3.2 Initial gas volume and working point

Summarizing the main characteristics the gas introduces in the twin tube damper behaviour:

- It introduces a force position dependent but velocity independent from the piston movement;
- The gas acts like a non-linear spring force in which pressure evolves according to (2.15);

It is necessary to point out that, even for the incompressible model, the pressure drop is also related to the piston movement. So that, the damper working point has to be chosen carefully. High pressure in the gas chamber can prevent cavitation from taking place. On the other side, a very high velocity movement of the piston causes a large pressure drop. This behaviour is illustrated in Figure 2.5 and 2.6 in which an incompressible model which does not consider cavitation phenomena is used.

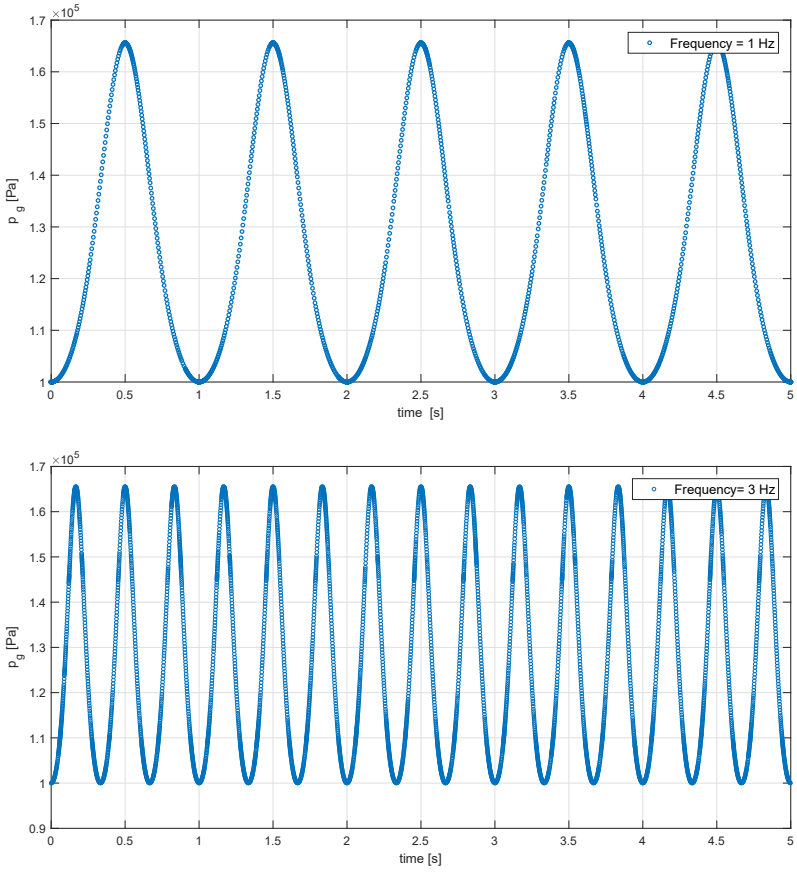

Figure 2.5: Gas pressure for same input geometry and different excitation frequency

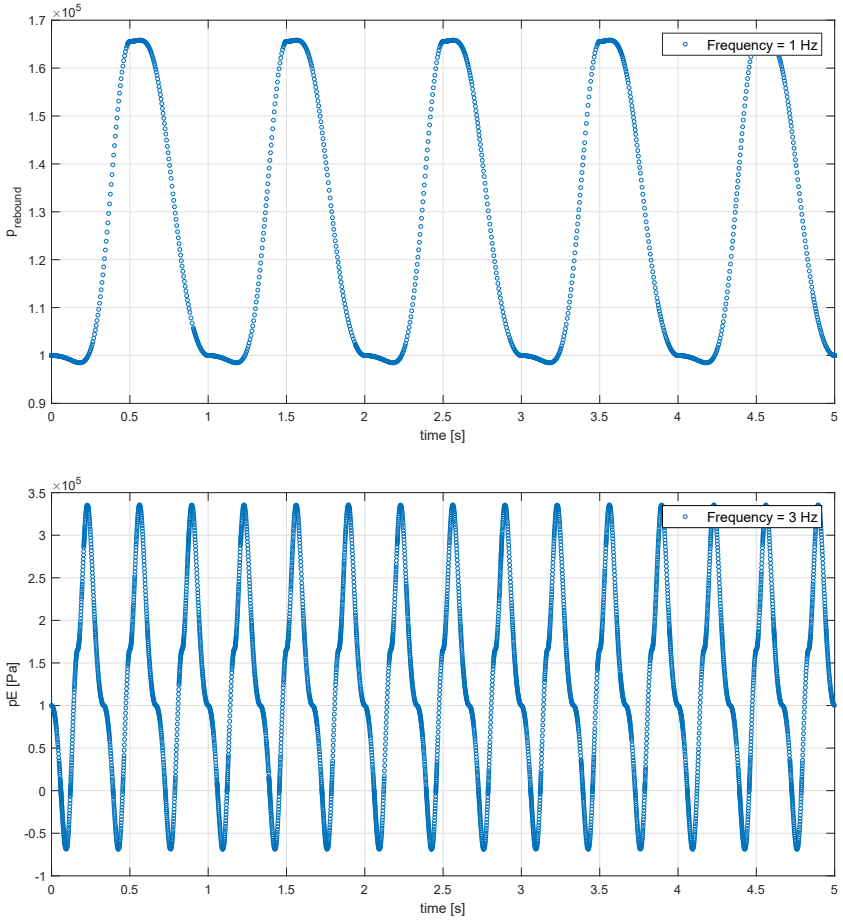

Figure 2.6: Reserve chamber pressure for same input geometry and different excitation frequency

It is clear that for different excitation frequencies gas pressure does not change (depending only on piston position) but very fast movements cause large pressure drop (negative pressure is not a physical situation, it means that cavitation phenomena will appear).

Chapter 3

Compressible model for an isothermal twin tube damper

3.1 Formulation of the compressible model

The aim of this section is to include the compressibility of the damper medium within the model. The formulation of a compressible model requires the revising of the continuity equation (1.10).

$$\frac{\partial(\rho V)}{\partial t} + \int_S \rho \mathbf{v} \mathrm{d}\mathbf{S} = 0 \tag{3.1}$$

The main difference with the incompressible model consists in considering the time variation of the density ρ. Expanding (3.1), using the definition of isothermal compressibility β (1.13):

$$\rho \frac{\partial V}{\partial t} + V \frac{\partial \rho}{\partial t} = \int_S \rho \mathbf{v} \mathrm{d}\mathbf{S} = 0$$

So that, for a generic chamber, we have:

$$V \frac{\partial p}{\partial t} \beta + \frac{\partial V}{\partial t} + \frac{1}{\rho} \int_S \rho \mathbf{v} \mathrm{d}\mathbf{S} = 0 \tag{3.2}$$

It is important noting that the value of ρ dividing the mass flux has to be chosen coherently with the value of density used to evaluate the velocity through the orifice. Otherwise, the mass conservation in the whole system is not respected. The last term in (3.2) is dimensionally a volumetric flow rate:

$$\frac{1}{\rho} \int_S \rho \mathbf{v} \mathrm{d}\mathbf{S} = Q$$

3.2 Mass conservation equation for the three chambers

Continuity equation (3.1) is specialized for each chamber as previously done for the incompressible model. Assuming no deformation of the cylinder containing the oil, the volume of each chamber is found. The negligible effect of cylinder compliance is treated in 3.3.

$$V_{reb} = x_p(t) \cdot (A_p - A_r) \tag{3.3}$$

$$V_{comp} = (L_c - x_p(t)) \cdot A_p \tag{3.4}$$

$$V_{res} = V_{B_0} + V_{g_0} - V_g \tag{3.5}$$

where L_c is the length of the internal cylinder, A_p the piston area, $x_p(t)$ the piston position while the subscript 0 stands for the initial configuration.

$$\beta V_{reb} \frac{\mathrm{d}p_{reb}}{\mathrm{d}t} + v_p(A_p - A_r) + Q_{reb-comp} = 0 \qquad \textbf{Rebound chamber} \tag{3.6}$$

$$\beta V_{comp} \frac{\mathrm{d}p_{comp}}{\mathrm{d}t} - v_p A_p - Q_{reb-comp} + Q_{comp-res} = 0 \qquad \textbf{Compression chamber} \tag{3.7}$$

$$\beta V_{res} \frac{\mathrm{d}p_{res}}{\mathrm{d}t} - \frac{\mathrm{d}V_g}{\mathrm{d}t} - Q_{comp-res} = 0 \qquad \textbf{Reserve chamber} \tag{3.8}$$

The equation for the gas chamber is the same used in the incompressible model (2.8). The presence of the compressibility term produces a system of *ordinary differential equations* (ODE).

Conceptually, the time derivative term brakes up the relation which bounds volume variation and volumetric flux. The compressibility introduces a time delay between the cause (volume variation) and the expected effect (volumetric flux).

Again, a parallel with a spring-damper system is possible: while in the incompressible formulation the oil is an infinitely stiff element, assuming a non-zero compressibility means admitting a finite value of stiffness for the damper medium. In particular, the oil behaves like a spring which stores and then release flow at the successive instant.

3.2.1 Compressibility influence on characteristic diagrams

On the basis of the same geometrical input used for the incompressible version (Table 4.1), the compressibility effect is analysed by varying the isothermal compressibility factor β. Figure 3.1 depicts the effects of compressibility for strokes characterized by low forces. The low forces are the direct consequence of the limited pressure differential between chamber. This is the reason why the compressibility effect is not appreciated and F-V diagrams seems to have nearly the same trend.
However, the compressibility is not negligible when the pressures (and forces) rise up.

Table 3.1: Value of compressibility used to highlight compressibility effect

Frequency f $= 1$ [Hz]						
β	0	$2.5 \cdot 10^{-9}$	$2.5 \cdot 10^{-10}$	$2.5 \cdot 10^{-8}$	$1.5 \cdot 10^{-8}$	$1.5 \cdot 10^{-6}$

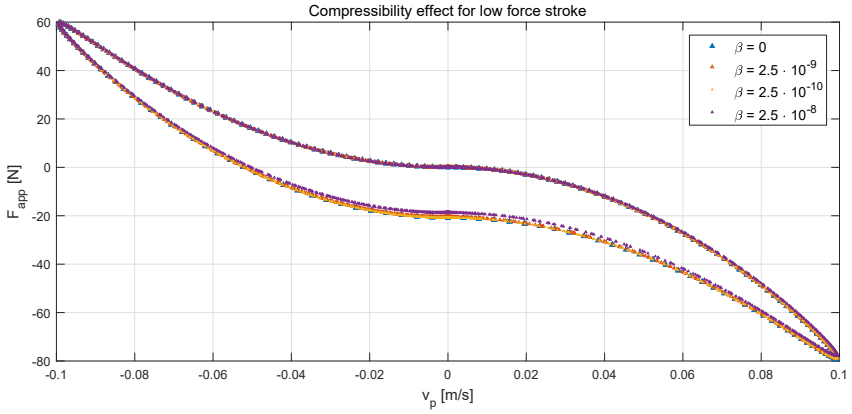

(a) *Hysteresis at low forces*

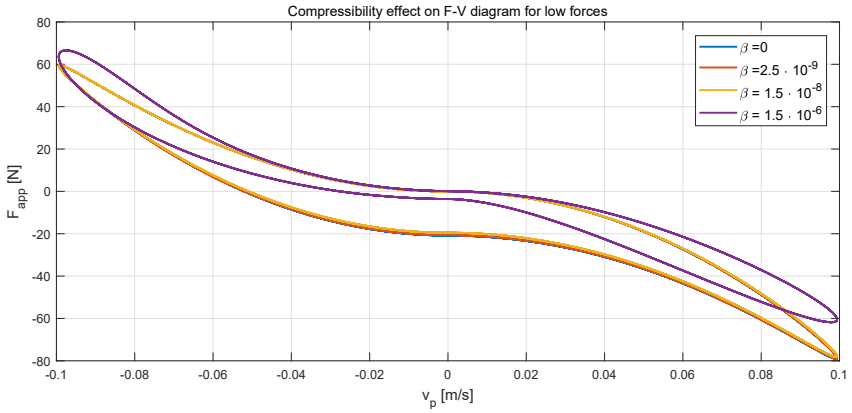

(b) *Hysteresis at low forces for higher value of β*

Figure 3.1: Hysteresis effect due to compressibility at frequency 1 Hz

What is more correct to say is that hysteresis becomes important in the range where $\frac{\mathrm{d}F}{\mathrm{d}v}$ is high.

The forces acting on the piston depends strictly on the geometry of the twin tube damper once the damper oil has been chosen. There are two main ways to get higher forces:

- Increasing the stroke frequency f;
- Working on the valve assembly, by varying the orifice diameters and/or inserting blow-off valves;

The first solution seems to be appropriate to emphasize the compressibility effect; in fact, maintaining the same geometry used in Table 4.1 a comparison with the incompressible model can be made. For further analysis, a more complex system valve will be introduced.

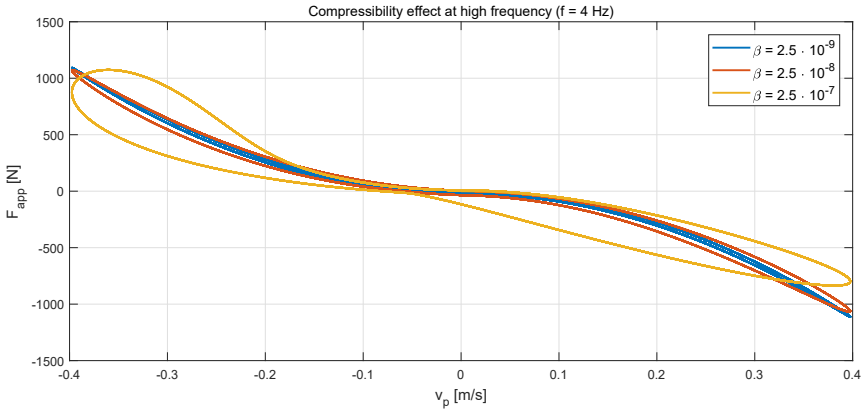

Figure 3.2: Compressibility effect at high frequency (f = 4 Hz)

As announced, high forces lead to large hysteresis as shown in Figure 3.2. In brief, the oil compressibility adds another non-linearity to the damper which needs to be considered.

3.2.2 Mass flow through orifices

In Figure 3.3, it is reported the mass flow rate through the orifices by varying the compressibility of the damper medium. The convention used for the flow sign is as following:

- $Q_{reb-comp}$ is assumed positive if the volumetric flow is from the rebound to the compression chamber;
- $Q_{comp-res}$ is assumed positive if the volumetric flow is from the compression to the reserve chamber;

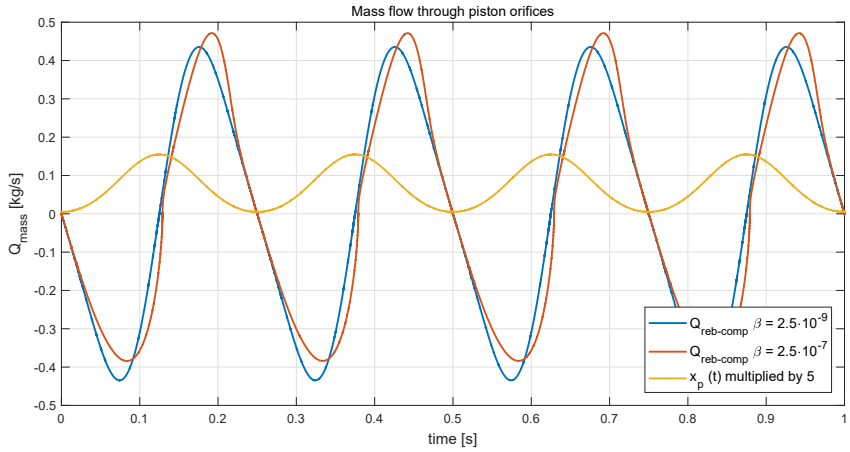

(a) *Comparison of mass flow through piston orifices for different* β

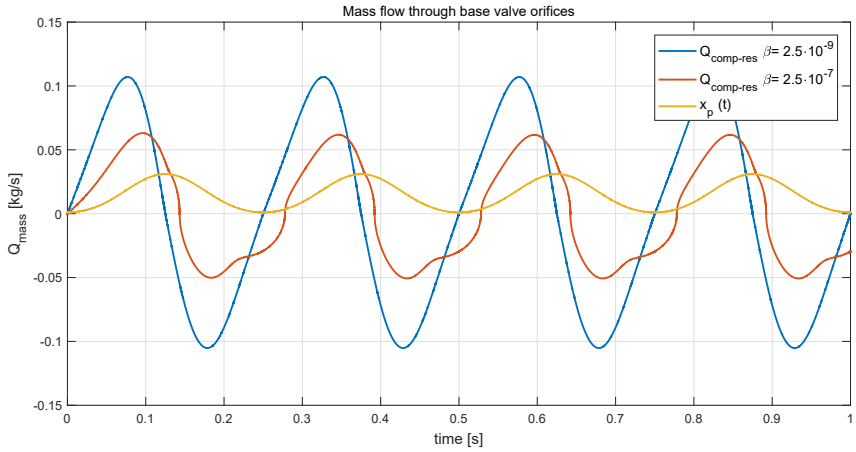

(b) *Comparison of mass flow through base valve orifices for different* β

Figure 3.3: Comparison of mass flow through orifices for different β at excitation frequency f= 4 Hz

It is possible nothing that when the compressibility effect is negligible (also meaning pressure variations not too high), the mass flow through orifices has a harmonic trend. In this case ($\beta = 2.5 \cdot 10^{-9}$ for Figure 3.3a), the mass flow rate directly depends on piston position and velocity.

For example, at the maximum extension of the cylinder, no flow through the base and the piston valve may occur in the incompressible assumption.
The more the compressibility is magnified the more the retarding effect takes place. In fact, considering again the fully extended condition but $\beta = 2.5 \cdot 10^{-7}$ we see that the flow through the base valve has still a positive value.

On the whole, a compressible medium stores and releases volumetric flow modifying the amount of oil flowing through the orifices. In Figure 3.3b), the compressibility causes

the mass flow rate through the base valve to reduce. The alteration of the mass flows changes the pressure field established in the chambers.

In general, increasing the compressibility factor β, the mean pressure in each chamber reduces (this fact explains why violet curve in Figure 3.1 shows less hysteresis in the range where $v_p \approx 0\ \mathrm{m\,s^{-1}}$).

3.3 Compliance of the cylinder wall

The pressure established in the working chamber may lead to a deformation of the cylinder walls. For a cylinder of inner radius R_i and outer radius R_e the compliance of the cylinder can be expressed according to [2], [1]:

$$\beta_c = \frac{2}{E}\left(\frac{R_i^2 + R_e^2}{R_e^2 - R_i^2} + \nu\right) \tag{3.9}$$

where ν denotes the Poisson's coefficient. The volume of the generic chamber can be written:

$$V_{i_{th}} = V_{0_{ith}}(1 + \beta_c \Delta p) \tag{3.10}$$

where Δp denotes the difference with respect to a reference pressure. In the following sections is investigated the influence of cylinder deformation due to pressure and its order of magnitude.

3.3.1 Another expression for cylinder compliance

In [19] the wall contribution to the volume change coming from the elastic strain of the cylinder is derived in this way. Expanding using a Taylor series around the inner diameter of the cylinder D_i, the internal area cross section change A_{cyl} can be evaluated:

$$A_{cyl} + \Delta A_{cyl} = \frac{\pi}{4}\left(D_i^2 + 2D_i \Delta D_i + \Delta D_i^2\right) \tag{3.11}$$

Indicating with U the circumference and multiplying by the length of the cylinder L, the volume variation follows:

$$\Delta V_{cyl} = \frac{\Delta U}{\pi}\left(2D_i + \frac{\Delta U}{\pi}\right)\frac{\pi}{4}L \tag{3.12}$$

where ΔU is the circumference variation. Neglecting terms superior to the second order:

$$\Delta V_{cyl} = \frac{\Delta U}{2} D_i L \tag{3.13}$$

Introducing the strain and Young's modulus

$$\varepsilon = \frac{\Delta U}{U} \qquad E = \frac{\sigma}{\varepsilon} \tag{3.14}$$

together with the tension in longitudinal direction:

$$\sigma = p\frac{D_i}{D_e - D_i} \tag{3.15}$$

where D_e corresponds to the external diameter. The expression for ΔU can be found:

$$\Delta U = \Delta p \pi \frac{D_i^2}{(D_e - D_i)\, E} \tag{3.16}$$

Combining (3.16) and (3.13) the volume variation is:

$$\Delta V_{cyl} = \frac{\Delta p \pi D_i^3 L}{2\,(D_e - D_i)\, E} \tag{3.17}$$

At this point it is possible to define an apparent compressibility factor which accounts for both the compressibility of the medium and the cylinder compliance. From the *bulk modulus* definition we have:

$$K = -V\frac{\mathrm{d}p}{\mathrm{d}V} = \rho\frac{\mathrm{d}p}{\mathrm{d}\rho} = \frac{1}{\beta} \tag{3.18}$$

Using the preceding relations (3.18) and (3.17) the final relation for the damper volume compliance yields:

$$\Delta V_{oil} = \frac{\Delta p V_{oil}}{K} \tag{3.19}$$

where K is the compressibility modulus of the oil.

$$\Delta V_{el} = \frac{\Delta p V_{oil}}{K_{oil}}\left[1 + \frac{V_{cyl}}{V_{oil}}\frac{K_{oil}}{E}\frac{D_i}{D_e - D_i}\right] = \frac{\Delta p V_{oil}}{K_{oil}}\kappa \tag{3.20}$$

In (3.20), κ stands for the dimensionless compression modulus. Making explicit β_c of the cylinder we write:

$$\beta_c = \frac{2}{E}\frac{D_i}{D_e - D_i} \tag{3.21}$$

3.3.2 Analysis of the compliance effect

It is analysed the impact the cylinder deformation has on the solution. Both of the proposed formulation given in (3.3) and (3.3.1) are compared. Assuming the same geometrical set of Table 4.1, the cylinder compressibility factor β_c is easily found.

Table 3.2: Cylinder compressibility factor

$E = 210000$ [N mm^{-2}]	$\boldsymbol{R_e = 0.052}$ [m]	$\boldsymbol{R_i = 0.045}$ [m]
$\boldsymbol{\beta_c}$	$6.947 \cdot 10^{-11}$ (3.3)	$6.122 \cdot 10^{-11}$ (3.3.1)

Dealing with oil which as approximatively $\beta \approx 2.5 \cdot 10^{-9}$, the hypothesis of neglecting the cylinder deformation is explained. Damper external structure is more than two order of magnitude stiffer than the damper medium. Figure 3.4 confirms the assumption made.

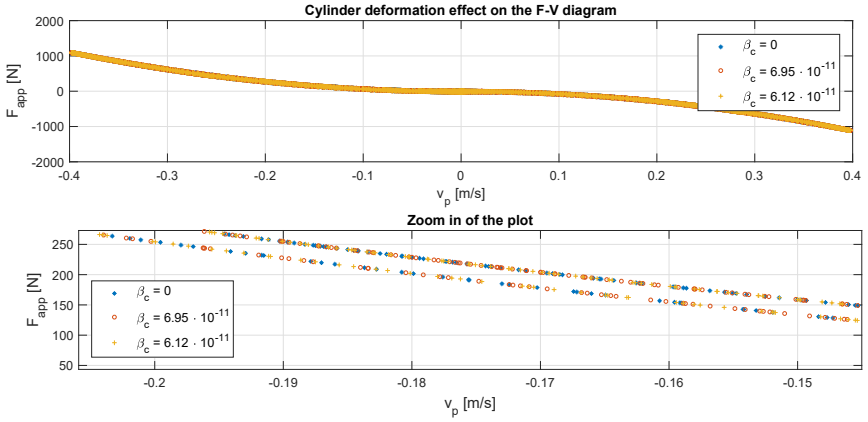

Figure 3.4: Deformation cylinder effect on F-V diagram

3.4 Piston-wall leakage modelling

The simple model introduced in 1.1 is now extended taking into account detailed phenomenologies, such as the leakage between the piston and the cylinder wall. In fact, a thin film of oil has a lubricating role filling the small mechanical backlash present. Otherwise, the damper is likely to seize up.

The leakage between the piston seal and the cylinder wall (Figure 3.5) can be modelled as a flow between two parallel plates [16]. In fact, assuming laminar flow, Navier-Stokes equations can be analytically resolved. By imposing the appropriate boundary conditions (no-slip condition for the inner cylinder and moving wall for the piston wall) the expression for velocity reads:

$$u(y) = \frac{v_p}{b}y - \frac{1}{2\mu}\frac{\mathrm{d}p}{\mathrm{d}x}y(b-y) \tag{3.22}$$

The volume flow rate Q per unit width of the channel is:

$$Q'(\text{per unit width}) = \int_0^b u(y)\,\mathrm{d}y = v_p\frac{b}{2}\left[1 - \frac{b^2}{6\mu v_p}\frac{\mathrm{d}p}{\mathrm{d}x}\right] \tag{3.23}$$

Approximating the pressure derivative with finite difference it is possible to obtain (3.24).

$$Q_{leakage} = \left(\frac{\Delta p b^3}{12\mu l} + \frac{v_p b}{2}\right)\pi D_p \tag{3.24}$$

The term D_p in (3.24) indicates the diameter of the piston, μ the dynamic viscosity while the geometrical parameters b and l represent the clearance between wall and cylinder and the thickness of the cylinder, respectively.

It is important to remind that this Navies-Stokes solution is founded on the assumption of incompressible and parallel flow. The cylinder curvature justifies to treat the flow as locally parallel.
The leakage term appears as a mass flux term in (3.2). Rewriting for instance the mass balance equation for the rebound and the compression chambers:

$$V_{reb}\beta\frac{\mathrm{d}p_{reb}}{\mathrm{d}t} + v_p(A_p - A_r) + Q_{reb-comp} + Q_{leak} = 0 \qquad \textbf{Rebound chamber} \tag{3.25}$$

$$V_{comp}\beta\frac{\mathrm{d}p_{comp}}{\mathrm{d}t} - v_p A_p - Q_{reb-comp} + Q_{comp-res} - Q_{leak} = 0 \qquad \textbf{Compression chamber} \tag{3.26}$$

As expected by adding (3.25) and (3.26), the leakage term vanishes as the mass leaving the rebound chamber is entering the compression chamber and vice-versa.

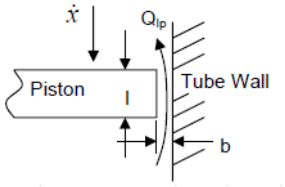

Figure 3.5: Schematic representation of the leakage between wall and cylinder [16]

3.5 A geometrical model with a simplified blow-off valve

The simple geometrical twin tube damper which has the piston and the base valve assembly both based on bleed orifices is now complicated. A blow-off valve is inserted in the piston assembly. It is modelled introducing a pre-charge force (a fixed value below that the valve does not open) and an elastic constant k which defines its spring rate.

Neglecting inertial effects, the progressive opening of the valve can be evaluated by considering a free-body diagram for the blow-off valve.
The static balance of forces acting reads:

$$ky = \Delta p_{valve} A_{valve} + F_{mom} - F_{pre-charge} \tag{3.27}$$

where Δp_{valve} denotes the pressure difference acting across the valve, A_{valve} the area the pressure acts on, F_{mom} the momentum force and $F_{pre-charge}$ the pre-charge force of the equivalent spring. The momentum force, term which often arises in the design of the valve, is equal to $\rho u^2 A_{valve}$. Rearranging (3.27) we have:

$$ky = \Delta p_{valve} A_{valve} + C_{corr} A_{valve} \rho u^2 - F_{pre-charge} \tag{3.28}$$

where C_{corr} is a corrective term because the flow is not completely known near the valve [16]. A blow-off valve is treated as an equivalent spring. In more detail, the valve implemented oppose no flow resistance when $p_{reb} < p_{comp}$ (it behaves like a simple orifice) while the passive self-tuning governed by (3.27) appears when $p_{reb} > p_{comp}$ (predominantly in the rebound movement of the piston).

MATLAB scripts have been implemented in app-designer to create a user-friendly interface which permits to set up the oil properties, the geometrical configuration and the initial conditions.

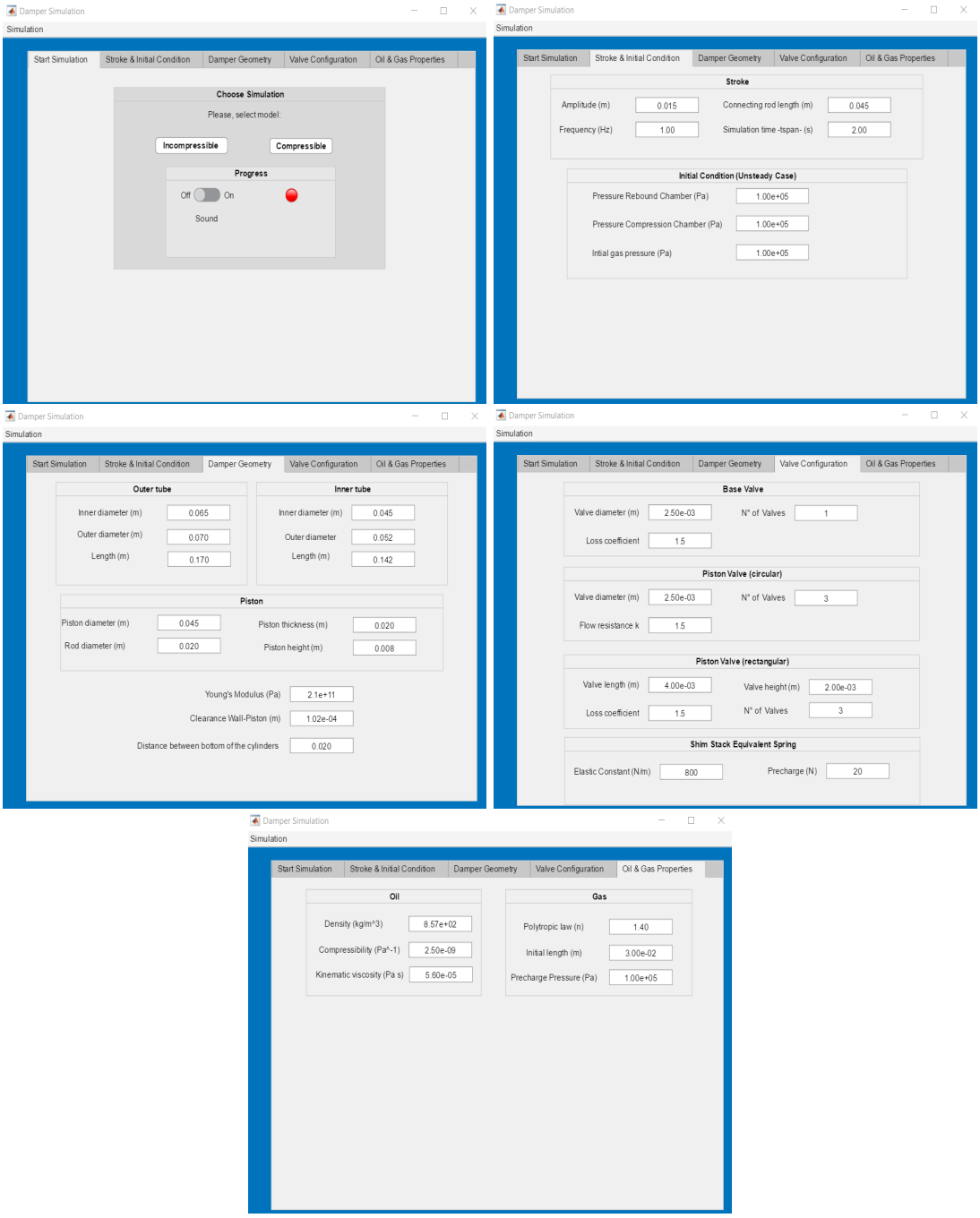

Figure 3.6: Interface implemented in app-designer

3.5.1 The impact of blow-off valve on damper characteristics

The behaviour of the blow-off valve is shown in Figure 3.7 and 3.8. In general, the presence of a valve system creates an asymmetrical response of the damper between compression and rebound phases.
For comfort reasons, the damping force during compression stroke should be small to respect the comfort requirements. If not, a large force force will be transmitted to the passenger compartment.
These constraints reveal two main non-linearities characteristic of a damper:

- The first non linearity appears approximatively at zero velocity due to the asymmetrical configuration;
- The second non linearity arises at medium-high velocity when the forces acting on the blow-off valve (or system) are enough to open completely the orifice;

Figure 3.7 and 3.8 show the typical trends for the characteristic diagrams. The level of forces can be adequately set choosing an appropriate geometrical configuration.

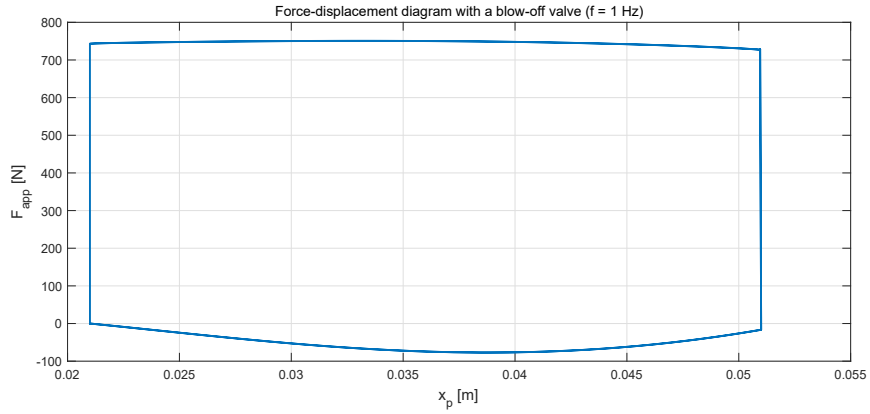

Figure 3.7: Force displacement diagram for excitation frequency 1 Hz, $k = 800\ \mathrm{N\,m^{-1}}$ and $\mathrm{F_{pre\text{-}charge}}$=20 N

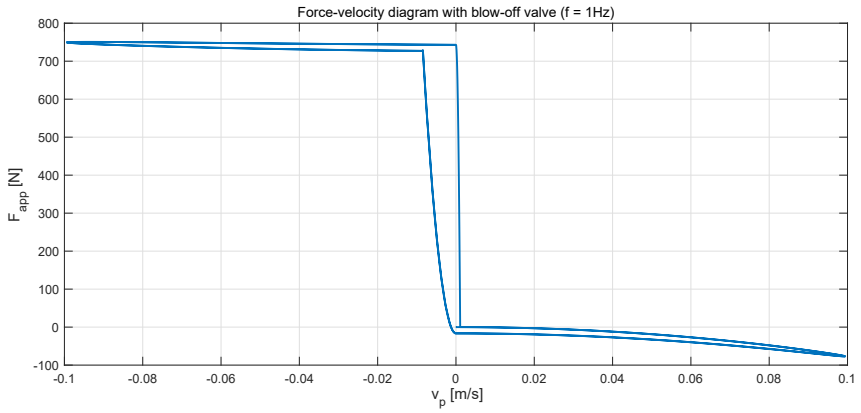

Figure 3.8: Force velocity diagram for excitation frequency 1 Hz, $k = 800\ \mathrm{N\,m^{-1}}$ and $\mathrm{F_{pre\text{-}charge}}$=20 N

The twin tube damper changes deeply its property with the insertion of a simple blow-off valve system. The non linearities mentioned above suddenly manifest; at the same time the compressibility effect is magnified by the high level of pressure caused by the blow-off valve.

A brief parameter study is done to understand the impact of the blow-off system on pressure establishes in chambers. The geometrical configuration used is reported in Table 3.3

Table 3.3: Geometrical configuration for parameter study

Data Geometry	
$\boldsymbol{A_p}$ [m^2]	$1.59{\cdot}10^{-3}$
$\boldsymbol{A_r}$ [m^2]	$3.14{\cdot}10^{-4}$
N° piston orifices	3
Diameter piston orifice [m]	$2.50{\cdot}10^{-3}$
N° base valve orifices	1
Diameter base valve orifice [m]	$2.50{\cdot}10^{-3}$
$\boldsymbol{L_{c_{in}}}$ [m]	$1.43{\cdot}10^{-1}$
$\boldsymbol{\gamma}$ **(specific heat ratio)**	1.4
$\boldsymbol{p_{g_0}}$ [Pa]	$1.00{\cdot}10^{5}$
$\boldsymbol{V_{g_0}}$ [m^3]	$3.58{\cdot}10^{-5}$

Compressibility effect: further comments

In Table 3.4 are listed the pair of values of compressibility factor used to underline, again, the compressibility effect. One corresponds to the typical value for the oil, while the other to that of an incompressible medium. The hysteresis phenomena is magnified by the blow-off valve.
The most interested area is the one located at damping force level between 0 N and 800 N on the rebound phase (when the blow-off controlling system is active).
Defining the damping stiffness as:

$$\frac{\mathrm{d}F_D}{\mathrm{d}v} \tag{3.29}$$

Hysteresis is clearly visible when damping stiffness reaches high values.
Considering that:

$$\frac{\mathrm{d}F_D}{\mathrm{d}t} \propto \frac{\mathrm{d}p}{\mathrm{d}t}$$

which can be rewritten as:

$$a\frac{\mathrm{d}F_D}{\mathrm{d}v} \propto \frac{\mathrm{d}p}{\mathrm{d}t}A_{ref} \tag{3.30}$$

In (3.30), a denotes the acceleration of the piston rod. We note that both the acceleration and the pressure derivative in time are especially high in the range of zero velocity of the piston.
Moreover, when the damping constant is important, also the term multiplied by the isothermal compressibility factor β in the continuity equation 3.1 gets high values.
Introducing the so called *elastic flow*:

$$Q_{elastic} = \frac{\mathrm{d}p}{\mathrm{d}t}V_{oil}\beta \tag{3.31}$$

However, even for low acceleration and damping stiffness the force-velocity diagram for a dynamic case may differ from a static one. The deviation takes birth in the difference of the pressurized volume between compression and rebound stroke.

Table 3.4: Value of β used to show compressibility effect

$\boldsymbol{k = 800}$ [N m^{-1}]	$\mathbf{F}_{\boldsymbol{precharge}} \boldsymbol{= 20}$ [N]	**f**= 1 [Hz]
$\boldsymbol{\beta}$ [Pa $^{-1}$]	$2.50 \cdot 10^{-9}$	$2.50{\cdot}10^{-11}$

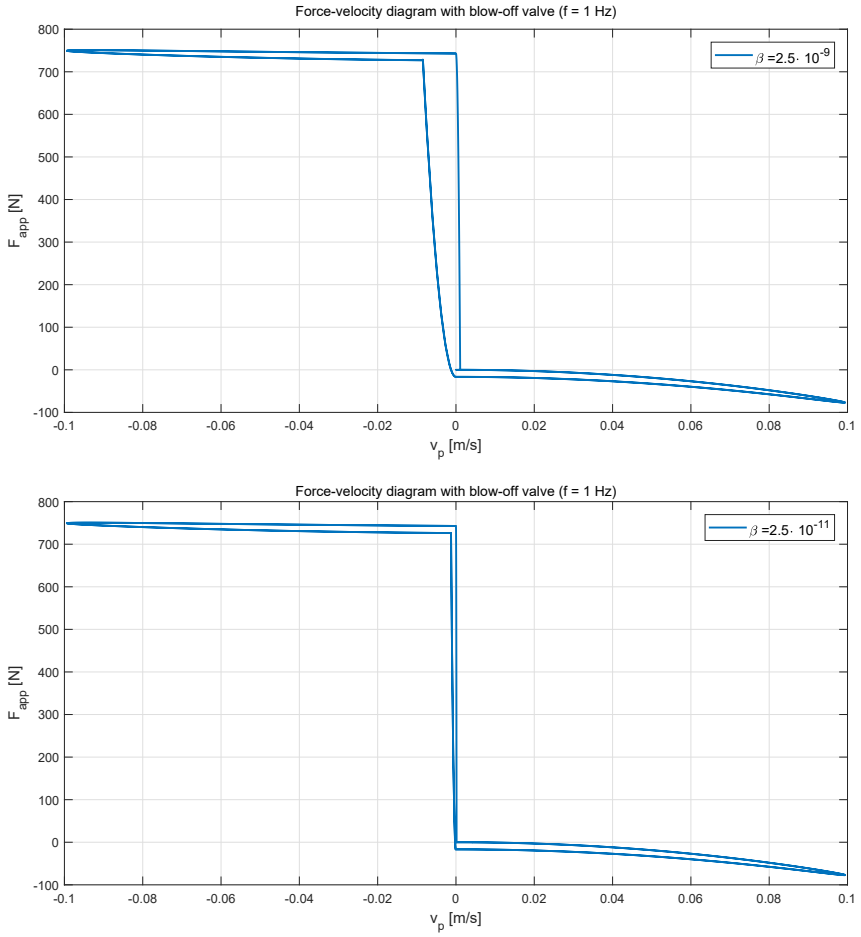

Figure 3.9: Hysteresis effect due to compressibility magnified by blow-off valve

Blow-off stiffness effect

Table 3.5 reports the values of spring stiffness varied in the parameter study. What emerges from the force-displacement (Figure 3.10) diagram is that increasing the stiffness of the equivalent spring brings to slightly higher damping forces. In fact, during rebound, the force-displacement curve assumes a trend which can resemble a parabolic one.

This behaviour is confirmed in the F-V diagram reported in Figure 3.11: the stiffer spring changes the slope of the F-V curve. As a matter of fact, the derivative of a parabolic function (which resembles the trend of the F-X curve in 3.10) is a linear one (as seen in 3.11).

Table 3.5: Blow-off equivalent effect on damper properties

$\boldsymbol{\beta = 2.5 \cdot 10^{-9}}$ [Pa $^{-1}$]	$\mathbf{F}_{precharge} = \mathbf{20}$ [N]	**f**= 1 [Hz]	
$\boldsymbol{k}$ [N m^{-1}]	80	800	10000

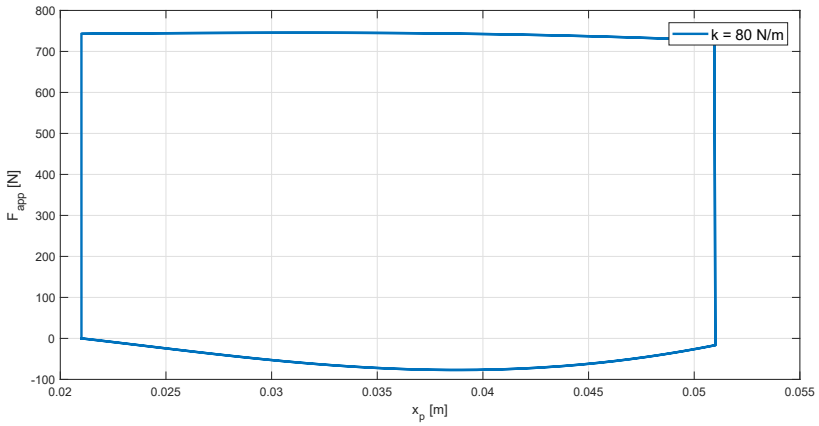

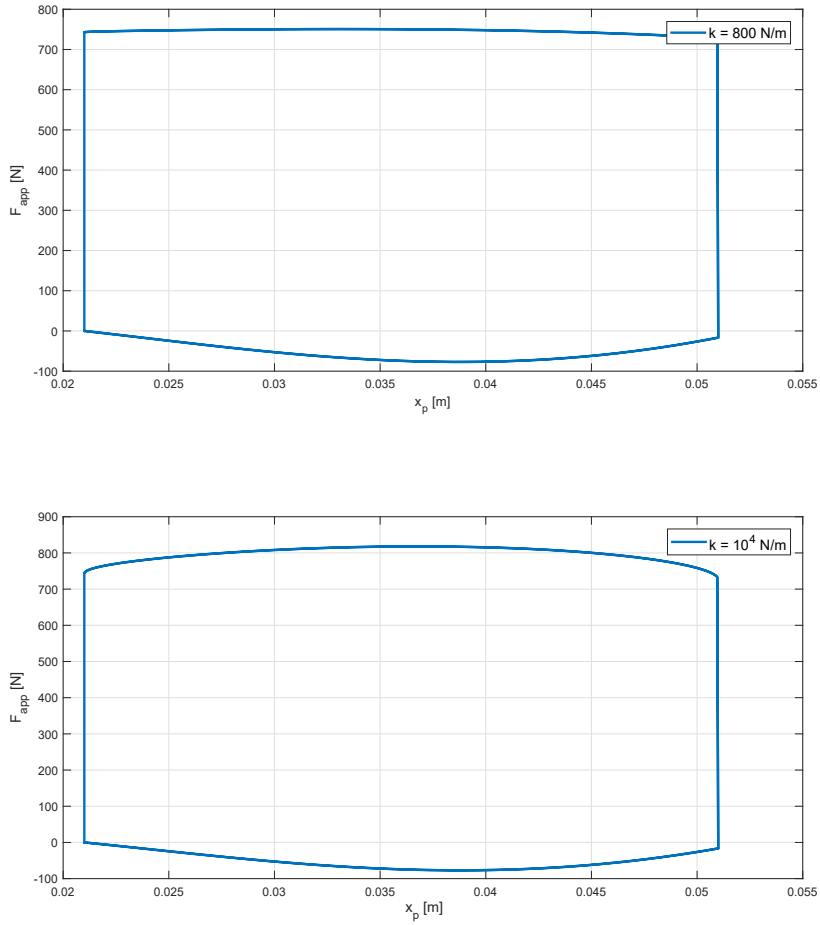

Figure 3.10: Force-displacement diagram for different k

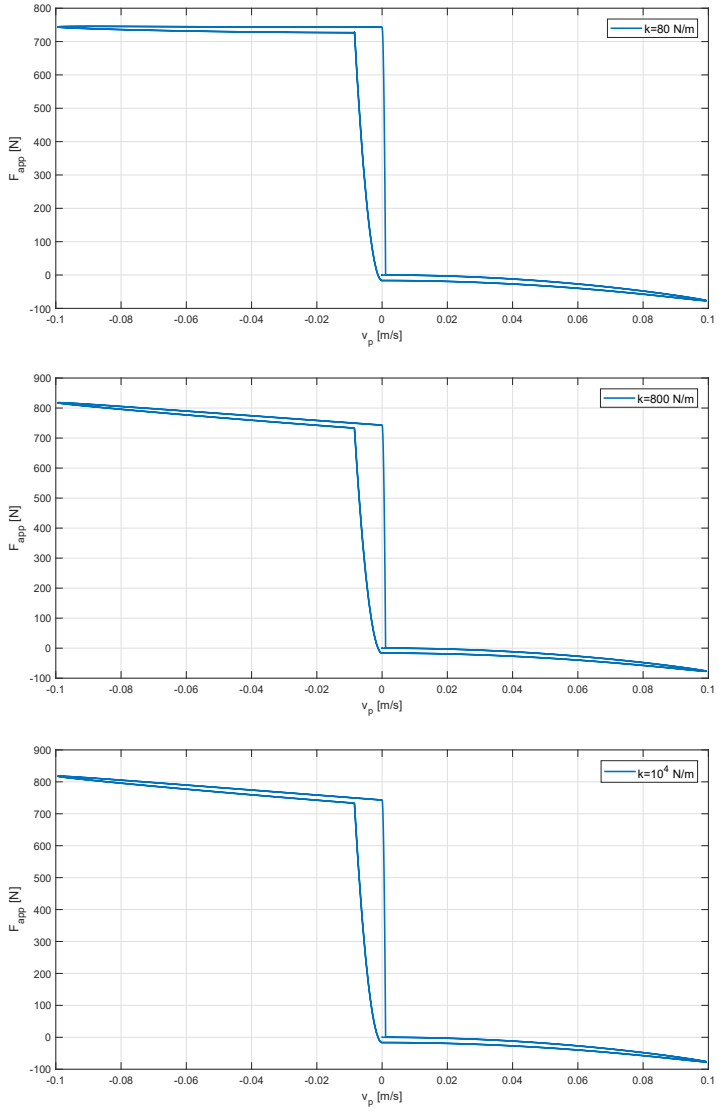

Figure 3.11: Force-velocity diagram for $k = 80$, 800 and 10^4 N/m

Pre-charge force effect

The pre-charge force $F_{pre-charge}$ defines the pressure differential between the rebound and the compression chamber necessary to open the blow-off valve. According to (3.28), the equivalent spring rate k has a role only when the valve begins to open.

In the simplified model implemented, by doubling the pre-charge force, also the maximum force detected in the rebound stroke doubles. The behaviour is appreciated in Figure 3.12.

Table 3.6: Input parameters to show the pre-load force effect

$\boldsymbol{\beta = 2.5 \cdot 10^{-9}}$ [Pa $^{-1}$]	$\mathbf{f} = 1$ [Hz]	$\mathbf{k}$= 800 [N m^{-1}]	$\boldsymbol{F_{precharge}}$**= 40** [N]

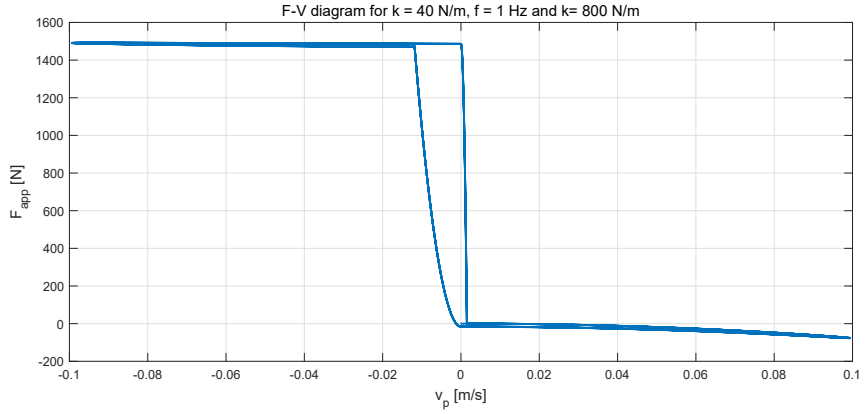

Figure 3.12: Force-velocity diagram for $F_{precharge} = 40$ N

Wall-cylinder leakage effect

Equation (3.24) implies a non-zero mass flow through the piston valve also when the pressure differential $\Delta p = 0$. In fact, a term depending only on the piston velocity is present. The presence of the leakage strongly modifies F-V diagram in the range of low velocity v_p.

When the piston velocity is relatively high, the wall-leakage contribution is negligible because the high pressure differentials lead to high flow rates. In Figure 3.13, it is possible to take view of the different slope in the rebound phase near zero velocity.

Table 3.7: Value of cylinder-wall gap simulated in the compressible model

$\boldsymbol{\beta = 2.5 \cdot 10^{-9}}$	**f= 1** [Hz]	**k= 800** [N m^{-1}]	$\boldsymbol{F_{precharge} = 20}$ [N]
Piston-wall gap [m]	$1.016{\cdot}10^{-4}$	$5.16{\cdot}10^{-5}$	$1.516{\cdot}10^{-4}$

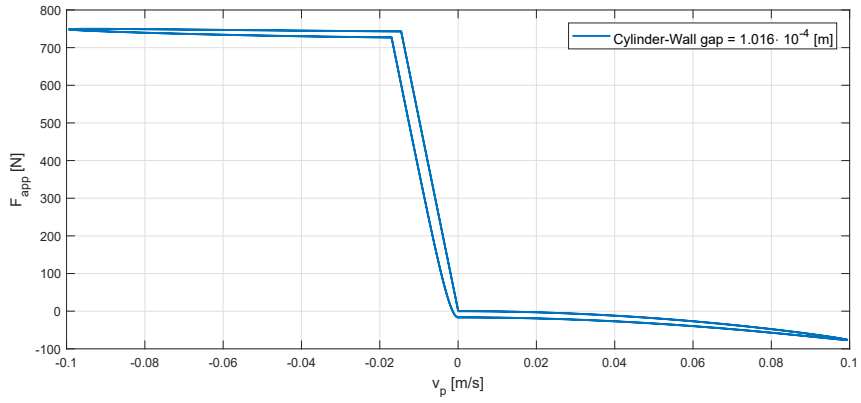

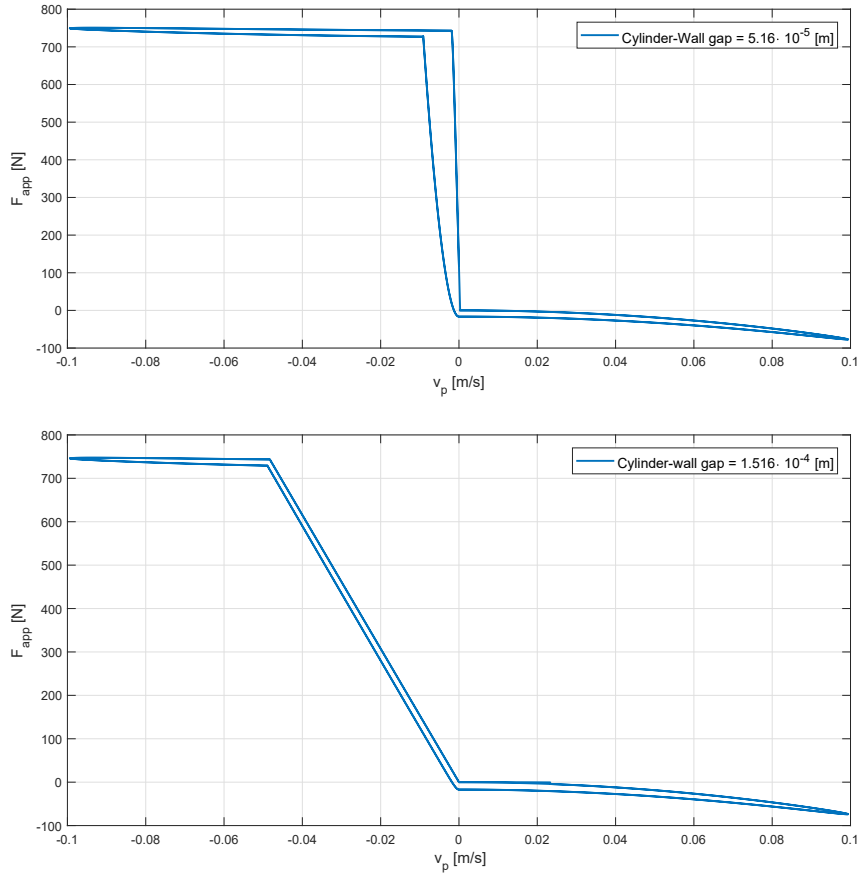

Figure 3.13: Force-velocity diagram for cylinder-wall gap listed in Table 3.7

3.5.2 Summary of the phenomenology appreciated

In the previous sections, several effects have been discussed separately. In general, in analysing the behaviour of a twin tube damper, all the below characteristics should be taken into account:

- Initial gas volume;
- Compressibility of damper medium;
- Piston-wall leakage;
- Geometry configuration of the valve system:
  1. Type of valves (i.e. simple orifices or blow-off valves);
  2. Equivalent spring rate of the blow-off valve;
  3. Pre-charge force of the blow-off valve;
- The cylinder compliance is in general negligible but can be taken into account depending on boundary conditions.

Figure 3.14 summarizes the mentioned aspects in typical F-X and F-V diagram.

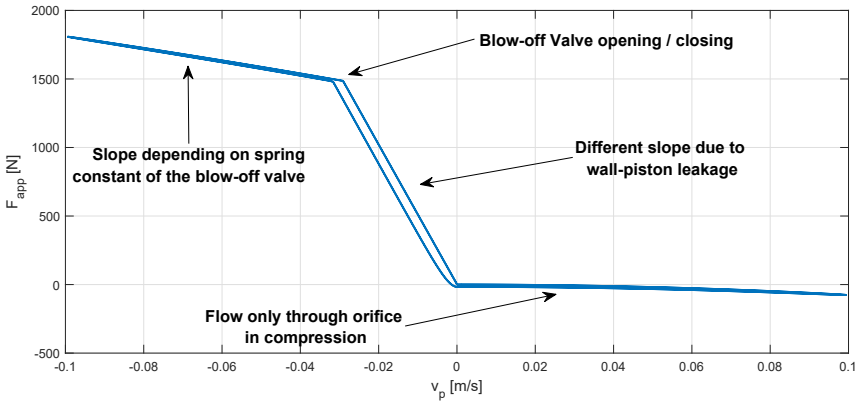

(a) *F-V diagram*

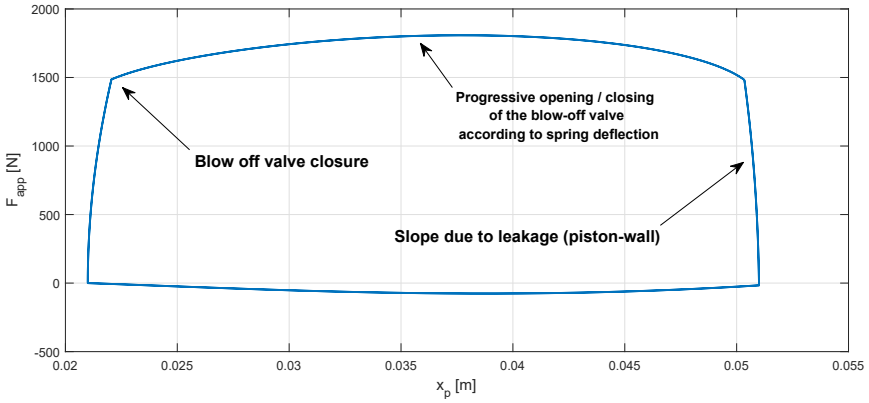

(b) *F-X diagram*

Figure 3.14: Characteristic diagram for a typical twin tube with blow-off valve

Chapter 4

A simplified non-caviting twin tube for experimental testing

The aim of the chapter is to define a simple twin tube damper configuration which meets two main requirements:

- Preventing cavitation phenomena inside the chambers;
- Achieving high forces, in particular in the rebound movement that can be measured by the test equipment;

The geometrical model has a reference geometry specified in Table 4.1.

Table 4.1: Geometry configuration for incompressible model

Data Geometry	
$\boldsymbol{A_p}$ [m^2]	$1.590 \cdot 10^{-3}$
$\boldsymbol{A_r}$ [m^2]	$3.142 \cdot 10^{-4}$
$\boldsymbol{L_{c_{in}}}$ [m]	$1.425 \cdot 10^{-1}$
$\boldsymbol{\gamma}$ **(specific heat ratio)**	1.4
$\boldsymbol{p_{g0}}$ [Pa]	$1.00 \cdot 10^5$
$\boldsymbol{V_{g0}}$ [m^3]	$3.584 \cdot 10^{-5}$

4.1 Orifices geometry analysis

The damper has no blow-off valves, so that only orifice diameters are the parameters of study. Prior to proceed further, the impact of orifice dimensions on pressure distribution is analysed. Reminding the govern equation for orifices 1.26 on page 12, it is possible to write:

$$Q \propto C_d A_{orifice} \sqrt{\Delta p} \tag{4.1}$$

The same value of flow rate requires an higher pressure drop for smaller orifices area $A_{orifice}$.

4.1.1 Piston orifices

The piston orifice role should be analysed distinguishing between rebound and compression phase.

Compression phase In the compression phase, the rebound chamber tends to expand. As a consequence, a pressure decrease is observed in the rebound chamber in the first phase. A wider orifice diameter in the piston permits the pressure not to drop below the vapour pressure value. According to 4.1, a larger flowing area limits the pressure drop on the rebound chamber. An example is reported in Figure 4.1.
However, enlarging the piston orifices cause a force decrease in the rebound movement. In fact, this operation limits the pressure drop across chambers.

Rebound phase The rebound phase is not critical for the rebound chamber as the oil is compressed by the piston. A drawback of having large orifices in the piston valve is the reduced rebound force, as already mentioned.

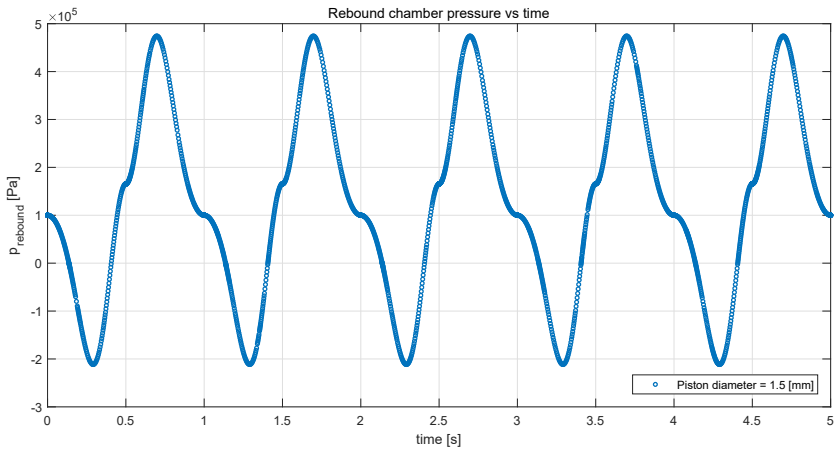

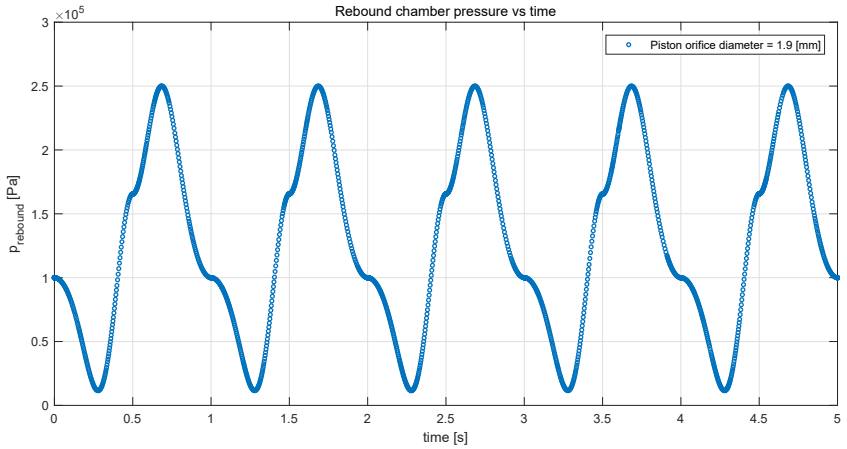

Figure 4.1: Rebound chamber pressure for two diameters of the piston orifices

4.1.2 Base valve orifices

The base valve orifice area has an important impact on the two upper chamber (compression and rebound). It has a direct influence on the compression chamber which in turn interacts with the rebound chamber. To simplify the comprehension, let's consider the incompressible model; rewriting (2.11):

$$v_{comp-res} = \frac{v_p A_r}{\sum A_{fcomp-res}} \tag{4.2}$$

$$v_{reb-comp} = -v_p \frac{A_p - A_r}{\sum A_{freb-comp}} \tag{4.3}$$

It follows that a small base valve orifice produces high velocities and high pressure in the compression compartment. A the same time, the pressure value in the rebound chamber depends on the pressure in the compression chamber and on the velocity of the flow through orifices. Making $p_{rebound}$ explicit, and assuming k_{loss} constant:

$$p_{reb} = p_{res} + \frac{1}{2} k_{loss} \left(\text{sgn}(v_{comp-res}) v_{comp-res}^2 + \text{sgn}(v_{reb-comp}) v_{reb-comp}^2 \right) \tag{4.4}$$

Compression phase Since p_{res} is defined mainly by the piston position [1], in the compression movement p_{reb} can display an increasing or decreasing trend depending on the mutual choice of piston and valve orifices. In fact, in (4.4) $\text{sgn}(v_{reb-comp})$ has a negative value in compression. These two kind of trends are shown in Figure 4.2.

[1] In a compressible model there is a small effect of *elastic flow* Q_{el} while in an incompressible model p_{res} depends only on the piston position.

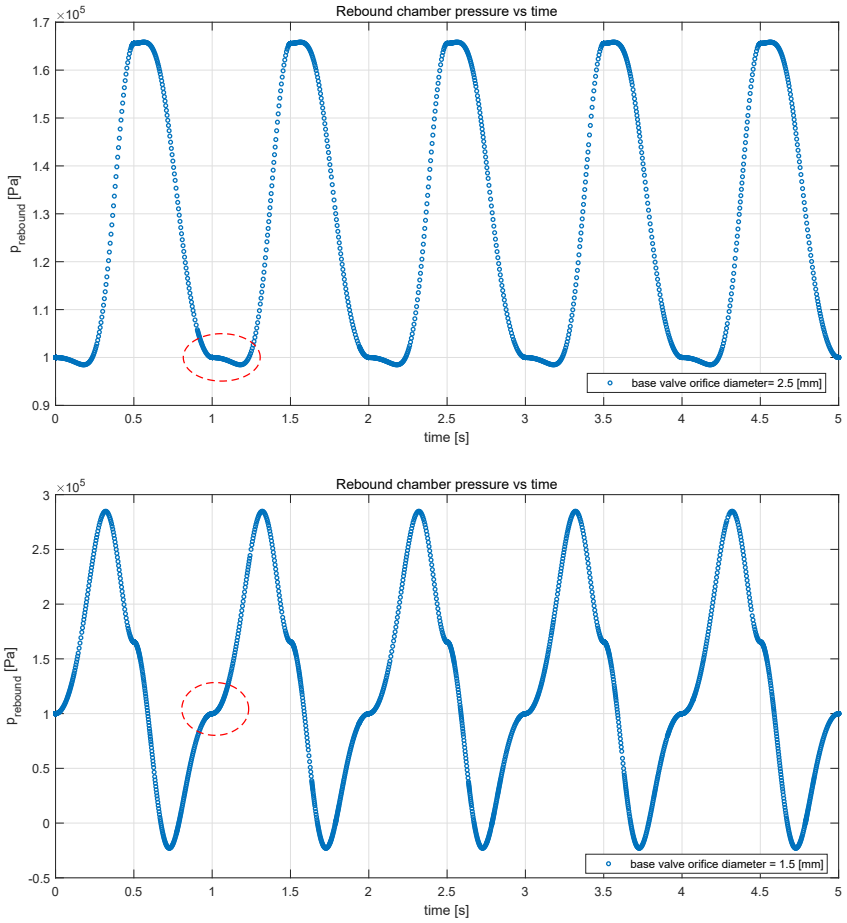

Figure 4.2: Rebound chamber pressure for two diameters of the piston orifices

Rebound phase The rebound phase is critical for the compression chamber. Very small diameters of the base valve can lead to pressure drops too high. For this reason, the most of base valve assemblies operate in different ways in rebound and compression stages.
Accordingly, higher orifice areas are preferable in the rebound phase. Consequence of not selecting the proper area is cavitation as reported in Figure 4.3.

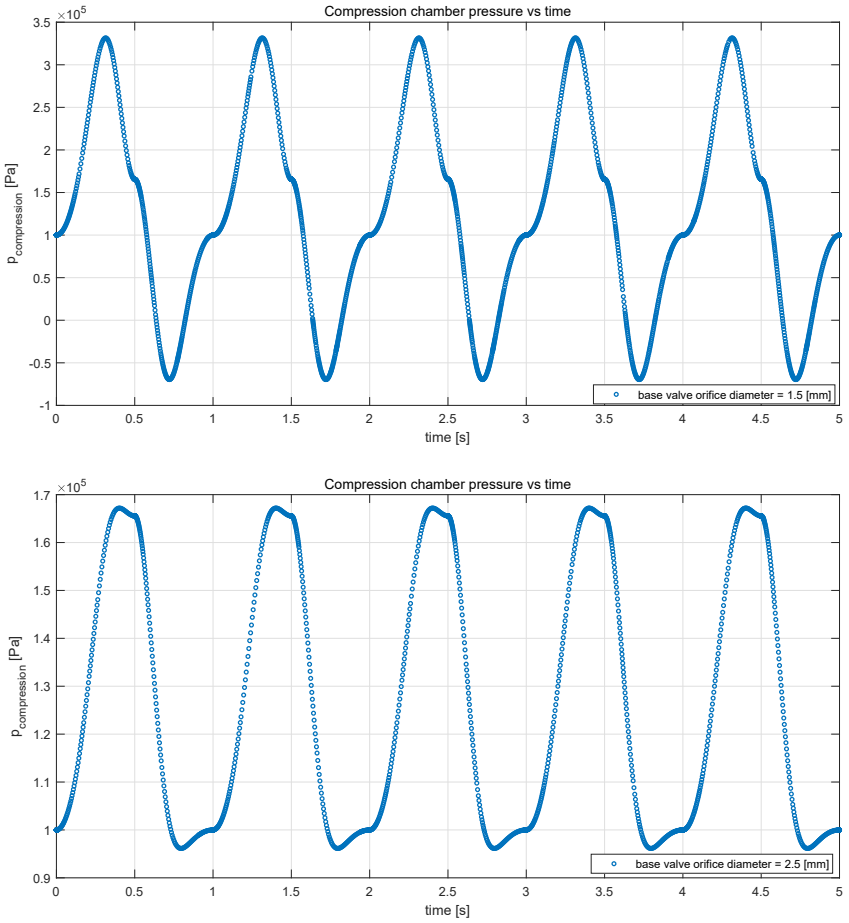

Figure 4.3: Compression chamber pressure for two diameters of the piston orifices, with a condition of cavitation

4.2 Possible configurations for experimental testing

To sum up what explained in the previous section, we have to deal with two main problems:

1. The reduction of piston orifice diameters cause the pressure in the rebound chamber to drop below zero; on the other side, enlarging too much the piston orifices diameters decreases the force;

2. The reduction of the base valve orifice diameters produce higher forces but can trigger cavitation during the rebound movement;

On these basis three configurations are proposed:

- Simple twin tube with fixed-diameter orifices;

- Twin tube with fixed orifices area in compression and reduction of the piston orifice area in rebound;

- Twin tube with fixed orifices area in compression and reduction of 50% of the piston area orifice in rebound;

The optimal configuration is found by running a MATLAB script of the compressible model by varying at each iteration the piston and the base valve orifice areas in the range $A_{search} = 10^{-5} - 10^{-6}$ [m^2]; the limits of the boundary lie in a ratio $\frac{A_{max_{search}}}{A_{min_{search}}} = 10$. The choice of the range has been made considering the absolute size of real-life damper orifices.
Due to time-consuming considerations, the model simulates flow resistance k_{loss} as constant. When the flow is turbulent, the viscous effects are negligible and both C_d and k_{loss} can be assumed as constant:

$$k_{loss} = \frac{1}{C_d^2} \qquad \text{with} \qquad k_{loss_\infty} \approx 2.6874$$

The configuration obtained is then compared to the one in which viscous effect are modelled.

4.2.1 Configuration with fixed orifice

In Table 4.2, the areas found for piston and base valve orifices are reported; also the corresponding number of holes are indicated.

Table 4.2: Orifice configuration for the fixed orifice model

Model with fixed orifice	
$\boldsymbol{F_{max}}$ [N]	341.97
$\boldsymbol{F_{min}}$ [N]	-357.80
$\boldsymbol{P_{min_{reb}}}$ [Pa]	$1.872 \cdot 10^3$
$\boldsymbol{P_{min_{comp}}}$ [Pa]	$2.048 \cdot 10^3$
$\boldsymbol{A_{base}}$ **orifice** [m^2]	$3.020 \cdot 10^{-6}$
$\boldsymbol{A_{piston}}$ **orifice** [m^2]	$8.714 \cdot 10^{-6}$

$\boldsymbol{n^\circ}$ **of holes**	**1**	**2**	**3**	**4**
diameter$_{\boldsymbol{base}}$ **orifice** [mm]	1.96	1.39	1.13	0.98
diameter$_{\boldsymbol{pist}}$ **orifice** [mm]	3.33	2.35	1.92	1.66

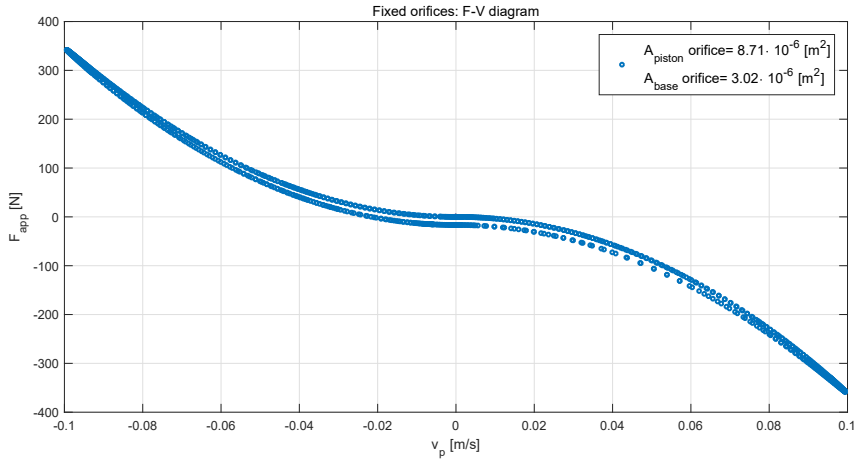

Figure 4.4: F-V diagram for fixed orifice model

4.2.2 Twin tube with 60% reduced piston orifice area in the rebound phase

The second configuration is found by considering three parameters as variables:

- The piston orifice area;
- The base valve orifice area;
- The percentage of closure of piston orifices in the rebound phase;

In the rebound movement, the piston orifices partially close in order to get higher damping forces.

Table 4.3: Orifice configuration for the third orifice model with 50% area reduction in rebound

Model with reduced orifice area in rebound	
$\boldsymbol{F_{max}}$ [N]	$1.987 \cdot 10^3$
$\boldsymbol{F_{min}}$ [N]	$-3.578 \cdot 10^2$
$\boldsymbol{P_{min_{reb}}}$ [Pa]	$1.872 \cdot 10^3$
$\boldsymbol{P_{min_{comp}}}$ [Pa]	$5.349 \cdot 10^3$
$\boldsymbol{A_{base}}$ **orifice** [m^2]	$3.020 \cdot 10^{-6}$
$\boldsymbol{A_{piston}}$ **orifice** [m^2]	$8.714 \cdot 10^{-6}$
% reduction in rebound	60%

$\boldsymbol{n^\circ}$ **of holes**^{2}	**1**	**2**	**3**	**4**
diameter$_{\boldsymbol{base}}$ **orifice** [mm]	-	1.39	-	0.98
diameter$_{\boldsymbol{pist}}$ **orifice** [mm]	-	2.35	-	1.66

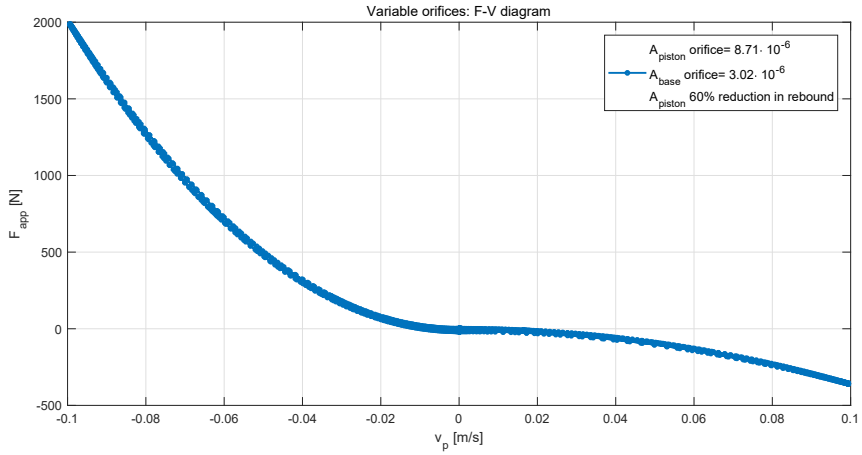

Figure 4.5: F-V diagram with 60% closure of orifice in piston valve in rebound phase

4.2.3 Twin tube with 50% reduced piston area orifice in the rebound phase

The final configuration introduces the constraint that the piston orifice area in rebound is 50% of the value we have in compression. This assumption allows to close half of the orifices in the rebound stage (the number of orifices must be even). The results obtained are reported in Table 4.4.

Table 4.4: Orifice configuration for the third orifice model with 50% area reduction in rebound

Model with fixed orifice	
$\boldsymbol{F_{max}}$ [N]	$1.280 \cdot 10^3$
$\boldsymbol{F_{min}}$ [N]	$-3.578 \cdot 10^2$
$\boldsymbol{P_{min_{reb}}}$ [Pa]	$1.872 \cdot 10^3$
$\boldsymbol{P_{min_{comp}}}$ [Pa]	$3.972 \cdot 10^3$
$\boldsymbol{A_{base}}$ **orifice** [m^2]	$3.020 \cdot 10^{-6}$
$\boldsymbol{A_{piston}}$ **orifice** [m^2]	$8.714 \cdot 10^{-6}$
% reduction in rebound	50%

$\boldsymbol{n}$**° of holes**	**1**	**2**	**3**	**4**
diameter$_{\boldsymbol{base}}$ **orifice** [mm]	-	1.39	-	0.98
diameter$_{\boldsymbol{pist}}$ **orifice** [mm]	-	2.35	-	1.66

[2]The system should be configured to allow 60% reduction of area in rebound phase.

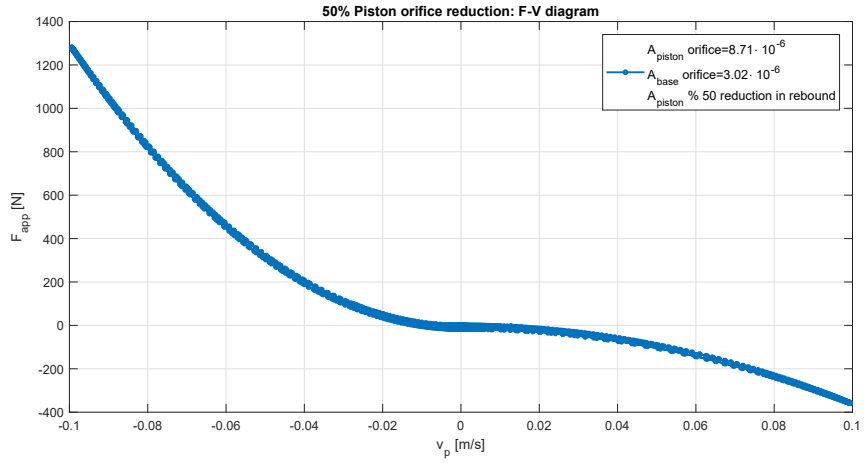

Figure 4.6: F-V diagram with closure of orifice in piston valve in rebound

4.3 Constant k model and Reynolds dependent model comparison

The configuration outlined assuming the flow resistance k_{loss} as constant is now compared with a model in which k_{loss} is function of Reynolds number. The modelling is based on both frictional losses along the channel and concentrated losses as described in 1.7 on page 10. In order to shorten the process of sizing, a first attempt with a simplified model in which Reynolds number has no influence is recommended. Then, a more complicated model in which viscous effects are expressed in function of Reynolds number can be invoked.
As reported in Figure 4.7, 4.9 and 4.8, differences of 5-10% in terms of forces can be seen between the two models.

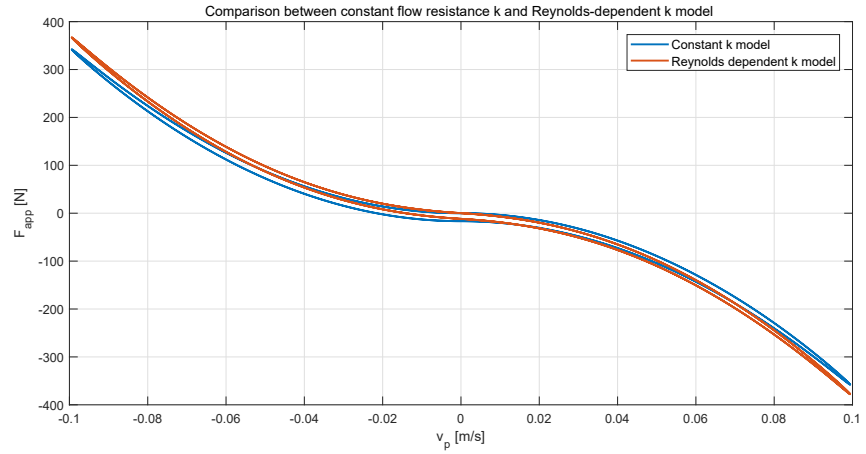

Figure 4.7: Constant k model and Reynolds dependent model for fixed orifice configuration

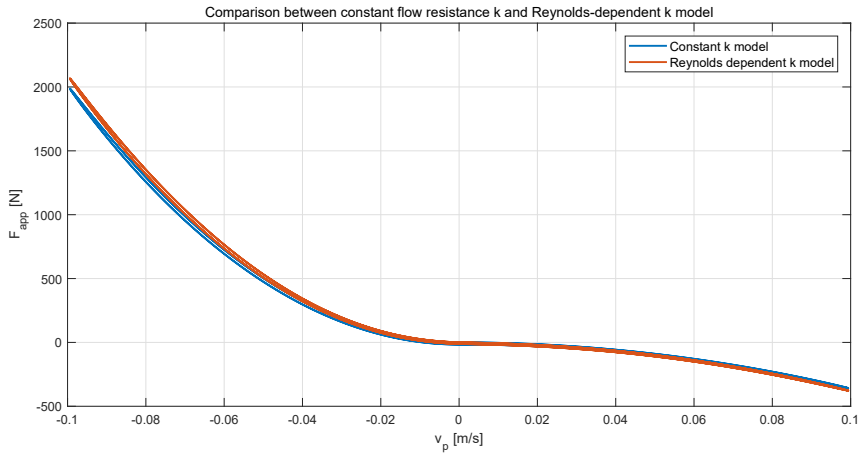

Figure 4.8: Constant k model and Reynolds dependent model with 60% reduction in rebound

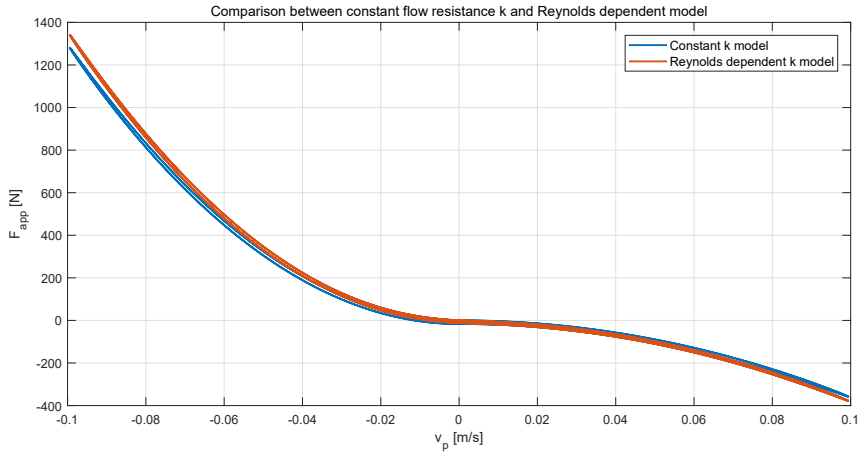

Figure 4.9: Constant k model and Reynolds dependent model with 50% reduction in rebound

Chapter 5

Dynamic behaviour of the damper at high frequency

This chapter treats the dynamical behaviour of a twin tube damper, analysing the response by changing the stroke frequency. Remembering the slider-crank motion discussed in 1.2 on page 6, it is clear that

$$v_{piston} \propto f \tag{5.1}$$

As a consequence, the damping force on the piston gets high with the excitation frequency. At the same time also the damping energy and the spring power increase. In first approximation $F_D \propto f^2$. In an incompressible model, F-V diagram is the same for all frequencies in the region where $v_p = 0$ [m/s].

Some discrepancies begin to appear if the medium is very compressible ($\beta \approx 10^{-8}$). This behaviour is compatible with what seen in Figure 3.3. Even at the beginning of each period where ($p_{rebound} = p_{compression}$), the pressure established depends slightly on the frequency, as underlined in Figure 5.2.

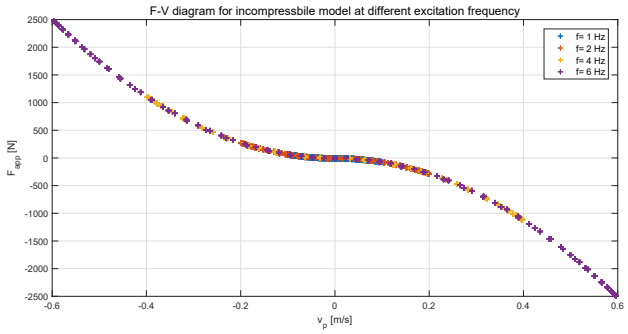

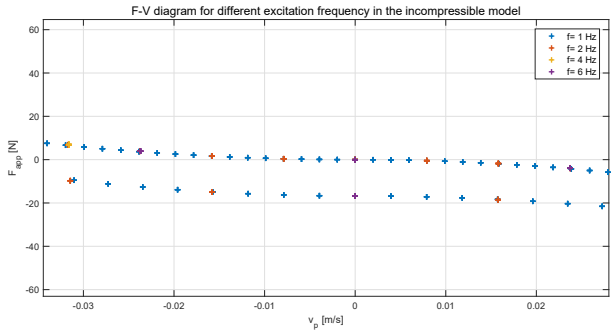

Figure 5.1: Frequency behaviour for incompressible model

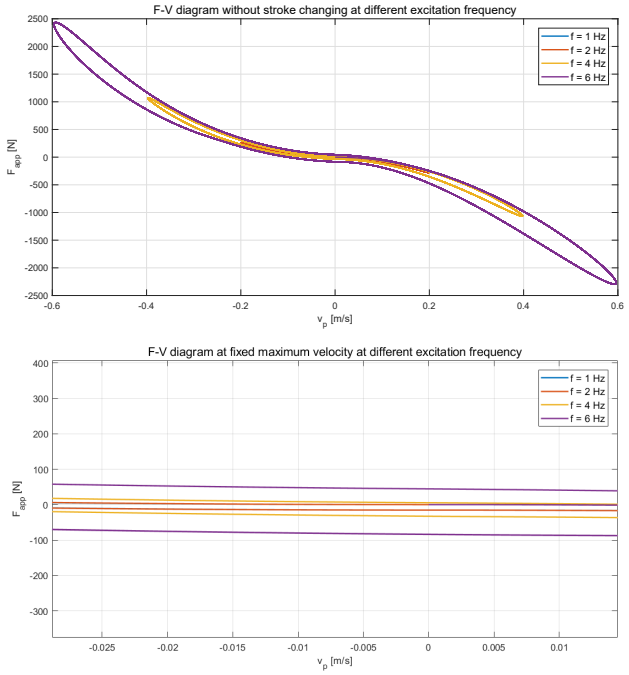

Figure 5.2: Frequency behaviour for compressible model

Another point to underline is that, in the compressible case (assuming the same piston law motion of the incompressible model), the rise of excitation frequency changes the F-V diagram . This result has the following meaning: rising the frequency, the compressibility effects are magnified and the so-called *spring power* gets higher values. Spring power is the area enclosed by F-V diagram and is the symptom of dissipative forces to become less important than spring forces (which are conservative).

5.1 Damping work

According to [19], it is possible to introduce the *damping energy* which is defined as:

$$W_d = \int_0^T F_D \, \mathrm{d}z \tag{5.2}$$

The dynamic behaviour is studied for one maximum excitation velocity by changing the stroke. Increasing the frequency, the damping work done per cycle by the system diminishes. An example is reported in Figure 5.3 for various frequency strokes.

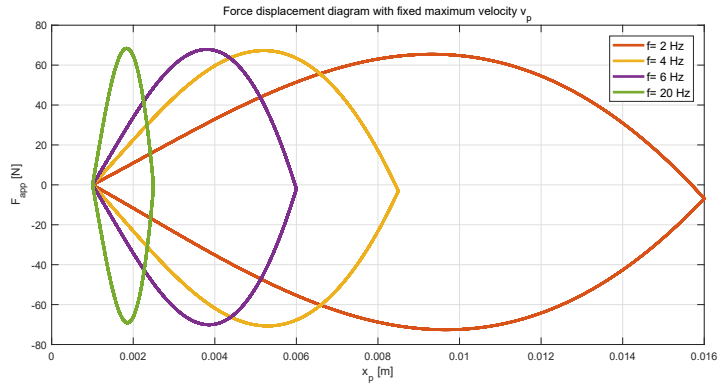

Figure 5.3: Damping work for various frequencies

In order to keep constant the maximum velocity, the stroke is changed according to the rule:

$$\mathrm{amp}' = \frac{\mathrm{amp}}{\mathrm{frequency}} \qquad L' = L \cdot \mathrm{amp}'/\mathrm{amp} \tag{5.3}$$

Modifying the stroke, the damper work (area enclosed in the F-X diagram) diminishes.

5.2 Spring Power

Introducing a new parameter, the so-called *spring power*, which is defined as:

$$P_{sp} = \int_0^T F_D \, \mathrm{d}v \tag{5.4}$$

We notice that it decreases when the frequency rises up and the maximum velocity is maintained; this is the consequence of the new motion law imposed to the piston.

The amplitude of the motion is reduced and the gas spring effect is reduced. In fact, the spring effect is provided both by the gas chamber and the compressibility of the oil. In this case, the important changes in the stroke limit the impact of the gas on hysteresis (visible in the F-V diagram). The unchanged stroke is reported in Figure 5.4a) for 5 cycles. The modified stoke to maintain constant the maximum velocity with frequency is shown in Figure 5.4b).
In Figure 5.6, the hysteresis effect due to the gas compression is plotted for increasing frequencies.

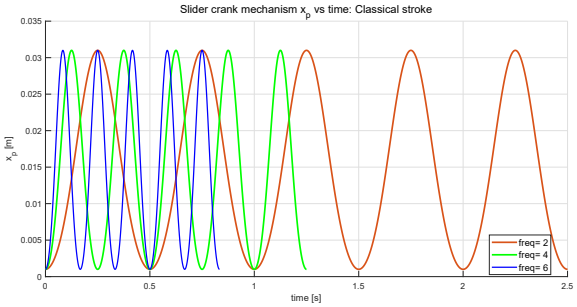

(a) *Classical stroke of the piston for various excitation frequencies (Hz)*

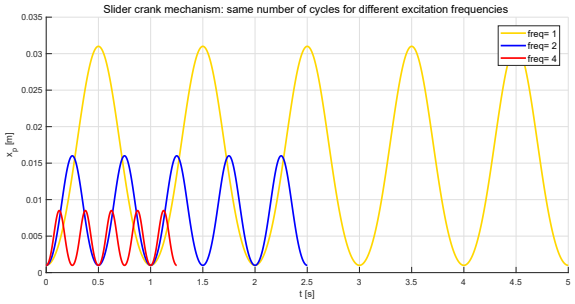

(b) *Stroke of the piston at fixed maximum velocity for different excitation frequencies (Hz)*

Figure 5.4: Stroke of the piston for different excitation frequencies (Hz), for classical stroke (a) and fixed maximum velocity (b)

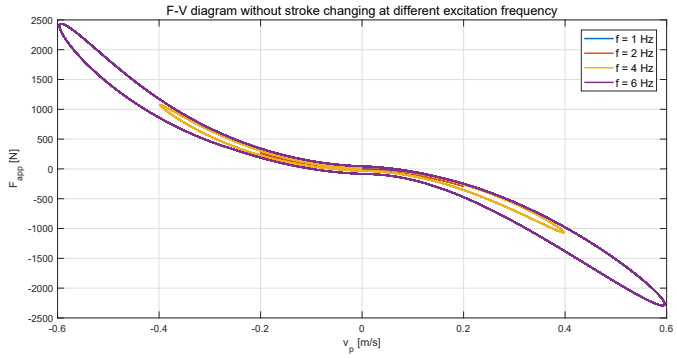

Figure 5.5: F-V diagram without stroke changing for various excitation frequencies [Hz]

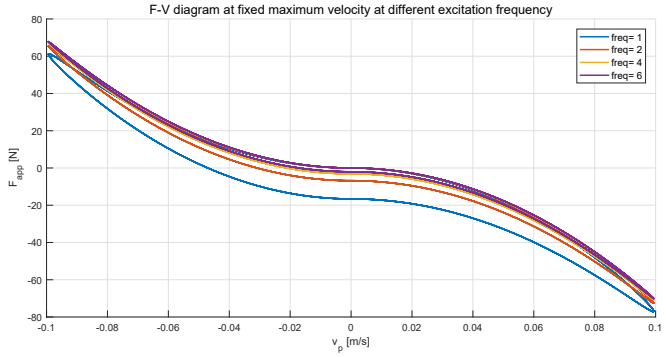

Figure 5.6: F-V diagram at fixed maximum velocity for various excitation frequencies [Hz]

Chapter 6

A compressible and thermal model for a dual tube damper

The purpose of this chapter is to extend the compressible model including the effect of temperature on the system. Therefore, the working fluid equation for density ρ is revisited. Two main models are presented: the first presents the temperatures of each chamber as new variables while the second models also the solid element temperatures such as the ones of inner cylinder, outer cylinder and piston.

The increased number of unknowns requires the energy equation to be involved. Two different ways for fluxes definition has been carried out in order to achieve numerical stability and physical results.

6.1 Thermal working fluid

The thermal model is developed considering the density variation due to pressure and temperature departures from their respective reference values. Reminding the definition of the coefficient of *isothermal compressibility*:

$$\frac{\partial \rho}{\partial p} = \beta \rho \tag{6.1}$$

and of the coefficient of *thermal expansion*:

$$\varphi = -\frac{1}{\rho}\frac{\partial \rho}{\partial T} \tag{6.2}$$

Solving the system in term of density ρ, we can find the dependence on temperature and pressure as:

$$\rho = \rho_0 e^{\beta(p-p_0)-\varphi(T-T_0)} \tag{6.3}$$

where p_0 and T_0 correspond to the pressure and to the temperature of reference. The basic assumptions under which the damper medium properties are modelled are:

$$\beta = constant \quad \varphi = constant \tag{6.4}$$

The density derivative term $\frac{\mathrm{d}\rho}{\mathrm{d}t}$ appearing in the mass conservation equations will lead to new terms which are temperature dependent:

$$\frac{\partial \rho}{\partial t} = \rho\beta\frac{\partial p}{\partial t} - \rho\varphi\frac{\partial T}{\partial t}$$

6.2 Equation of state for gas

The reserve chamber oil is in direct contact with the gas chamber with no physical separation between them. The gas (usually nitrogen) is treated as ideal. The constitutive equation reads:

$$p_g V_g = m_g \frac{R}{M_{mg}} T_g \tag{6.5}$$

The state equation is needed to compute the gas temperature in the thermal model; by the way, the specific heat ratio does not appear on equation. However, assuming no heat flux between parts (solid and fluid ones) the isothermal condition can be reproduced.

6.3 Mass conservation equations for the thermal model

Continuity equation is rewritten for each of the three damper chambers (rebound, compression and reserve). The volume chamber deformation caused by thermal expansion and elastic deformation (due to pressure) has a negligible impact and therefore it is not considered in the proposed model.

For clearness, the following symbols are adopted to refer briefly to each chamber property:

* rebound → E
* compression → C
* reserve → B
* gas → g

The mass conservation equations for the damper configuration analysed are:

$$V_E\left(\frac{\mathrm{d}p_E}{\mathrm{d}t}\beta - \frac{\mathrm{d}T_E}{\mathrm{d}t}\varphi\right) = -v_p(A_p - A_r) - Q_{EC} \tag{6.6}$$

$$V_C\left(\frac{\mathrm{d}p_C}{\mathrm{d}t}\beta - \frac{\mathrm{d}T_C}{\mathrm{d}t}\varphi\right) = vA_p - Q_{BC} + Q_{EC} \tag{6.7}$$

$$V_B\left(\frac{\mathrm{d}p_B}{\mathrm{d}t}\beta - \frac{\mathrm{d}T_B}{\mathrm{d}t}\varphi\right) - \frac{\mathrm{d}V_g}{\mathrm{d}t} = Q_{BC} \tag{6.8}$$

The gas volume variation has a key role also in the energy equation; for clearness, $\frac{\mathrm{d}V_g}{\mathrm{d}t}$ is explained:

$$\frac{\mathrm{d}V_g}{\mathrm{d}t} = m_g \frac{R}{M_{mg}}\left(\frac{p_g\frac{\partial T_g}{\partial t} - T_g\frac{\partial p_g}{\partial t}}{p_g^2}\right) \tag{6.9}$$

6.4 Energy equations

The closure of the system of differential equations needs the energy equation to be taken into account. The general form of the first principle of Thermodynamics takes the form:

$$\frac{\mathrm{d}}{\mathrm{d}t}\int_{V(t)}\rho u \mathrm{d}V = \Phi - \dot{W} \tag{6.10}$$

where Φ denotes the heat flow, u the internal energy of the fluid and $\dot{W}$ the power the system interchange with the environment, assuming as positive the work (or power if derived in time) done by the system on the external.

Expression (6.10) is equivalent to the following in which the total derivative has been expanded in the eulerian time derivative and convection term:

$$\frac{\partial}{\partial t}\int_{V(t)}(\rho E)\mathrm{d}V + \int_{S(t)}(\rho E)\mathbf{v}\cdot\mathrm{d}\mathbf{S} = \Phi - \int_{V(t)}\boldsymbol{\nabla}\cdot(p\mathbf{v})\mathrm{d}V + \int_{V(t)}\boldsymbol{\nabla}\cdot(\tau\cdot\mathbf{v})\mathrm{d}V - \int_{V(t)}\boldsymbol{\nabla}\cdot q\mathrm{d}V - \dot{W}_a \tag{6.11}$$

where $\dot{W}_a$ denotes the external power provided to the control volume. Remembering that

$$E = u + e_k + e_p$$

Under the assumption that the kinetic energy e_k and the potential energy e_p are negligible:

$$E \approx u$$

$$\frac{\partial}{\partial t}(\rho u V) = \Phi - \int_{S(t)}\rho\left(u + \frac{p}{\rho}\right)\mathbf{v}\cdot\mathrm{d}\mathbf{S} - \dot{W}_a \tag{6.12}$$

The integration has been carried out considering constant the fluid properties on the chamber. Expanding the time derivative:

$$\frac{\partial\rho}{\partial t}uV + \frac{\partial T}{\partial t}c_p\rho V + \frac{\partial V}{\partial t}u\rho = \Phi - \dot{W}_a - \int_{S(t)}\rho h\mathbf{v}\cdot\mathrm{d}\mathbf{S} \tag{6.13}$$

The energy is redistributed in the system through the enthalpy fluxes coming from the orifices interconnecting each chamber to the other.
For the rebound chamber it is possible to write:

$$\frac{\mathrm{d}p_E}{\mathrm{d}t}\rho_E u_E V_E\beta + \frac{\mathrm{d}T_E}{\mathrm{d}t}(c_p\rho_E V_E - \rho_E u_E V_E\varphi) = \Phi_E - v_p(A_p - A_r)(p_E + \rho_E u_E) - \sum\rho\cdot Q\cdot h|_{EC} \tag{6.14}$$

While for the compression chamber:

$$\frac{\mathrm{d}p_C}{\mathrm{d}t}\rho_C u_C V_C\beta + \frac{\mathrm{d}T_C}{\mathrm{d}t}(c_p\rho_C V_C - \rho_C u_C V_C\varphi) = \Phi_C + vA_p(p_C + \rho_C u_C) - \sum\rho Q\cdot h|_{BC} + \sum\rho Q\cdot h|_{EC} \tag{6.15}$$

The gas chamber energy equation must account for the gas volume variation (6.9):

$$\frac{\mathrm{d}p_B}{\mathrm{d}t}\rho_B u_B V_B\beta + \frac{\mathrm{d}T_B}{\mathrm{d}t}(c_p\rho_B V_B - \rho_B u_B V_B\varphi) + p_B\frac{\mathrm{d}V_B}{\mathrm{d}t} + \rho_B u_B\frac{\mathrm{d}V_B}{\mathrm{d}t} = \Phi_B \tag{6.16}$$

Introducing (6.5), we obtain:

$$\frac{\mathrm{d}p_B}{\mathrm{d}t}\rho_B u_3 V_B \beta + \frac{\mathrm{d}T_B}{\mathrm{d}t}(c_p \rho_B V_B - \rho_B u_B V_B \varphi) - m_g \frac{R}{M_{mg}}\left(\frac{\mathrm{d}T_g}{\mathrm{d}t} - \frac{T_g}{p_g}\frac{\mathrm{d}p_g}{\mathrm{d}t}\right) + \\ - \rho_B u_B \frac{\mathrm{d}T_g}{\mathrm{d}t}\frac{m_g}{p_g}\frac{R}{M_{mg}} + m_g \rho_B u_B \frac{R}{M_{mg}}\frac{T_g}{p_g^2}\frac{\mathrm{d}p_g}{\mathrm{d}t} = \Phi_B + \sum \rho \cdot Q \cdot h|_{BC} \tag{6.17}$$

6.4.1 Gas energy equation

It is important to point out that the gas in the reserve chamber is treated as ideal because the pressure it is subjected to does not justify the characterization as real. Writing the first principle for a closed system, assuming reversible process:

$$\mathrm{d}u = \mathrm{d}\Phi - \mathrm{L} \tag{6.18}$$

The pressure work is:

$$\mathrm{d}L = p\mathrm{d}V$$

introducing the enthalpy:

$$h = u + \frac{p}{\rho} = c_p \mathrm{d}T$$

which lead to:

$$\frac{\mathrm{d}T_g}{\mathrm{d}t} = \frac{1}{m_g c_p}\left(\Phi + V_g \frac{\mathrm{d}p_g}{\mathrm{d}t}\right) \tag{6.19}$$

6.4.2 Energy equation for orifices

It is necessary to introduce the total energy equation for the flow inside the orifices:

$$\rho V \frac{\mathrm{d}E}{\mathrm{d}t} + \int_V \boldsymbol{\nabla} \cdot (p\mathrm{v})\mathbf{d}V = \dot{m}(h + e_k + e_p)_{inlet} - \dot{m}(h + e_k + e_p)_{outlet} + \cancel{\rho V \frac{\partial E}{\partial t}} \tag{6.20}$$

there is no energy transfer as heat flux or power through the control volume so those terms have been omitted. Unsteady effects are negligible in the orifice so the time derivative can be neglected [14].
Assuming negligible the potential energy and the kinetic energy time variation, the enthalpy conserves throughout the pipe:

$$h_{inlet} = h_{outlet} \tag{6.21}$$

Although the enthalpy is conserved, according to the generalized Bernoulli's equation, the internal energy is increased by friction and irreversibilities:

$$\frac{v_{out}^2 - v_{in}^2}{2} + g(z_{out} - z_{in}) + \int_1^2 v\mathrm{d}p + R_{12} = 0 \tag{6.22}$$

Under the listed assumptions, assuming incompressible flow inside the pipe:

$$\frac{p_{out} - p_{in}}{\rho} = -R_{12} \tag{6.23}$$

The pressure drop due localized and distributed loss indicated with the term R_{12} causes the oil to leave the orifice with an increased temperature. Since the flow direction in orifices is determined by the relative velocity of the piston, the enthalpy (or in general the physic property) assumed at the inlet of the orifice (and conserved through outlet as seen in (6.21)) depend on the piston movement.
A way to choose the right value at the inlet can be made by a `if - else statement` or referring to the function sgn:

$$s_1 = \frac{1 + \mathrm{sgn}(\dot{x}(t))}{2} \qquad s_2 = \frac{1 - \mathrm{sgn}(\dot{x}(t))}{2}$$

6.5 Heat transfer modelling on solid parts

The right hand side Φ appearing in the energy equations represents the heat flux absorbed by the fluid elements (gas and oil) which fill the respective chambers. In order to provide the information about the temperature reached by the solid parts, also three main damper components are introduced in the thermal model: the inner cylinder, the outer cylinder and the piston.

The field of temperature is considered uniform inside the entire part. This assumption allows to express the first principle of thermodynamics for the generic part as:

$$m_i c_v \frac{\mathrm{d}T_i}{\mathrm{d}t} = \Phi_i \tag{6.24}$$

The terms m_i and c_v stands for the mass of the solid part and the specific heat at constant volume. The only kind of heat transfer considered is a convection flux between the solid part and the fluid region.
According to Newton's equation for convection the heat flux can be expressed through:

$$\Phi_i = \alpha_c A (T_i - T_f) \tag{6.25}$$

where α_c is the convection coefficient which depends not only on the fluid involved but mostly on the condition under which the flow takes place. For its calculations, semi-empirical correlation will be used. Symbols A, T_i and T_f refer to the area involved in the heat interchange, to the temperature of the solid component and to the temperature of the fluid respectively.
It is important to underline that the gas oil interface changes position due to the piston movement. In evaluating the heat fluxes this consideration has to be taken into account.

6.6 Justification of the lumped system analysis

In general, the temperature of a body varies with time and position. Assuming this dependence, in rectangular coordinates the temperature can be expressed as $T(x, y, z, t)$. In a lumped system, the temperature is considered uniform at the generic time instant during the heat transfer process. The energy balance for the body can be expressed as in (6.24). Denoting with m the mass of the body, A the area of heat exchange and c_v the specific heat:

$$m \cdot c_v \mathrm{d}T = \alpha_c (T_\infty - T)\mathrm{d}t \tag{6.26}$$

The equation takes the form of a first order model with a time constant τ which can be defined as:

$$\tau = \frac{m \cdot c_v}{\alpha_c A} \tag{6.27}$$

The time constant identifies the time required by the system to reach the 63% of the final value. Moreover, integrating (6.24), it easy to show that it has an exponential trend.

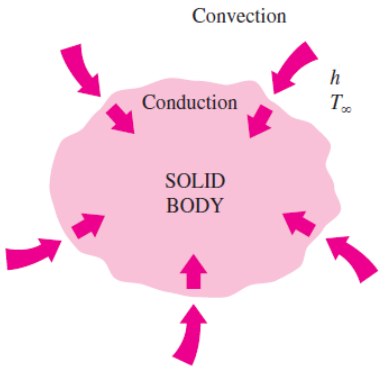

Figure 6.1: The convection-conduction in the lumped system, [5], pp.212

According to [5], the criterion which establishes the applicability of the lumped system idealization is based on the *Biot* number:

$$\mathrm{Bi} = \frac{\alpha_c \cdot L_c}{\lambda} \tag{6.28}$$

where in (6.28) L_c defines a characteristic length:

$$L_c = \frac{V}{A} \tag{6.29}$$

The Biot number can be viewed as the ratio between the convection involving the heat exchange area A and the conduction which takes place inside the body:

$$\mathrm{Bi} = \frac{\alpha_c}{\lambda / L_c} \frac{\Delta T}{\Delta T} = \frac{\text{Convection at the body surface}}{\text{Conduction within the body}} \tag{6.30}$$

At the same time (6.30) can be rearranged in the ratio between the conduction resistance and the convection resistance at the surface of the body.

$$\mathrm{Bi} = \frac{L_c/\lambda}{1/\alpha_c} = \frac{\text{Conduction resistance within the body}}{\text{Convection resistance at the body surface}} \tag{6.31}$$

Assuming as uniform the temperature of the generic element means that the Biot number is zero. Thus, when the thermal resistance to conduction is zero, the lumped system analysis is exact and rigorous.
However, a good approximation is obtained if

$$\mathrm{Bi} \leqslant 0.1$$

When the above criterion is satisfied, the temperature field varies very slight inside the body and can be approximated as uniform.

6.6.1 Biot number computation for the solid parts

The Biot number for the three solid parts modelled in the damper is calculated.

Table 6.1: Calculation of Biot number for solid parts

Conductivity $\boldsymbol{\lambda}$ [$\mathrm{W\,m^{-1}\,K^{-1}}$]	≈ 40
Coefficient of thermal convection oil-wall [$\mathrm{W\,m^{-2}K^{-1}}$]	100-1000
Lc_{inner} [m]	0.007
Lc_{outer} [m]	0.005
Lc_{Piston} [m]	0.045
Biot number	
Inner Cylinder	0.0125-0.125
Outer Cylinder	0.0175-0.175
Piston	0.05625-0.5625

Table 6.1 shows the Biot number for the range of the thermal convection coefficient oil-cylinder wall $100 - 1000\ \mathrm{W\,m^{-2}\,K^{-1}}$. It can be seen that also in the worst condition the assumption of the lumped system modelling is acceptable. In fact, the value of $1000\ \mathrm{W\,m^{-2}\,K^{-1}}$ is over estimated and reported as a limit case. An important information is that the most problematic part to which apply the lumped analysis is the piston. In fact, it is characterized by the largest Biot number.

6.7 Temperature influence on viscosity

The implementation of the thermal model in which temperatures of the system appears explicitly in govern equations allow to consider their influence on viscosity. The linear approximation

$$\mu = \mu_{ref}\Big(1 + k_{\mu T}(T - T_{ref})\Big) \qquad k_{\mu T} \approx -2\%\,^{\circ}\mathrm{C} \tag{6.32}$$

is acceptable only for a narrow temperature range so the Guzmann-Carrancio equation is preferred:

$$\mu = \mu_0 e^{\frac{E}{RT}} \tag{6.33}$$

in which E is the characteristic energy value, R the universal gas constant and T the absolute temperature. Re-expressing (6.33):

$$\mu = \mu_0 e^{C(\frac{1}{T} - \frac{1}{T_1})} \tag{6.34}$$

denoting with C a positive coefficient and μ_0 is the viscosity at temperature (absolute) T_0. Moreover we have:

$$\log \mu = \log \mu_0 + \frac{C}{T} - \frac{C}{T_1} \tag{6.35}$$

$$\log \mu = A + \frac{C}{T} \tag{6.36}$$

By inspection of (6.36), this model of viscosity predicts a linear relation between the logarithm of the viscosity and the reciprocal of the temperature.
In absence of other data, a reasonable estimate of parameter C is

$$C = 5693 - 304\log_{10}(\mu_{ref}) - 646\log_{10}^2(\mu_{ref}) \qquad T_{ref} = 15^{\circ}\mathrm{C} \tag{6.37}$$

Once the values of μ and ρ have been computed, the contribution of concentrated and distributed friction loss can be evaluated. In particular, reminding 1.26 on page 12, flow rate and velocity is readily known:

$$Q = C_d A\sqrt{\frac{2\Delta P}{\rho}}$$

If in the first phase C_d is considered constant, the temperature influences only the density value. The decreasing trend of density with temperature diminishes the damping force:

$$Q = C_d A\sqrt{\frac{2\Delta P}{\rho_0}\frac{\rho_0}{\rho}} \qquad \frac{\rho_0}{\rho} > 1 \quad \textbf{for} \quad T > T_0$$

In general, the evaluation of the global C_d (due to distributed and concentrated losses) needs an iterative process with an initial guess. In fact, Reynolds number is also a function of flow rate:

$$Re = \frac{\rho\frac{Q}{A}D_h}{\mu} \tag{6.38}$$

The calculation is carried on with the analytical formulation of C_d given in 1.7 on page 10.

6.8 Definition of fluxes through boundaries

We refer to flux of a property f through a surface S as the integral:

$$\text{flux of f} = \int_S f \cdot \mathbf{v} \cdot \mathbf{n} \mathrm{d}S$$

where in this case the advected is a scalar property (e.g. density or enthalpy).

Implementing the thermal model of the damper, the definition of how the enthalpy flux is defined within orifices is found to have an important impact on solution. Precisely, two ways are exploited:

1. Approximating the enthalpy as the mean of the value assumed in the adjacent chambers;

2. Choosing the value of enthalpy according to piston movement;

The solution 2, as mentioned in 6.4.2, is considered more suitable for modelling approach and for stability reasons, as it will be investigated later.
Denoting with Q_m the mass flow rate, for the approach 1 the enthalpy flux is:

$$h_{ij} = c_v \cdot \frac{T_i + T_j}{2} + \left(\frac{p_i + p_j}{2}\right)/\rho_{ij} \qquad \text{where i, j = E, C, B} \tag{6.39}$$

while in the second case the appropriate value of enthalpy is assigned according the to sign of the mass flow; in particular, the properties of the fluid in the orifice are the same of the chamber the oil is coming from. A possible choice to implement this condition is a if-else statement:

$$\begin{aligned} &\textbf{if } Q_{m_{ij}} > 0 \\ &h_{ij} = c_v \cdot T_i + p_i/\rho_{ij} \\ &\textbf{else} \\ &h_{ij} = c_v \cdot T_j + p_j/\rho_{ij} \qquad \text{where i,j = E, C, B} \end{aligned} \tag{6.40}$$

In order to study the difference the above implementations offer, the more general thermal model with heat fluxes enabled is considered as reference. With "heat fluxes enabled" we refer to the thermal model in which also the solid parts are present. From inspection of Figure 6.2 and Figure 6.3 the dependence of the solution from the enthalpy definition is remarked.

When the enthalpy is computed with the algebraic method considering the mean of the properties (temperature and pressure) of the adjoining chambers, the amplitude of temperature oscillations increase in a non-physical way. The increasing amplitude is evident in expansion and compression chamber.
This divergent behaviour is responsible for the abortion of simulation when either the simulation time or the frequency are increased. As announced, the second solution is implemented because shows a more stable evolution. To be coherent with enthalpy definition

also the mass fluxes are computed taking into account the value of density appropriate:

$$\begin{aligned} &\textbf{if } \operatorname{sgn}(p_i - p_j) > 0 \\ &\rho_{ij} = \rho(p_i, T_i) \\ &\textbf{else} \\ &\rho_{ij} = \rho(p_j, T_j) \qquad \text{where i,j = E,C,B} \end{aligned} \tag{6.41}$$

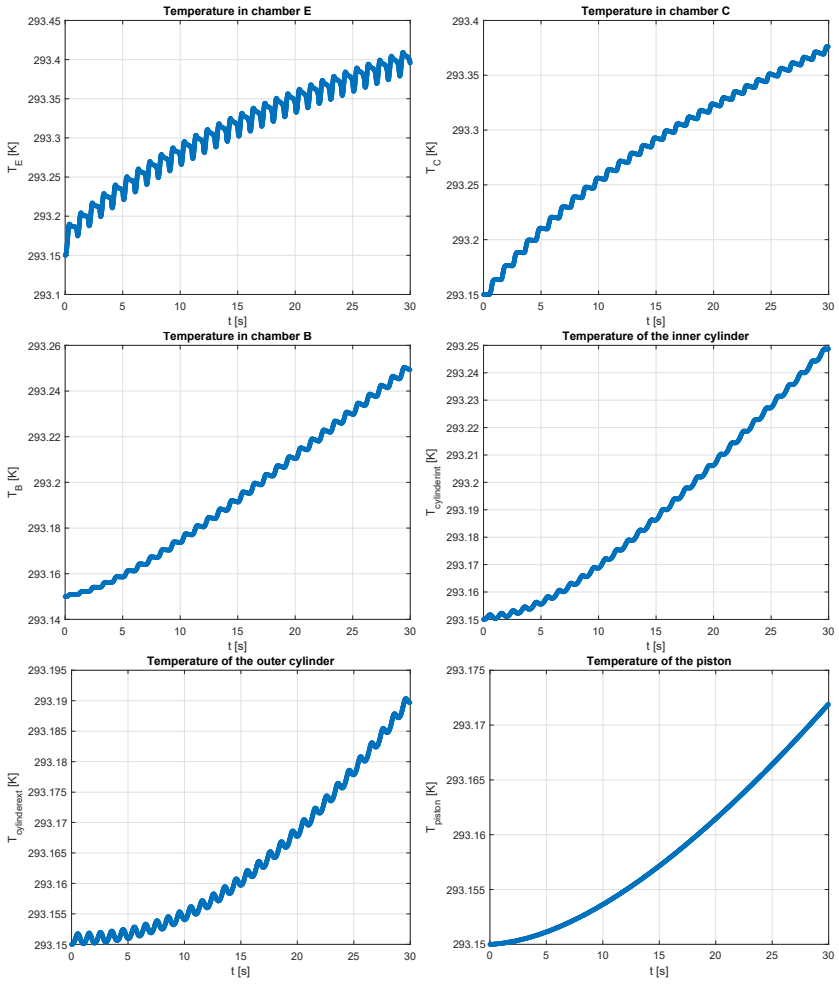

Figure 6.2: Pressure and temperature trends with enthalpy convected by the mass flow rate Q_m

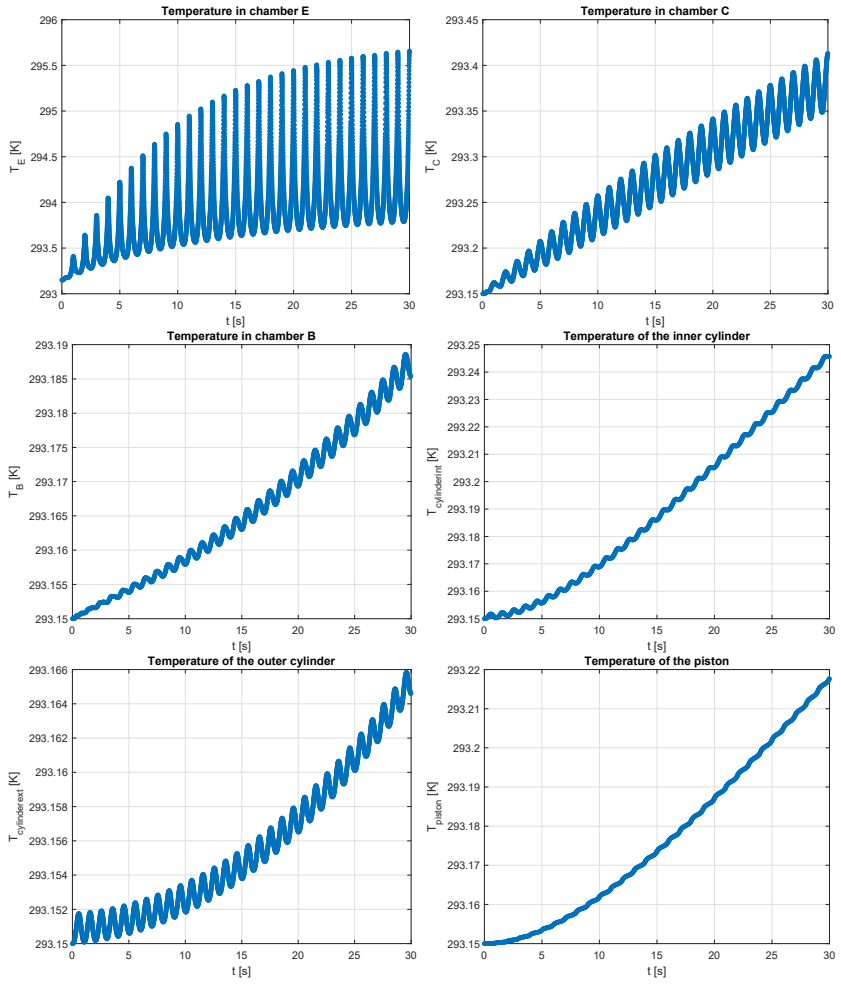

Figure 6.3: Pressure and temperature trends with enthalpy computed as mean value of the properties of adjacent chambers

Chapter 7

Implementation of the model in Matlab

The system of equation presented in Chapter 6 is implemented in MATLAB. Two different methods are exploited. The mathematical model consists in a system of ordinary differential equations (ODE). The number of equation depends also on the number of the solid parts modelled. A typical dual tube is considered with: three chambers filled with the oil, one gas chamber and piston assembly, inner cylinder and outer cylinder as solid parts.

On this basis, the number of equations sets to 11. In fact, we have six equations for the oil (3 eqns. of continuity + 3 eqns. of energy), two equations for the gas (1 eqn. of state + 1 eqn. of energy) and one for each solid element (1×3 - three solid parts -).

7.1 Classical ODE resolution

The first method implemented is the classical method for resolution of a system of ODE. Once the equations are written, the linear system of equation is solved. In particular, calling A the matrix of coefficients of the ODE systems:

$$A(t, y)\mathbf{y}' = \mathbf{b}(t) \tag{7.1}$$

where $\mathbf{y}$ denotes the dependent variables which in the specific case is a 11×1 vector. When the linear system is solved by MATLAB command \ (mldivide) the vector of derivatives is the input for the MATLAB ODE solver.

$$\mathbf{y}' = A(t, y)^{-1}\,\mathbf{b}(t) \tag{7.2}$$

where

$$A = \begin{bmatrix} a_{11} & \dots & a_{1n} \\ \vdots & \ddots & \vdots \\ a_{n1} & \dots & a_{nn} \end{bmatrix}_{n \times n} \qquad \mathbf{b} = \begin{bmatrix} b_1 \\ \vdots \\ b_n \end{bmatrix}_{n \times 1} \qquad n = 11$$

7.2 Mass matrix implementation method

A different way to solve the system of ODE is to exploit MATLAB functionality of solving problems containing a mass matrix $M(t, y)\mathbf{y}' = \mathbf{b}(t)$ where M is a sparse or full matrix. The `ode15s` solver is able to solve systems where the mass matrix is time dependent. In the specific case, the mass matrix coincides with the matrix A previously introduced.

7.3 CPU time measurements for the two methods

The CPU time taken by each method is measured for different simulation times and frequency excitations. The results obtained are reported below. Table 7.1 refers to the model in which the heat fluxes interesting the solid parts are disabled while Table 7.2 to the case in which the heat fluxes are enabled. The resolution involving the mass matrix appear to be always faster than the classical resolution. The comparison of the solution at the same instant of time is not possible since in the variable step approach of ode 15s time vectors (in which solutions are computed) are different.

However, reconstructing the solution at the desired time using the function deval, the difference between the solutions are compatible with the relative and absolute tolerances given as input. The CPU time obtained justifies the implementation of the thermal model according to the mass matrix approach.

7.3.1 CPU time: Heat fluxes disabled

Table 7.1: CPU time required by the simulation with the with heat flux disabled model

		CPU time [s]	CPU time [s]
Simulation time [s]	**Freq. [Hz]**	**Classical ODE**	**Mass Matrix Resolution**
3	1	16.56	16.55
3	2	21.09	15.41
3	3	28.67	20.41
12	1	31.16	14.75
12	2	81.45	54.86
12	3	124.77	90.25
24	1	74.83	39.47
24	2	168.50	115.55
24	3	264.20	174.63
64	1	306.30	111.83
64	2	649.61	403.48
64	3	875.52	543.78
300	1	926.47	519.97
300	2	3333.73	1453.06
300	3	5044.75	4007.94

7.3.2 CPU time: Heat fluxes enabled

Table 7.2: CPU time required to run the simulation by the thermal model with heat flux enabled

		CPU time [s]	CPU time [s]
Simulation time [s]	**Freq.** [Hz]	**Classical ODE**	**Mass Matrix Resolution**
3	1	15.78	11.48
3	2	19.55	13.17
3	3	46.72	27.23
12	1	34.48	19.86
12	2	88.86	60.27
12	3	131.17	92.38
24	1	77.22	42.64
24	2	276.72	178.44
24	3	412.38	269.75
64	1	322.53	166.63
64	2	452.02	343.50
64	3	1030.80	513.14
300	1	1494.61	753.44
300	2	3087.20	2121.05
300	3	5070.42	3297.00

Analysing the results obtained it is possible to point out the following peculiarities:

- The resolution time increases with frequency as speeding up the dynamic a smaller step integration time is required to achieve the tolerances;
- The implementation with the mass matrix is faster than the classical resolution;
- The CPU time difference taken by the two methods is less evident for short simulation times because MATLAB `ode15s` makes attempts with different step time to respect the tolerances;

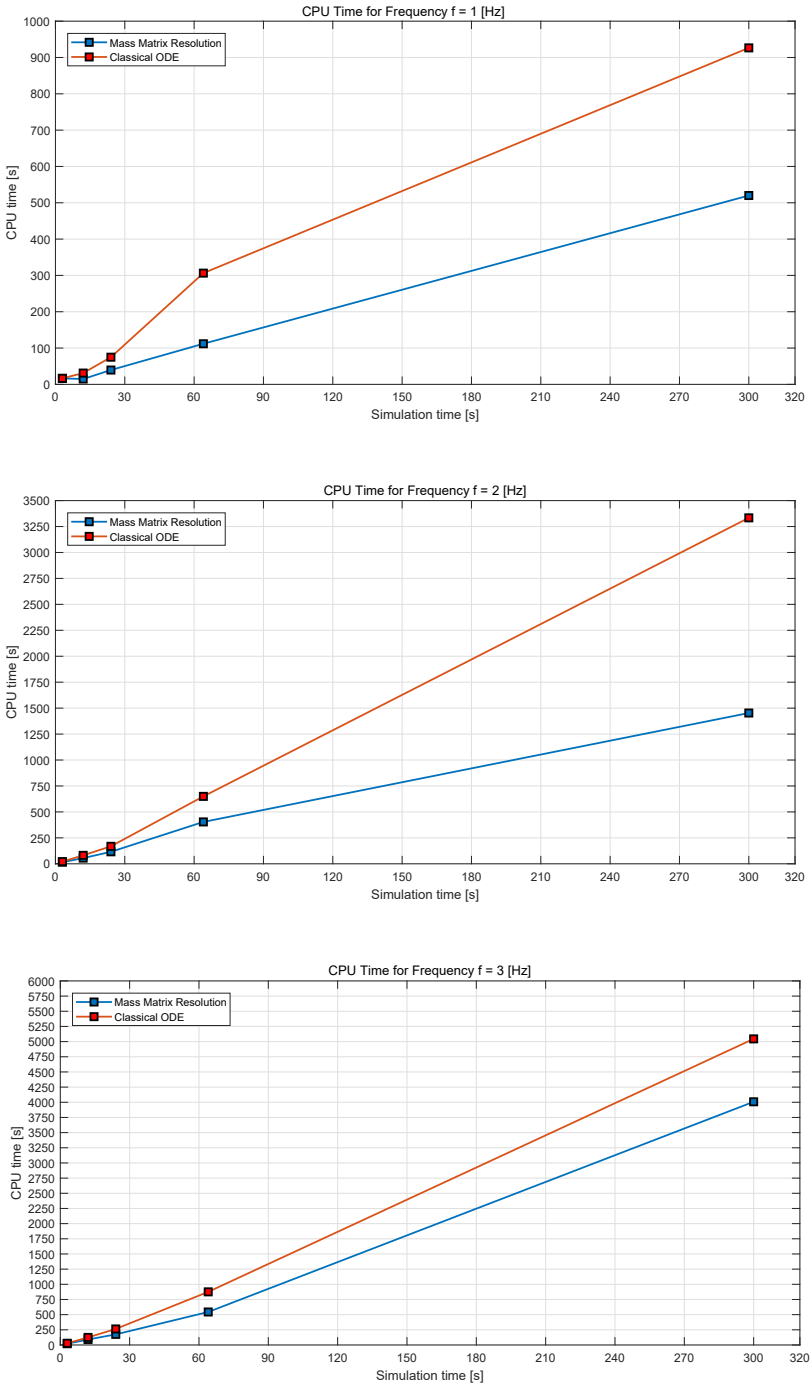

Figure 7.1: CPU time comparison for the thermal model with heat flux disabled

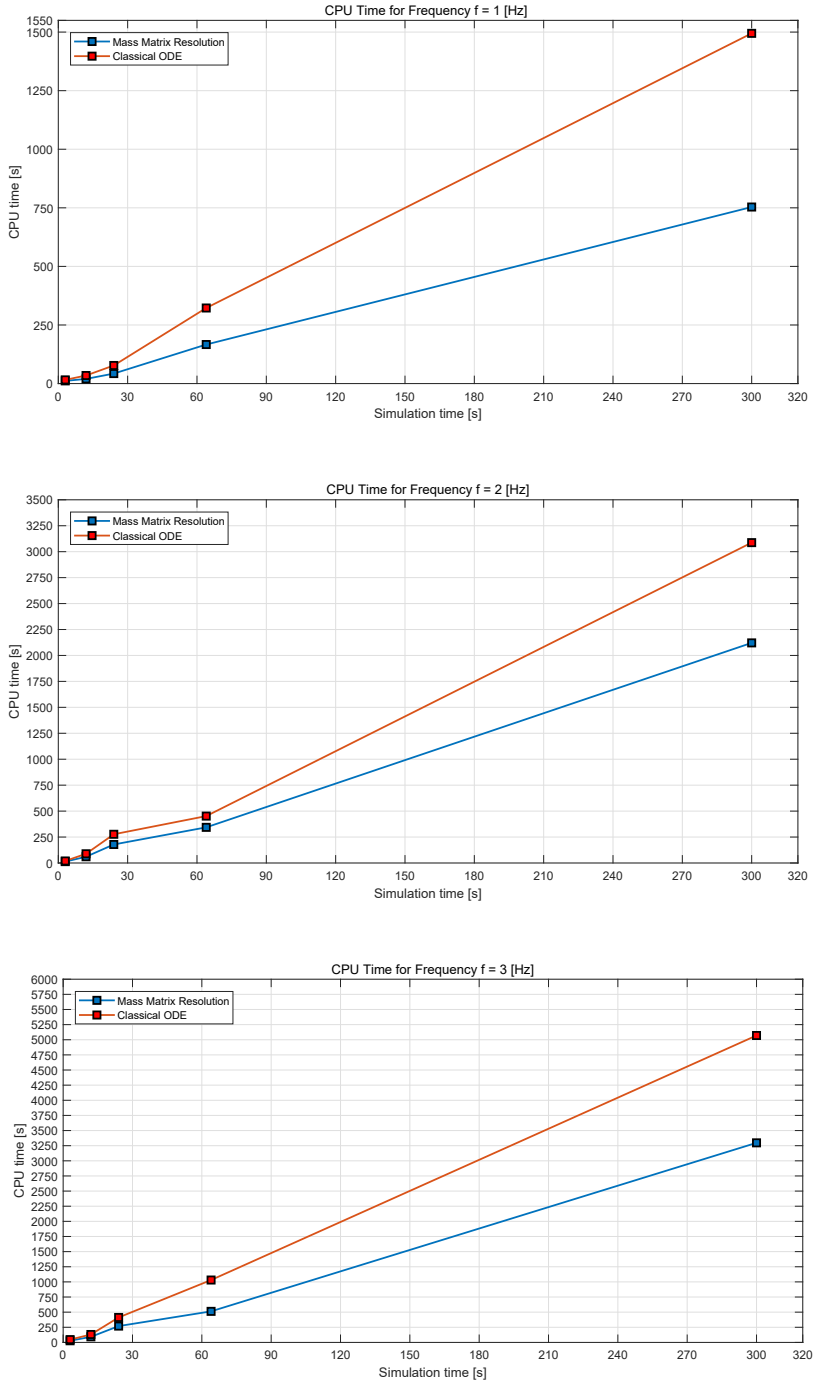

Figure 7.2: CPU time comparison for the thermal model with heat flux enabled

7.4 Numerical verification of mass and energy conservation

The present section is dedicated to the description of the numerical verification of the code. In particular, it is important to verify that the system of ODE implemented in the system works correctly. Since the equation written are essentially the conservation of mass and the conservation of energy (first principle of thermodynamics) it is possible to check:

1. If the final mass equals (within numerical errors) the initial one;
2. If the energy input on the system has been transformed in internal energy;

The condition number 2 is easily applicable to an adiabatic system that is a system which does not exchange heat with the environment. Two thermal versions are reported: in the first one the heat fluxes are suppressed while in the second the heat fluxes are enable and solid parts will see their temperature changing in time.

7.4.1 Thermal model with no heat fluxes

The first thermal model developed does not contemplate the thermal fluxes between the fluid elements and the solid parts. Under the basis of this modelling, the solid part temperature remains constant in time to the initial value.

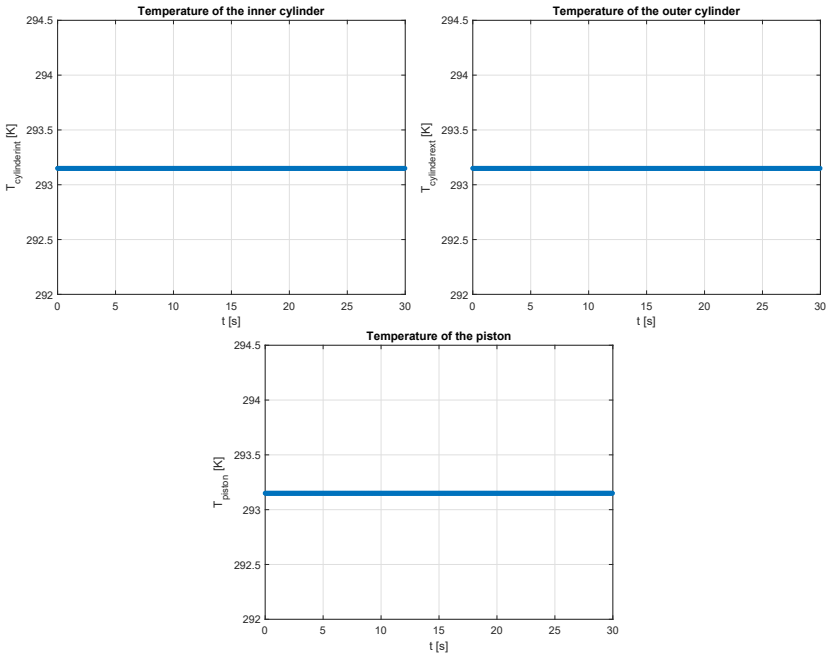

Figure 7.3: Temperature trends for solid parts (heat fluxes disabled)

From Figure 7.3 is evident that the temperature of the solid elements is stuck to the initial one, since the heat fluxes inside the solid parts are set to zero. However, this modelling provides the information of evolution of the temperature in the oil chambers: on average, it increases monotonically because energy is continually inserted in the system.

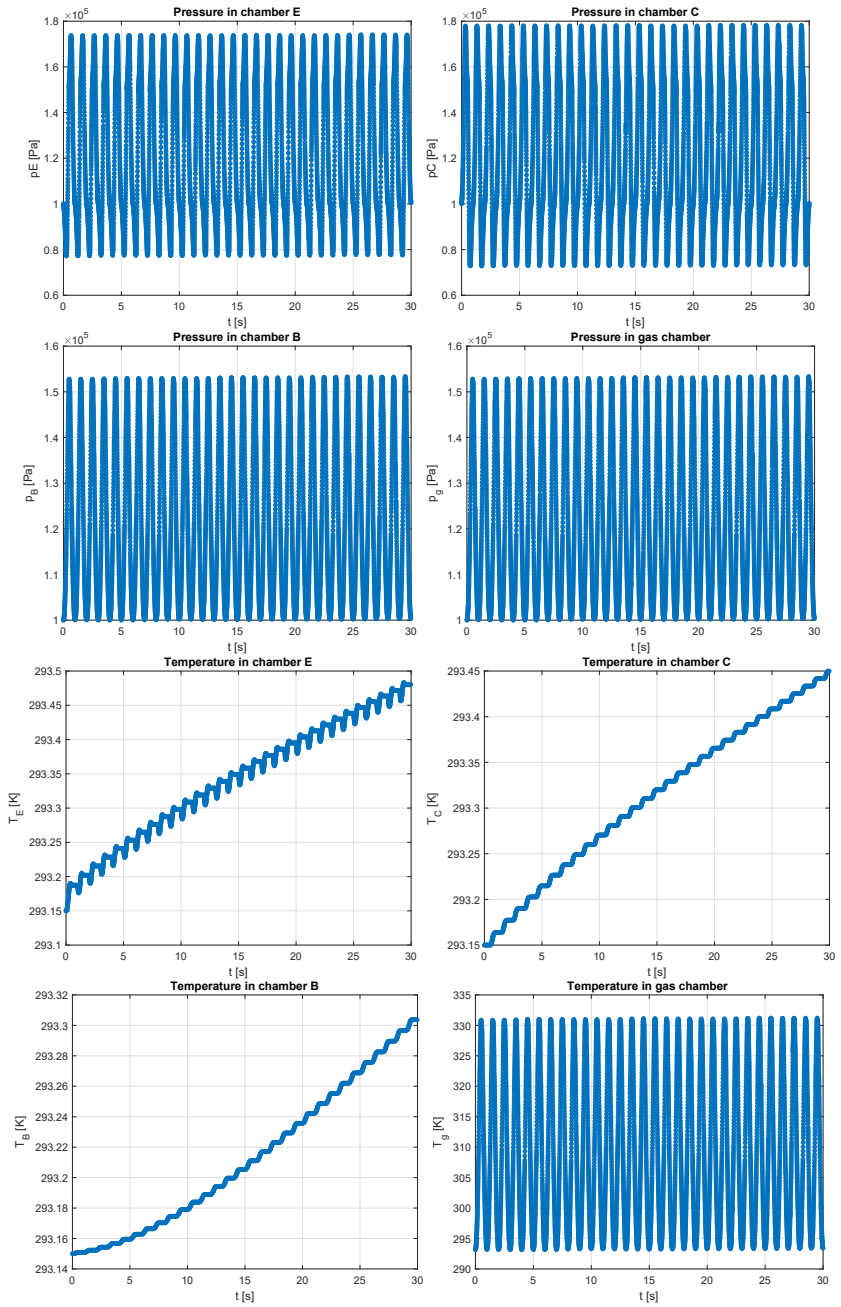

Figure 7.4: Pressure and temperature trends for fluid parts in the thermal model with no heat fluxes

7.4.2 Thermal model with heat fluxes enabled

A more complete system is modelled considering the presence of the solid parts and the heat fluxes they interchange with the solid elements. In this case also the piston, the inner and the outer cylinder increase their temperature with time.

The internal energy stored by the solid elements is removed from the one potentially available for the fluids region: this is found to be the reason why the fluid regions reach in the same time of simulation a lower maximum temperature if compared to the system in which the fluxes are disabled (Figure 7.3, 7.4). Moreover, as highlighted by Figure 7.5, their mean temperature trends resemble an exponential evolution, coherently with what explained in 6.6.

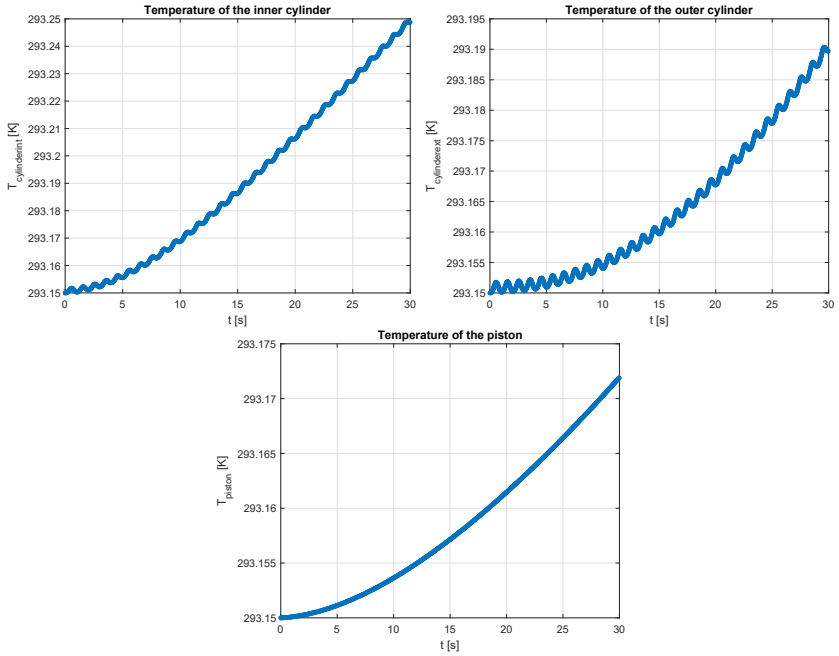

Figure 7.5: Temperature trends for solid parts (heat fluxed enabled)

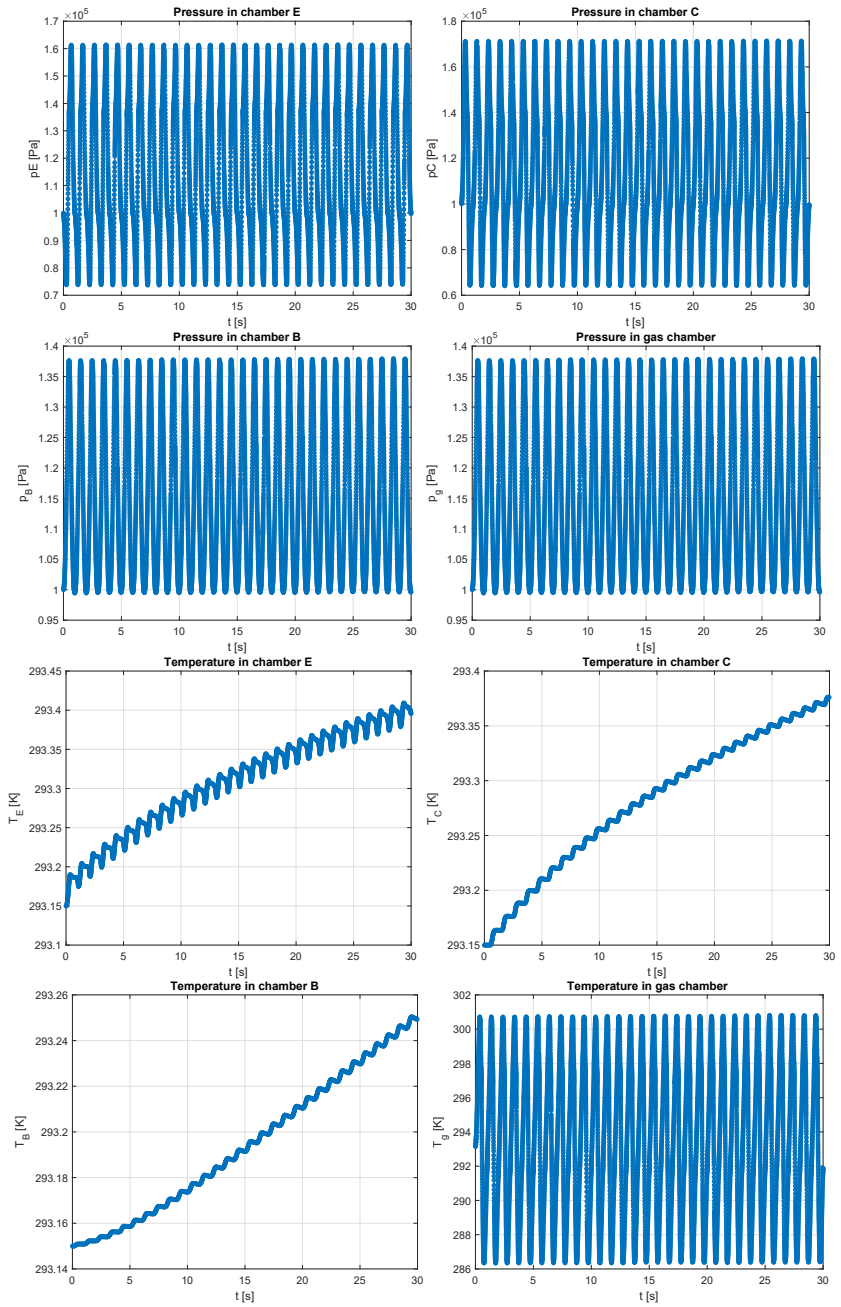

Figure 7.6: Pressure and temperature trends for fluid parts in the thermal model with heat fluxes enabled

In Table 7.3 the initial and the final mass value are computed. It can be stated that the absolute error is of order $\approx 10^{-8} - 10^{-9}$, which is compatible with the relative and the absolute errors set in MATLAB solver `ode 15s` to 10^{-8} and 10^{-10}, respectively. The adiabatic modelling towards the external environment allows also to verify if the energy has been conserved integrally in the system.
The difference of energy is computed once the temperatures, the densities and the volumes occupied are known at the beginning and at the end of the simulation. The reference value for the energy check can be computed analysing the energy dissipated by the system:

$$\Delta E = \int_0^T F_D \, \mathrm{dx} \qquad \text{or equivalently} \qquad \Delta E = \int F_D \cdot v \, \mathrm{d}t \tag{7.3}$$

These two modes are considered because the integral is computed numerically using trapezoidal rule (second order accuracy). In both cases, the energy dissipated by the system is converted in internal energy (temperature), confirming the conservativeness of energy in the system.

Table 7.3: Mass and energy conservation for the thermal model - numerical verification

Fluxes Disabled	Yes	No
$\boldsymbol{\beta}$	$2.50{\cdot}10^{-9}$	$2.50{\cdot}10^{-9}$
tspan [s]	30	30
Freq [Hz]	1	1
$\boldsymbol{\Delta E}$ [J]	$1.5879657227 \cdot 10^{2}$	$1.5996459066 \cdot 10^{2}$
$\boldsymbol{\Delta E}$ $(\boldsymbol{F_x})$ [J]	$1.5878240222 \cdot 10^{2}$	$1.5994962704 \cdot 10^{2}$
$\boldsymbol{\Delta E}$ $(\boldsymbol{F_{v_t}})$ [J]	$1.5879562390 \cdot 10^{2}$	$1.5996314449 \cdot 10^{2}$
Δ **Energy Error** [J](%)	$7.55921{\cdot}10^{-3}(4.76{\cdot}10^{-3}$ %)	$8.204895{\cdot}10^{-3}(5.13{\cdot}10^{-3}$ %)
Initial Mass [kg]	2.08823475451	2.08823475451
Final mass [kg](%)	2.08823475615	2.08823475379
Δ **Mass Error** [kg] (%)	$1.64{\cdot}10^{-9}(7.85{\cdot}10^{-8}$ %)	$7.20{\cdot}10^{-10}(3.44{\cdot}10^{-8}$ %)

7.5 A mass non-conserving model

A mass conservative model is a model in which the total final mass matches the initial mass value. The above statement is guaranteed if the following conditions are verified:

1. The model should provide a density variation due to pressure (and also due to temperature if the temperature effects are implemented);

2. The mass flow rate needs to be computed coherently referring to the value of density used in the velocity calculation;

Non conservation of mass can be appreciated not only comparing the mass values at the beginning and at the end of the time simulation; in fact, it can be seen in Figure 7.7

that when mass is non conserved but decreases in time, also the gas pressure shows a decreasing trend. If the mass conservation is respected, the gas pressure has a constant mean value (Figure 7.8).

Table 7.4: Mass value comparison for excitation frequency f=3 Hz and simulation time T=5 s

f= 3 [Hz], **T=5** [s]	**Initial Mass** [kg]	**Final Mass** [kg]
Non conserving model	$3.7369 \cdot 10^{-1}$	$3.7337 \cdot 10^{-1}$
Conserving model	$3.7369 \cdot 10^{-1}$	$3.7369 \cdot 10^{-1}$

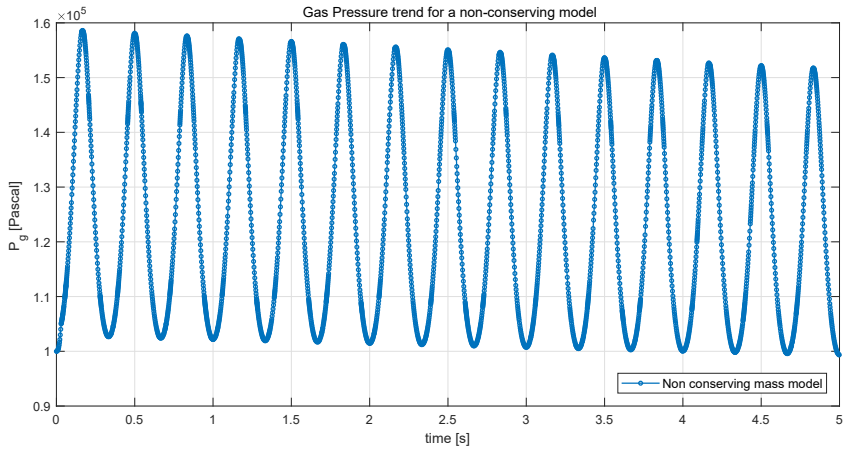

Figure 7.7: Example of pressure trend for a non conserving model

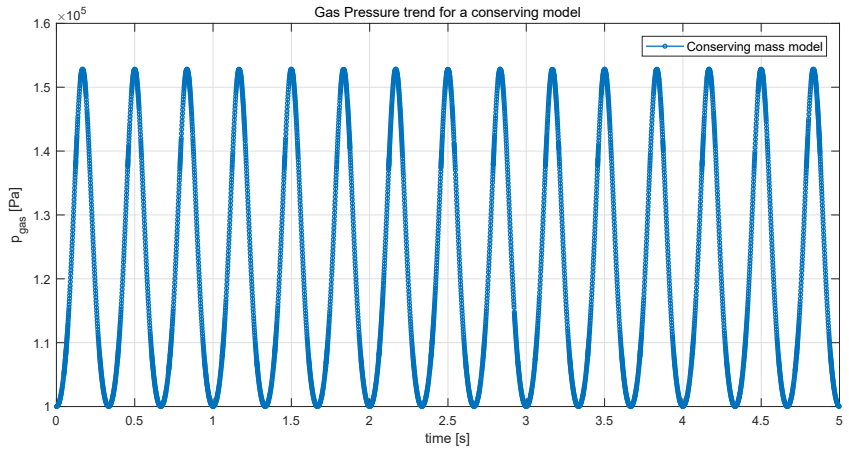

Figure 7.8: Example of pressure trend for a conserving model

As a consequence, the investigation of the gas pressure evolution can be regarded as a check to ensure the correct implementation of the code. The condition 1 assures that a

pressure increase in a compressible model causes a density increase in that chamber while the condition 2 guarantees that the mass flux entering the orifice is the same amount leaving it.

What it is important to underline is that the mean value of the gas pressure takes a constant value strictly in isothermal condition. In the thermal model the effect of coefficient of thermal expansion can be seen.

Let's consider the thermal model of a damper which is adiabatic with respect to the environment in more depth.
The system does not exchange heat with the surroundings. Hence, the dissipative force acting on the piston introduces power into the system which converts this energy per unit time in internal energy. Then, the mean temperature of the system increases. The volume of oil for the rebound and the compression chambers is defined by the piston movement but according to (6.3) the density falls down with the temperature increase.

This fact means that less mass is contained in these two chambers if compared to the analogous system under isothermal assumption. To preserve mass, the volume occupied by the oil in the reserve chamber must increase (the mean value of density is decreasing due to temperature if compared to the isothermal one). If the oil in the reserve chamber occupies more volume, the pressure in the gas chamber increases because of the less volume available for the gas.

7.5.1 Coefficient of thermal expansion effect on density

The evolution of the gas pressure is reported for two values of coefficient of thermal expansion φ. One is a typical value for a damper medium while the other is for a liquid which does not expands ($\varphi \ll 1$) with the temperature variation . Figure 7.9 shows that when the temperature effect on density is negligible, the mean value of the gas pressure tends to switch back to a constant value (as in the isothermal model). Below trends are obtained for f= 3 Hz and simulation time T= 15 s.

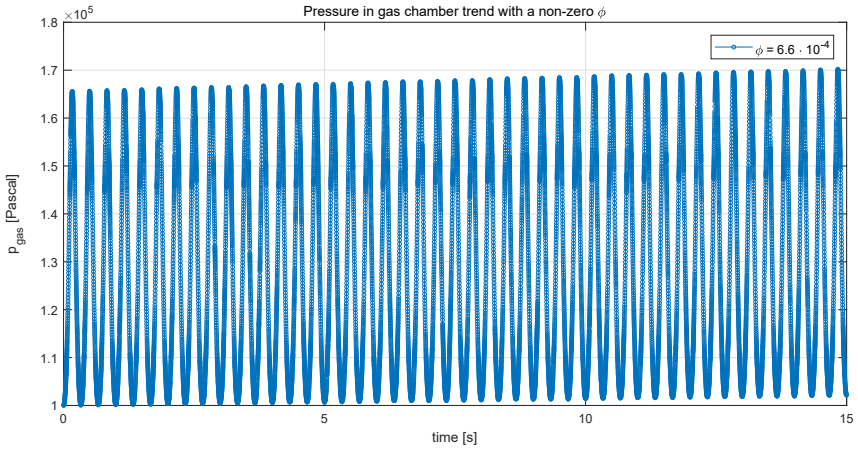

Figure 7.9: Pressure trend for a typical coefficient of thermal expansion

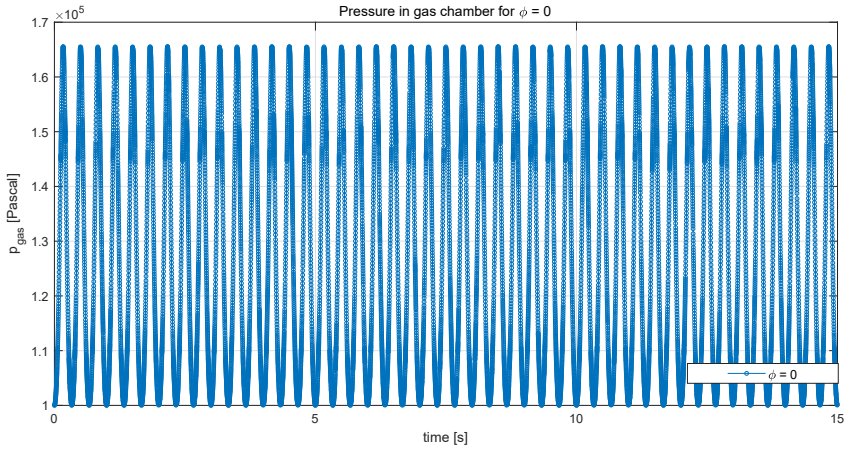

Figure 7.10: Pressure trend for coefficient of thermal expansion $\varphi \ll 1$ (in this case $\varphi = 0$)

Chapter 8

Conclusions

A compressible and thermal model of a pure twin tube damper has been developed. It was pointed out that the compressibility introduces a delay between the piston motion and the flow rate Q. The results is a reduced stability of the system: very small integration time step have to be taken and the problem becomes numerically stiff.

It has been shown that the compressibility is responsible of an *elastic flow* $Q_{elastic} = \frac{\mathrm{d}p}{\mathrm{d}t} V_{oil}\beta$, which is not negligible at high excitation frequency. The compliance of the cylinder wall may enlarge the compressibility effects; for the geometrical configuration considered, its value is two orders of magnitude smaller than the oil compressibility. However, its impact can be easily taken into account once the physical properties of the cylinder are known.

The piston-wall leakage, if not accurately limited, has an impact on the characteristic diagrams because an undesirable flow rate reduces the effectiveness of the blow-off valve. In fact, for the same flow displacement (and therefore flow rate) a wider "equivalent" cross-sectional area limits the flow lamination producing a minor pressure differences between chambers.

The original contribution provided comes from the inclusion of the thermal effects. The energy equation has been considered and coupled with the state equation for gases. The modelling has been carried out accordingly to a lumped system analysis, which offers the opportunity of speeding up the process of sizing in a preliminary phase compared to a time-consuming detailed CFD process.

A preliminary identification of the heat exchange coefficients may be needed to set the correct range of values. The presence of orifices with geometry different from the sharp-edge proposed is easily implemented in MATLAB script adapting the empirical correlation for the discharge coefficient C_d.
The state equation for the oil is based on the assumption $\beta = \text{const}$ and $\varphi = \text{const}$ but in the presence of detailed information about the damper medium properties, their value can be parametrized as function of temperature and pressure. This will lead to an

additional term in $\frac{\mathrm{d}\rho}{\mathrm{d}p}$ and $\frac{\mathrm{d}\rho}{\mathrm{d}t}$ according to the derivative chain rule.

The implementation of the model in the mass-matrix form (DAE's systems of equations) showed better performance in terms of CPU time than the classical ODE resolution. The numerical verification with an integral approach confirms that the model is mass and energy conservative.
A possible definition of fluxes through boundary is given to provide numerical stability and to prevent non-physical oscillations.

The temperature affects not only the density value ρ but also the dynamic viscosity μ. Both terms influence the Reynolds number whose value governs *friction* and *local* losses. In order to be evaluated correctively, an iterative loop is required to compute the total flow resistance $k_{loss_{tot}}$.

The proposed model can be extended to more complex configurations which contemplate complicated piston valve and base valve assemblies. Depending on the information required, different ways of modelling can be chosen:

1. Writing the mass and energy balance equations for each region of interest;
2. Modelling the regions inside the piston and the valve assemblies as compressible but isothermal;
3. Modelling the piston and the base valve assemblies as self entities ("black box") with a characteristic $\Delta p = f(Q)$;

The approach 1 gives more accurate results but for each new region two new equations (mass and energy) are needed. Clearly, having many regions the systems of equation becomes progressively larger and the quick implementation-evaluation quality of lumper parameter analysis may be lost.
The third approach is the quicker one if no information about the pressure and the temperature distributions inside valves are requested. On the other hand, the procedure 2 stands in the middle between the choices 1 and 3: the pressure distribution is known while the temperature information may be provided by interpolation methods. A combined implementation (1-2-3) is even possible.

Appendix

MATLAB code used for thermal and compressible model implementation is reported below.

```
%% Dynamic and Thermal model of a twin tube damper
function [Energy,Energy2,DeltaE,Potinitial,Potfin,y,t,mgas,Minitial,...
         Mfinal,Fapp,xpist,vpist,DM]=Thermal_model_Damper
close all;
clear all;
%% Initialization
trasporto=true;      %% Model enthalphy choice: true=convection,
                     %                          false= mean value
heat_fluxes=true;    %% Presence of solid part choice:
                     %                          true= heat fluxes enabled,
                     %                          false=heat fluxes disabled;
Abs=1e-10;           %% Absolute tolerance ODE solver
Rel=1e-8;            %% Relative tolerance ODE solver
pio4 = atan(1);
pi = 4*pio4;
amp=15.e-3;          %% Crank length                      [m]
freq=1.0;            %% Excitation frequency              [m]
tmax=30;             %% Simulation time                   [s]
ome=2*pi*freq;
L=0.045;             %% Connecting rod length             [m]
%%%%%%%%%%%%%%%%%%%%%%%%%%%%%%
%% Activate to simulate stroke with same max velocity
% amp=amp*1/freq;
% L=L*amp/15e-3;
%%%%%%%%%%%%%%%%%%%%%%%%%%%%%%
%% Geometry and cylinders data
% ***************************
% ***************************
Lc1 = 142.5e-3;      %% Inner cylinder length               [m]
dc1e = 52.e-3;       %% Diameter of external cylinder       [m]
Ac1e = pio4*dc1e^2;
Lc2  = 170e-3;       %% External cylinder lenght            [m]
dc2i = 65.e-3;       %% Internal diameter of outer cylinder [m]
Ac2i = pio4*dc2i^2;
dc2e=70e-3;          %% Outer diameter of outer cylinder    [m]
Ac2e=pio4*dc2e^2;
%% Orifices length
Lh=1e-2;             %% Piston orifice length            [m]
```

```
Ld=7.5e-3;          %% Base valve orifice length        [m]
EOD=0;              %% Absolute roughness               [m]
%% Oil properties
% ***********
% ***********
rhooil  = 8.57e2;     %% Oil density                   [kg/m^3]
nuoil = 46.e-6;       %% Kinematic viscosity            [m^2/s]
muoil = rhooil*nuoil; %% Dynamic viscosity              [Pa*s]
% **********

%% Initial length of gas in gas chamber
Lg0=3.e-2;
%%
Vg0 = Lg0*(Ac2i-Ac1e);  %% Gas chamber intial volume  [m^3]
pg0 = 1.0e5;            %% Initial gas pressure        [Pa]
%% Geometry and piston data
% *************************
% *************************
dp=45.e-3;              %% Piston diameter            [m]
dr=20.e-3;              %% Rod diameter               [m]
Ap=pio4*dp^2;           %% Piston area              [m^2]
Ar=pio4*dr^2;           %% Rod area                 [m^2]
tp = 22.5e-3;           %% Piston height              [m]

dc1i=dp;

kEC = 1/0.61^2;        %% Flow resitance k for piston assembly orifices
nhp1=3;                %% n. of orifices in piston assembly
dhp1=2.50e-3;          %% Orifice diameter for piston assembly       [m]
sumAfEC = nhp1*pio4*dhp1^2; %% Total area of piston valve orifices [m^2]

%% Geometry and base valve data
% ************************
% ************************
kBC = 1/0.61^2;       %% Flow resistance k for base valve assembly orifices
nhbc1=1;              %% n. of orifices in base vake assembly
dhbc1=2.5e-3;         %% Diameter of base valve orifices              [m]
hB = 2.e-2;           %% Distance between inner and outer cylinder    [m]
sumAfBC = nhbc1*pio4*dhbc1^2;  %% Total area of base valve orifices [m^2]

%%-----------------------------------------
%% Intial and reference pressure/temperature
Ti=293.15;           %% Initial temperature                   [K]
T_air=293.15;         %% Environmental temperature            [K]
pref=1e5;            %% Reference pressure                  [Pa]
Tref=293.15;         %% Reference temperature                [K]
%%-----------------------------------------
%% Thermodynamics data
Mmg=28.96;           %% Gas molar mass                     [g/mol]
cpg=1005;            %% cp of the gas                     [J/kg/K]
cpoil=1850;          %% cp of the oil                     [J/kg/K]
betaf=2.5e-9;        %% Isothermal compressibility of oil   [1/Pa]
%betaf=0;           % for incompressbile model
phif=6.6e-4;         %% Coefficient of thermal expansion     [1/K]
%phif=0;             % for isothermal model
```

```
94  R=8314.47;           %% Universal constant for gases
95  n=cpg/(cpg-R/Mmg);   %% specific heat ratio
96  rhogas=pg0*Mmg/(R*Ti);  %% Initial gas density            [kg/m^3]
97  mgas=rhogas*Vg0;        %% Gass mass                        [kg]
98  E=210000e6;             %% Young's modulus inner cylinder     [Pa]
99  Ri=45e-3;               %% Internal radius inner cylinder      [m]
100 Re=52e-3;               %% External radius inner cylinder      [m]
101 %betac=2/E*((Ri^2+Re^2)/(Re^2-Ri^2) +0.33);  %% Compliance of cylinder wall
102 betac=0;
103 alpha=450;    %% Coefficient of thermal convection oil-wall [W/m^2/K]
104 alphagas=50;  %% Coefficient of thermal convection gas-wall [W/m^2/K]
105 alpha_air=20; %% Natural convection with environmment       [W/m^2/K]
106 lamb_oil=0.15;%% Oil conductivity                           [W/mK]
107 lamb_air=0.03;%% Air conductivity                           [W/mK]
108 alpha_oil_gas=8*lamb_air/Lc2+...
109               8/3*lamb_oil/Lc2; %% Thermal conductivity oil-gas [W/m^2/K]
110 %% Piston material properties
111 rhocylE=7860; %% Inner cylinder density                     [kg/m^3]
112 rhocylB=7860; %% Outer cylinder density                     [kg/m^3]
113 rhopist=7860; %% Piston density                            [kg/m^3]
114 ccyl=460;     %% cv specific heat cylinder                 [J/kg/K]
115 cpist=460;    %% cv specific heat piston                   [J/kg/K]
116 F_Coul=10;    %% Coulumbian Friction                           [N]
117 %-------------------------------------------------------------------------------
118 %%
119 %**************************************************
120 % Expression for density
121 rho=@ (p,T) rhooil*exp(betaf*(p-pref)-phif*(T-Tref));
122 u=@ (T) cpoil*T;
123 rhoc=@(p)rhooil*exp(betaf*(p-pref));
124
125 mcyl=Lc1*(Ac1e-Ap)*rhocylE;
126 mB=(Ac2e-Ac2i)*Lc2*rhocylB;
127 mpist=(Ar*(Lc1-tp)+tp*Ap)*rhopist;
128
129 str=sprintf('Discharge_time%2dfreq_%2d_Rel_%3e_Abs_%3e.txt',...
130             tmax,freq,Rel,Abs);
131 filePA5=fopen(str,'w');
132 fprintf(filePA5, '%20s %20s %20s %20s %20s %20s %20s %20s %20s %20s ...
        %20s\r\n','tempo','CdEC','ReEC','\Delta ...
        PEC','muEC','ncicli','CdbC','ReBC','\Delta PBC','muBC','ncicli');
133 fclose(filePA5);
134 %% Mass and Energy Check
135 [t,y,Fapp,xpist,vpist]=dumper;
136 Potenza=Fapp.*vpist;
137 Energy=trapz(t,Potenza);
138 Energy2=trapz(xpist,Fapp);
139 %*****************************
140 % Initial and final volume computation + energy computations
141 VolEf_finale=(Ap-Ar)*xpist(end);
142 VolCf_finale=Ap*(Lc1-xpist(end));
143 VolBf_finale=Ac1e*hB+(Ac2i-Ac1e)*Lc2-mgas*R/Mmg*y(end,8)/y(end,7);
144 rhogas0=pg0*Mmg/(R*Ti);
145 mgas=rhogas0*Vg0;
146 cvg=cpg/n;
```

```
147 Potfin=cpoil*rho(y(end,1),y(end,2))*VolEf_finale*((y(end,2)))+...
148        cpoil*rho(y(end,3),y(end,4))*VolCf_finale*((y(end,4)))+...
149        cpoil*rho(y(end,5),y(end,6))*VolBf_finale*((y(end,6)))+...
150        cvg*mgas*((y(end,8)))+ccyl*mcyl*((y(end,9)))+...
151        ccyl*mB*((y(end,10)))+cpist*mpist*(y(end,11));
152
153 VolEf_baseinizio=(Ap-Ar)*xpist(1);
154 VolCf_baseinizio=Ap*(Lc1-xpist(1));
155 VolBf_baseinizio=Ac1e*hB+(Ac2i-Ac1e)*Lc2-mgas*R/Mmg*y(1,8)/y(1,7);
156
157 Potinitial=cpoil*rho(y(1,1),y(1,2))*VolEf_baseinizio*((y(1,2)))+...
158            cpoil*rho(y(1,3),y(1,4))*VolCf_baseinizio*((y(1,4)))+...
159            cpoil*rho(y(1,5),y(1,6))*VolBf_baseinizio*((y(1,6)))+...
160            cvg*mgas*((y(1,8)))+ccyl*mcyl*((y(1,9)))+...
161            ccyl*mB*((y(1,10)))+cpist*mpist*(y(1,11));
162 DeltaE=Potfin-Potinitial;
163 Minitial=rho(y(1,1),y(1,2))*VolEf_baseinizio+...
164          rho(y(1,3),y(1,4))*VolCf_baseinizio+...
165          rho(y(1,5),y(1,6))*VolBf_baseinizio+...
166          mgas+mcyl+mB+mpist;
167 Mfinal=rho(y(end,1),y(end,2))*VolEf_finale+...
168        rho(y(end,3),y(end,4))*VolCf_finale+...
169        rho(y(end,5),y(end,6))*VolBf_finale+...
170        mgas+mcyl+mB+mpist;
171 %% Text file Output
172 filePARAMETRI=fopen('Damperdata.txt','a');
173 if fseek(filePARAMETRI, 1, 'bof') == -1
174    fprintf(filePARAMETRI, '%18s %18s %18s %18s %18s %18s %18s %18s ...
          %10s\r\n','tspan','freq', 'DeltaE', ...
          'Energia(F_x)','Energia(F_v_t)','Massa_iniziale',...
175                          'Massa_finale','Adiabatic','beta');
176    fprintf(filePARAMETRI, '%18.6f %18.6f %18.8f %18.8f %18.8f %18.11f ...
          %18.11f %18s %10.8e\r\n', [max(t); freq; DeltaE; Energy2; ...
          Energy; Minitial; Mfinal; heat_fluxes; betaf]);
177 else
178    frewind(filePARAMETRI)
179    fprintf(filePARAMETRI, '%18.6f %18.6f %18.8f %18.8f %18.8f %18.11f ...
          %18.11f %18s %10.8e\r\n', [max(t); freq; DeltaE; Energy2; ...
          Energy; Minitial; Mfinal; heat_fluxes; betaf]);
180
181 end
182
183 fclose(filePARAMETRI);
184 Miniziale0=Minitial-mgas-mB-mcyl-mpist;
185 [DM]=scrivi(t,y,Miniziale0);
186 %%
187
188 function [t,y,Fapp,xpist,vpist]=dumper
189 %% ODE call with Mass Matrix formulation (DAE's systems)
190 tspan = [0 tmax];
191     y0 = [1e5 Ti 1e5 Ti 1e5 Ti 1e5 Ti Ti Ti Ti];
192     opts=odeset('Mass',@(t,y) ...
          myode1(t,y),'RelTol',Rel,'AbsTol',Abs,'MaxStep',0.9,...
193                 'MStateDependence','strong');
194     [t,y] = ode15s(@(t,y) myode(t,y), tspan, y0, opts);
```

```
195     xpist = xp(t);
196     vpist = vp(t);
197 %************************************
198 % Damping force computation
199 Fapp = y(:,1)*(Ap-Ar)-y(:,3)*Ap+pg0*Ar;
200 % Uncomment to take friction into account
201 Fapp_c=Fapp-sign(vpist).*F_Coul;
202 % % Uncomment for Stribeck curve formulation for friction
203 % % Fs=0  static friction force                                          [N]
204 % % Ft=0  value of friction in Stribeck curve at zero relative velocity [N]
205 % % Fv=0  Viscous friction                                              [N]
206 % % Fc=0  Dynamic friction force                                        [N]
207 % % vfs=0 Value of vel. corresponding to max force in Stribeck curve  [m/s]
208 % % vs=0  Stribeck velocity                                            [m/s]
209
210 % for i=1:length(vpist)
211 %  if abs(vpist(i))<vfs
212 %     Fric(i)=sign(vpist(i)).*((Fs-(Fs-Ft)*(1-abs(vpist(i)/vfs).^c).^d)+...
213 %             +Fv.*vpist(i).^2);
214 %  else
215 %     Fric(i)=sign(vpist(i)).*((Fc-(Fs-Fc)*(abs(vpist(i)/vs).^c).^d)...
216 %             +Fv.*vpist(i).^2);
217 %  end
218 % Fapp=Fapp-Fric;
219 %% Plot of the results
220 figure
221 plot(t,y(:,1),'-o','LineWidth',1.5,'MarkerSize',3)
222 xlabel('t [s]')
223 ylabel('pE [Pa]')
224 title('Pressure in chamber E');
225 grid on;
226 print('-depsc2','pE');
227
228 figure
229 plot(t,y(:,3),'-o','LineWidth',1.5,'MarkerSize',3)
230 xlabel('t [s]')
231 ylabel('pC [Pa]')
232 title('Pressure in chamber C');
233 grid on;
234 print('-depsc2','pC');
235
236 figure
237 plot(t,y(:,7),'-o','LineWidth',1.5,'MarkerSize',3)
238 xlabel('t [s]')
239 ylabel('p_g [Pa]')
240 title('Pressure in gas chamber');
241 grid on;
242 print('-depsc2','pg');
243
244 figure
245 plot(t,y(:,2),'-o','LineWidth',1.5,'MarkerSize',3)
246 xlabel('t [s]')
247 ylabel('T_E [K]')
248 title('Temperature in chamber E');
249 grid on;
```

```
250 print('-depsc2','TE');
251
252 figure
253 plot(t,y(:,4),'-o','LineWidth',1.5,'MarkerSize',3)
254 xlabel('t [s]')
255 ylabel('T_C [K]')
256 title('Temperature in chamber C');
257 grid on;
258 print('-depsc2','TC');
259
260 figure
261 plot(t,y(:,5),'-o','LineWidth',1.5,'MarkerSize',3)
262 xlabel('t [s]')
263 ylabel('p_B [Pa]')
264 title('Pressure in chamber B');
265 grid on;
266 print('-depsc2','pB');
267
268 figure
269 plot(t,y(:,6),'-o','LineWidth',1.5,'MarkerSize',3)
270 xlabel('t [s]')
271 ylabel('T_B [K]')
272 title('Temperature in chamber B');
273 grid on;
274 print('-depsc2','TB');
275
276 figure
277 plot(t,y(:,8),'-o','LineWidth',1.5,'MarkerSize',3)
278 xlabel('t [s]')
279 ylabel('T_g [K]')
280 title('Temperature in gas chamber ');
281 grid on;
282 print('-depsc2','Tg');
283
284 figure
285 plot(t,y(:,9),'-o','LineWidth',1.5,'MarkerSize',3)
286 xlabel('t [s]')
287 ylabel('T_{cylinderint} [K]')
288 title('Temperature of the inner cylinder');
289 grid on;
290 print('-depsc2','Tci');
291
292 figure
293 plot(t,y(:,10),'-o','LineWidth',1.5,'MarkerSize',3)
294 xlabel('t [s]')
295 ylabel('T_{cylinderext} [K]')
296 title('Temperature of the outer cylinder');
297 grid on;
298 print('-depsc2','Tce');
299
300 figure
301 plot(t,y(:,11),'-o','LineWidth',1.5,'MarkerSize',3)
302 xlabel('t [s]')
303 ylabel('T_{piston} [K]')
304 title('Temperature of the piston');
```

```
grid on;
print('-depsc2','Tp');

figure
plot(t,Fapp,'-o','LineWidth',1.5,'MarkerSize',3)
xlabel('time [s]')
ylabel('Fapp [N]')
grid on;

figure
plot(xpist,Fapp,'-o','LineWidth',1.5,'MarkerSize',3)
xlabel('x_p [m]')
ylabel('Fapp [N]')
grid on;

figure
plot(vpist,Fapp,'-o','LineWidth',1.5,'MarkerSize',3)
xlabel('v_p [m/s]')
ylabel('Fapp [N]')
grid on;

figure
plot(xpist,Fapp_c,'-o','LineWidth',1.5,'MarkerSize',3)
xlabel('x_p [m]')
ylabel('Fapp (Friction included) [N]')
grid on;

figure
plot(vpist,Fapp_c,'-o','LineWidth',1.5,'MarkerSize',3)
xlabel('v_p [m/s]')
ylabel('Fapp (Friction included) [N]')
grid on;

%% Right-hand side term of DAEs : Ay'=bb
    function bb=myode(t,y)
%% Heat Exchage areas for fluid regions
AcE=dc1i*pi*xp(t);                      %% Internal area rebound
AcC=dc1i*pi*(Lc1-xp(t));                %% Internal area compression
Lgas=mgas*R/Mmg*y(8)/y(7)/(Ac2i-Ac1e);  %% Position of gas-oil interface
AcB=dc2i*pi*(Lc2-Lgas);                 %% Area reserve (outer cyl)
AcB_i=dc1e*pi*(Lc2-Lgas);               %% Area reserve (inner cyl)
Acgas=dc2i*pi*Lgas;                     %% Area gas (outer cyl)
Acgas_i=dc1e*pi*Lgas;                   %% Area gas (inner cyl)
Ap_scambioC=Ap-sumAfEC;                 %% Piston area within compression
Ap_scambioE=Ar+(Ap-Ar-sumAfEC);         %% Piston area within rebound

%uncomment to heat exchage with surroundings
Ac_environ=dc2e*pi*Lc2;                 %% External area of outer cylinder
%%
Volg=mgas*R/Mmg*y(8)/y(7);
flagEC=2;
flagBC=2;
b=zeros(11,1);
if trasporto==false

```

```
360      rhoEC=rho((y(1)+y(3))/2, (y(2)+y(4))/2);
361      rhoBC=rho((y(3)+y(5))/2,(y(4)+y(6))/2);
362
363  else
364
365      flagEC=0;
366      flagBC=0;
367
368  if sign(y(1)-y(3))>0
369      rhoEC=rho(y(1),y(2));
370  else
371      rhoEC=rho(y(3),y(4));
372      flagEC=1;
373  end
374  if sign(y(3)-y(5))>0
375       rhoBC=rho(y(3),y(4));
376  else
377       rhoBC=rho(y(5),y(6));
378       flagBC=1;
379  end
380  end
381
382  %% Discharge coefficient definition
383  cd0=0.61;
384  cdEC=cd0;
385  cdBC=cd0;
386
387  %**********************************
388  % Flow velocity through piston assembly
389  Δp12 = abs(y(1)-y(3));
390  if Δp12 == 0
391      vEC = 0;
392  else
393       % Initial velocity guess for Cd(Re) loop
394      vECguess = abs(vp(t))*(Ap-Ar)/sumAfEC;
395      if vECguess == 0
396         vECguess = 1.e-6;
397      end
398      vEC=nr(y(1),y(3),rhoEC,dhp1,Lh,EOD,kEC,vECguess,flagEC,y(2),y(4),muoil);
399  end
400
401  fluxvEC=vEC*sign(y(1)-y(3))*rhoEC;
402  %**********************************
403  % Flow velocity through base valve
404  Δp = abs(y(3)-y(5));
405  if Δp == 0
406      vBC = 0;
407  else
408      vBCguess = vp(t)*Ar/sumAfBC;
409      if vBCguess == 0
410          vBCguess = 1.e-6;
411      end
412     vBC=nr(y(3),y(5),rhoBC,dhbc1,Ld,EOD,kBC,vBCguess,flagBC,y(4),y(6),muoil);
413  end
414
```

```
fluxvBC=vBC*sign(y(3)-y(5))*rhoBC;

Reduction=0.0; %% Piston orifice closure in rebound [0-1]

if sign(y(1)-y(3))>0
    QECm=fluxvEC*sumAfEC*(1-Reduction);
else
    QECm=fluxvEC*sumAfEC;
end
QBCm=sumAfBC*fluxvBC;
ΔpE=y(1)-pref;
ΔpC=y(3)-pref;

%% Heat exchange to fluid regions (3 of oil + 1 of gas)
if heat_fluxes==true
    % heat flux oil in rebound receives
    qE=alpha*AcE*(y(9)-y(2))+alpha*Ap_scambioE*(y(11)-y(2));
    % heat flux oil in compression receives
    qC=alpha*AcC*(y(9)-y(4))+alpha*Ap_scambioC*(y(11)-y(4));
    % heat flux oil in reserve receives
    qB=alpha*AcB*(y(10)-y(6))+alpha*AcB_i*(y(9)-y(6))+...
        (Ac2i-Ac1e)*alpha_oil_gas*(y(8)-y(6));
    % heat flux gas receives
    qgas=alphagas*(Acgas*(y(10)-y(8))+Acgas_i*(y(9)-y(8)))+...
         (Ac2i-Ac1e)*alpha_oil_gas*(y(6)-y(8));
else
    % heat fluxes are disabled
    qE=0;
    qB=0;
    qC=0;
    qgas=0;
end

%% Right hand side of continuity equations
    b(1)=-vp(t)*(Ap-Ar)*(1+betac*ΔpE)-QECm/rho(y(1),y(2));
    b(2)=vp(t)*Ap*(1+betac*ΔpC)-QBCm/rho(y(3),y(4))+QECm/rho(y(3),y(4));
    b(3)=QBCm/rho(y(5),y(6));


%% Enthalpy fluxes
switch trasporto
    case false
        hEC=cpoil*((y(2)+y(4))/2)+(y(1)+y(3))/2/rhoEC;
        HfluxEC=-QECm*hEC;
    case true
        if sign(QECm)>0
            HfluxEC=-QECm*(cpoil*y(2)+y(1)/rho(y(1),y(2)));
        else
            HfluxEC=-QECm*(cpoil*y(4)+y(3)/rho(y(3),y(4)));
        end

end

switch trasporto
    case false
```

```
470          hBC=cpoil*((y(6)+y(4))/2)+(y(3)+y(5))/2/rhoBC;
471          HfluxBC=-QBCm*hBC;
472      case true
473          if sign(QBCm)>0
474              HfluxBC=-QBCm*(cpoil*y(4)+y(3)/rho(y(3),y(4)));
475          else
476              HfluxBC=-QBCm*(cpoil*y(6)+y(5)/rho(y(5),y(6)));
477          end
478
479  end
480  %************************************
481  % Right hand side of energy equations
482      b(4)=qE-vp(t)*(Ap-Ar)*(y(1)+rho(y(1),y(2))*u(y(2))*(1+betac*ΔpE))+...
483           HfluxEC;
484      b(5)=qC+vp(t)*Ap*(y(3)+rho(y(3),y(4))*u(y(4))*(1+betac*ΔpC))-...
485           HfluxEC+HfluxBC;
486      b(6)=qB-HfluxBC;
487  %**********************************
488  % Right hand side of compatibility condition at the interface oil-gas
489      b(7)=0;
490  if heat_fluxes==true
491  %**************************************
492  %Right hand side of energy equation
493      b(8)=qgas;
494      b(9)=-alpha*AcE*(y(9)-y(2))-alpha*AcC*(y(9)-y(4))-...
495           alphagas*Acgas_i*(y(9)-y(8))-alpha*AcB_i*(y(9)-y(6));
496      b(10)=-alpha*AcB*(y(10)-y(6))-alphagas*(Acgas*(y(10)-y(8)));
497      b(11)=-alpha*Ap_scambioE*(y(11)-y(2))-alpha*Ap_scambioC*(y(11)-y(4));
498  %Uncomment if heat exchange with surroundings is possible
499  %    b(11)=-alpha_air*Ac_environ*(y(11)-T_air)+b(11);
500  end
501  bb=b;
502
503  end
504
505  %% Mass matrix A computation Ay'=b(t)
506  % Columns matrix A: [pE TE pC TC pB TB pg Tg Tinncyl Toutercyl Tpist]
507  function A=myode1(t,y)
508  t
509  VolEf_base=(Ap-Ar)*xp(t);
510  VolCf_base=Ap*(Lc1-xp(t));
511  VolBf_base=Ac1e*hB+(Ac2i-Ac1e)*Lc2-mgas*R/Mmg*y(8)/y(7);
512
513  Volg=mgas*R/Mmg*y(8)/y(7);
514  VolCcyl=VolCf_base;
515  VolEcyl=VolEf_base;
516
517  ΔpE=y(1)-pref;
518  ΔpC=y(3)-pref;
519  ΔpB=y(5)-pref;
520  VolEf=VolEf_base*(1+betac*ΔpE);
521  VolCf=VolCf_base*(1+betac*ΔpC);
522  VolBf=VolBf_base;
523  A=zeros(10,10);
524
```

```
%*******************************************
% Coefficients relative to continuity equation
AA(1,1)=VolEf*betaf+VolEcyl*betac;
AA(1,2)=-VolEf*phif;

AA(2,3)=VolCf*betaf+VolCcyl*betac;
AA(2,4)=-VolCf*phif;

AA(3,5)=VolBf*betaf+mgas*R/Mmg*y(8)/((y(5))^2);
AA(3,6)=-VolBf*phif;
AA(3,8)=-mgas*R/Mmg/y(5);
%*******************************************
% Energy equation coefficients
AA(4,1)=rho(y(1),y(2))*u(y(2))*(VolEf*betaf+VolEcyl*betac);
AA(4,2)=cpoil*rho(y(1),y(2))*VolEf-rho(y(1),y(2))*u(y(2))*(VolEf*phif);

AA(5,3)=rho(y(3),y(4))*u(y(4))*(VolCf*betaf+VolCcyl*betac);
AA(5,4)=cpoil*rho(y(3),y(4))*VolCf-rho(y(3),y(4))*u(y(4))*(VolCf*phif);

AA(6,5)=rho(y(5),y(6))*u(y(6))*(VolBf*betaf+...
        mgas*R/Mmg*y(8)/(y(5))^2)+mgas*R/Mmg*y(8)/y(5);
AA(6,8)=-rho(y(5),y(6))*u(y(6))*mgas*R/Mmg/(y(5))-mgas*R/Mmg;
AA(6,6)=cpoil*rho(y(5),y(6))*VolBf-rho(y(5),y(6))*u(y(6))*(VolBf*phif);

A(1:6,1:8)=AA;
%***********************************
% Compatibility condition at the interface pg=pB
A(7,7)=1;
A(7,5)=-1;
%***********************************
% Energy equation for gas
A(8,8)=mgas*cpg;
A(8,7)=-Volg;

%***********************************
% Solid parts coefficient equations
A(9,9)=mcyl*ccyl;
A(10,10)=mB*ccyl;
A(11,11)=mpist*cpist;
end

end
%% Output file (writing)
 function DeltaM=scrivi(t,y,Miniziale0)
s=sprintf('DeltaM_time_%2dfreq_%2d_Rel_%3e_Abs_%3e.txt',tmax,freq,Rel,Abs);
s1=sprintf('Density_time_%2dfreq_%2d_Rel_%3e_Abs_%3e.txt',...
            tmax,freq,Rel,Abs);
s2=sprintf('Volume_time_%2dfreq_%2d_Rel_%3e_Abs_%3e.txt',tmax,freq,Rel,Abs);
filePA1=fopen(s1,'w');
fprintf(filePA1, '%38s\r\n',' ...
    Density-------------------------------------');
fprintf(filePA1, '%18s %18s %18s\r\n','rhoE','rhoC','rhoB');
filePA2=fopen(s2,'w');
fprintf(filePA2, ...
    '%38s\r\n','Volumi-------------------------------------');
```

```
fprintf(filePA2, '%18s %18s %18s %18s\r\n','VolE','VolC','VolB','Volg');

filePA=fopen(s,'w');
fprintf(filePA, ...
    '%38s\r\n','-----------------------------------------');
fprintf(filePA, '%18s %18s %18s\r\n','ΔM',['tspan=',num2str(tmax)],...
       ['freq=', num2str(freq)]);
for i=1:length(t)
VolEf_corr=(Ap-Ar)*xp(t(i));
VolCf_corr=Ap*(Lc1-xp(t(i)));
VolBf_corr=Ac1e*hB+(Ac2i-Ac1e)*Lc2-mgas*R/Mmg*y(i,8)./y(i,7);

Mfin=rho(y(i,1),y(i,2)).*VolEf_corr+rho(y(i,3),y(i,4)).*VolCf_corr+...
     rho(y(i,5),y(i,6)).*VolBf_corr;
DeltaM=Mfin-Miniziale0;

   fprintf(filePA, '%18.10e\r\n', DeltaM);
   fprintf(filePA1, '%20.12e %20.12e %20.12e\r\n', rho(y(i,1),y(i,2)),...
            rho(y(i,3),y(i,4)),rho(y(i,5),y(i,6)));
   fprintf(filePA2, '%20.12e %20.12e %20.12e %20.12e\r\n', VolEf_corr,...
           VolCf_corr,VolBf_corr,mgas*R/Mmg*y(i,8)./y(i,7));

end
fclose(filePA);
fclose(filePA1);
fclose(filePA2);
 end
%% Piston rod motion (Slider crank mechanism)
function disp = xp(t)
        disp = 1e-3 + sqrt(L^2-(amp*sin(ome*t)).^2)-...
               amp*cos(ome*t)-L+amp;
    end
    function vel = vp(t)
        vel = ...
            ome*amp*sin(ome*t)-.5*ome*amp*sin(2*ome*t)./sqrt((L/amp).^2-...
              (sin(ome*t)).^2);
    end


function voil    = nr(p1,p2,rho,D,L,EOD,klossin,v,flag,T1,T2,muoil)
    Δp=abs(p1-p2);
    f = fval(v);
    eps = 0.01;
    it = 0;
    vn = v;
    fneg = -10000000;
    fpos =  10000000;
    vfneg = 10000000;
    vfpos = 10000000;
    dvmin = 1e9;
    pw = 0;
    nw = 0;
    while abs(f)>1.e-10
        it = it + 1;
        if f < 0
```

```
631             if abs(v-vfpos) ≤ dvmin
632                 vfneg = v;
633                 fneg = f;
634             end
635             nw=1;
636         else
637             if abs(v-vfneg) ≤ dvmin
638                 vfpos = v;
639                 fpos = f;
640             end
641             pw=1;
642         end
643         if it > 50 & pw == 0
644             vd = logspace(-15,4,20);
645             fd = fval(vd);
646             fpos=min(fd(fd≥0));
647             ip = find(fpos==fd);
648             vfpos= vd(ip);
649             pw = 1;
650         end
651         if it > 50 & nw == 0
652             vd = logspace(-15,4,20);
653             fd = fval(vd);
654             fneg=min(fd(fd<0));
655             in = find(fneg==fd);
656             vfneg= vd(in);
657             nw = 1;
658         end
659         dvmin = abs(vfpos-vfneg);
660         if it > 50
661             v = min(vfpos,vfneg) + .5*dvmin;
662             sw = 1;
663         end
664         if it ≤ 50
665         vm = v*(1-eps);
666         fm = fval(vm);
667         vp = v*(1+eps);
668         fp = fval(vp);
669         df = (fp-fm)/(vp-vm);
670         vn = v - f/df;
671         if vn < 0
672             vn = 1.e-10;
673         end
674         v = vn;
675         end
676         f = fval(v);
677     end
678     voil = v;
679     return
680     function fdum = fval(vdum)
681         [klossdum,klossin] = loss(vdum,D,L,EOD,rho,muoil,flag,T1,T2);
682         fdum = vdum-sqrt(2*Δp/rho./(klossdum+klossin));
683     end
684 end
685 function [kloss,klossin]=loss(vel,D,L,EOD,rho,muoil,flag,T1,T2)
```

```
686
687 %     Laminar, transitional and turbulent friction in cylidrical pipes
688 if flag==2
689              T=(T1+T2)/2;
690 elseif flag==0
691              T=T1;
692     else
693              T=T2;
694 end
695     C=5693-304*log10(muoil)-646*(log10(muoil))^2;
696     % Variation of dynamic viscosity with temperature
697     mu=muoil*exp(C*(1/T-1/(293.15)));
698     % Reynolds number
699     Re=abs(vel).*D*rho/mu;
700
701 %*********************************************************
702 % Correlation for friction coeffcient
703 if EOD==0
704     if (Re<1.e-15)
705         F=0;
706     else
707         FA = 64./Re;
708         FB = 4.1e-16*Re.^4.;
709         FC = 0.351*Re.^-0.255;
710         FD = 0.118*Re.^-0.165;
711         F1 = FA+(FB-FA)./sqrt(1.+(Re/2900.).^-50.);
712         F2 = FC+(FD-FC)./sqrt(1.+(Re/240000.).^-1.);
713         F  = F1+(F2-F1)./sqrt(1.+(Re/3050.).^-50.);
714     end
715 else
716     indici=Re<2300;
717     F(indici)=PowRe(Re(indici));
718     F(¬indici)=colebrook(Re(¬indici),EOD/D);
719 end
720 %*****************************************************
721 %Discharge coefficient computation
722 cd_new=0.61*(1+1.07*exp(-0.126*sqrt(Re))-2.07*exp(-0.246*sqrt(Re)));
723 %*****************************************************
724 % Flow resitance for concentrated and distributed losses
725 klossin=1./(cd_new).^2;
726 kloss=F*L/D;
727
728 end
729 function F = colebrook(R,K)
730 % F = COLEBROOK(R,K) fast, accurate and robust computation of the
731 %     Darcy-Weisbach friction factor F according to the Colebrook equation:
732 %                                 -                          -
733 %       1                        |    K        2.51         |
734 %   ---------   =   -2 * Log_10  |   ----- + -------------   |
735 %    sqrt(F)                     |    3.7     R * sqrt(F)    |
736 %                                 -                          -
737 % INPUT:
738 %    R : Reynolds' number (should be ≥ 2300).
739 %    K : Equivalent sand roughness height divided by the hydraulic
740 %        diameter (default K=0).
```

```
%
% OUTPUT:
%   F : Friction factor.
%
% Method: Quartic iterations.
% Reference: http://arxiv.org/abs/0810.5564
% Author: D. Clamond, 2008-09-16.

% Check for errors.
if any(R(:)<2300) == 1,
   warning('The Colebrook equation is valid for Reynolds'' numbers ≥ ...
       2300.');
end,
if nargin == 1 || isempty(K) == 1,
   K = 0;
end,
if any(K(:)<0) == 1,
   warning('The relative sand roughness must be non-negative.');
end,

% Initialization.
X1 = K .* R * 0.123968186335417556;   % X1 <- K * R * log(10) / 18.574.
X2 = log(R) - 0.779397488455682028;   % X2 <- log( R * log(10) / 5.02 );

% Initial guess.
F = X2 - 0.2;

% First iteration.
E = ( log(X1+F) - 0.2 ) ./ ( 1 + X1 + F );
F = F - (1+X1+F+0.5*E) .* E .*(X1+F) ./ (1+X1+F+E.*(1+E/3));

% Second iteration (remove the next two lines for moderate accuracy).
E = ( log(X1+F) + F - X2 ) ./ ( 1 + X1 + F );
F = F - (1+X1+F+0.5*E) .* E .*(X1+F) ./ (1+X1+F+E.*(1+E/3));

% Finalized solution.
F = 1.151292546497022842 ./ F;    % F <- 0.5 * log(10) / F;
F = F .* F;                       % F <- Friction factor.

end
function Fric=PowRe(Rey)
        FA = 64./Rey;
        FB = 4.1e-16*Rey.^4.;
        FC = 0.351*Rey.^-0.255;
        FD = 0.118*Rey.^-0.165;
        F1 = FA+(FB-FA)./sqrt(1.+(Rey/2900.).^-50.);
        F2 = FC+(FD-FC)./sqrt(1.+(Rey/240000.).^-1.);
        Fric  = F1+(F2-F1)./sqrt(1.+(Rey/3050.).^-50.);
end
end
```

Bibliography

[1] M. Alonso and Á. Comas. «Modelling a Twin Tube Cavitating Shock Absorber». In: *Proceedings of the Institution of Mechanical Engineers, Part D: Journal of Automobile Engineering* 220.8 (2006), pp. 1031–1040.

[2] M. Alonso and Á. Comas. «Thermal model of a twin-tube cavitating shock absorber». In: *Proceedings of the Institution of Mechanical Engineers, Part D: Journal of Automobile Engineering* 222.11 (2008), pp. 1955–1964.

[3] W. Bauer. *Hydropneumatic Suspension Systems*. VDI-Buch. Springer Berlin Heidelberg, 2010.

[4] A. Cavallini and L. Mattarolo. *Termodinamica applicata*. CLEUP, 2013.

[5] Y.A. Cengel. *Heat Transfer: A Practical Approach*. McGraw-Hill, 2007.

[6] Didier Clamond. «Efficient Resolution of the Colebrook Equation». In: *Industrial & Engineering Chemistry Research* 48.7 (2009), pp. 3665–3671.

[7] Daniel D. Joseph and Haoping Yang. «Friction factor correlations for laminar, transition and turbulent flow in smooth pipes». In: *Physica D-nonlinear Phenomena - PHYSICA D* 239 (July 2010).

[8] J.C. Dixon. *The Shock Absorber Handbook: Second Edition*. Nov. 2007, pp. 1–415.

[9] Stefann Duym, Randy Stiens, and Koenraad Reybrouck. «Evaluation of Shock Absorber Models». In: *Vehicle System Dynamics* 27.2 (1997), pp. 109–127.

[10] Urszula Ferdek and Jan Luczko. «Modeling and analysis of a twin-tube hydraulic shock absorber». In: *Journal of Theoretical and Applied Mechanics* 50 (Jan. 2012).

[11] L. He and G.T. Zheng. «Effect of viscous heating in fluid damper on the vibration isolation performance». In: *Mechanical Systems and Signal Processing* 21.8 (2007), pp. 3060–3071. ISSN: 0888-3270.

[12] Kwangjin Lee. «Numerical Modelling for the Hydraulic Performance Prediction of Automotive Monotube Dampers». In: *Vehicle System Dynamics* 28.1 (1997), pp. 25–39.

[13] Javier Lizarraga, José A. Sala, and Jorge Biera. «Modelling of friction phenomena in sliding conditions in suspension shock absorbers». In: *Vehicle System Dynamics* 46.sup1 (2008), pp. 751–764.

[14] J.C. Ramos et al. «Development of a thermal model for automotive twin-tube shock absorbers». In: *Applied Thermal Engineering* 25.11 (2005), pp. 1836–1853. ISSN: 1359-4311.

[15] W.M. Rohsenow, J.P. Hartnett, and Y.I. Cho. *Handbook of heat transfer*. McGraw-Hill handbooks. McGraw-Hill, 1998.

[16] Michael S. Talbott and John Starkey. «An Experimentally Validated Physical Model of a High-Performance Mono-Tube Damper». In: *SAE Technical Paper 2002-01-3337* (Dec. 2002), pp. 776–4841.

[17] Adrian Simms and David Crolla. «The Influence of Damper Properties on Vehicle Dynamic Behaviour». In: *SAE Technical Paper 2002-01-0319* (Mar. 2002).

[18] Paulius Skackauskas et al. «Development and verification of a shock absorber and its shim valve model based on the force method principles». In: *Eksploatacja i Niezawodnosc - Maintenance and Reliability* 19 (Dec. 2016), pp. 126–133.

[19] R. Sonnenburg and A. Stretz. *Dynamics of Hydraulic Damper Modules*. Mechanical Engineering Theory and Applications. Nova Science Publishers, Incorporated, 2014.

[20] Hitesh K. Tare and C.S. Dharankar. «Determination of damping coefficient of automotive hydraulic damper using sinusoidal testing». In: *International Journal of Current Engineering and Scientific Research, ISSN (Print): 2393-8374, (Online): 2394-0697, Vol 3, Issue 7* 3 (2016).

[21] B. Yung Victor Y. and David J. Cole. «Modelling high frequency force behaviour of hydraulic automotive dampers». In: *Vehicle System Dynamics* 44.1 (2006), pp. 1–31.

[22] Duqiang Wu, Richard Burton, and Greg Schoenau. «An Empirical Discharge Coefficient Model for Orifice Flow». In: *International Journal of Fluid Power* 3.3 (2002), pp. 13–19.